INFORMATION TO USERS

This manuscript has been reproduced from the microfilm master. UMI films the text directly from the original or copy submitted. Thus, some thesis and dissertation copies are in typewriter face, while others may be from any type of computer printer.

The quality of this reproduction is dependent upon the quality of the copy submitted. Broken or indistinct print, colored or poor quality illustrations and photographs, print bleedthrough, substandard margins, and improper alignment can adversely affect reproduction.

In the unlikely event that the author did not send UMI a complete manuscript and there are missing pages, these will be noted. Also, if unauthorized copyright material had to be removed, a note will indicate the deletion.

Oversize materials (e.g., maps, drawings, charts) are reproduced by sectioning the original, beginning at the upper left-hand corner and continuing from left to right in equal sections with small overlaps.

Photographs included in the original manuscript have been reproduced xerographically in this copy. Higher quality 6" x 9" black and white photographic prints are available for any photographs or illustrations appearing in this copy for an additional charge. Contact UMI directly to order.

Bell & Howell Information and Learning
300 North Zeeb Road, Ann Arbor, MI 48106-1346 USA

UMI®
800-521-0600

Flow injection methods for drug-receptor interaction studies, based on probing cell metabolism

by

Ilkka Johannes Lähdesmäki

A dissertation submitted in partial fulfillment of the requirements for the degree of

Doctor of Philosophy

University of Washington

1999

Program Authorized to Offer Degree: Chemistry

UMI Number: 9952855

Bell & Howell Information and Learning Company
300 North Zeeb Road
P.O. Box 1346
Ann Arbor, MI 48106-1346

In presenting this thesis in partial fulfillment of the requirements for the Doctoral degree at the University of Washington, I agree that the Library shall make it's copies freely available for inspection. I further agree that extensive copying of the dissertation is allowable only for scholarly purposes, consistent with "fair use" as prescribed in the U.S. Copyright Law. Requests for copying or reproduction of this dissertation may be referred to University Microfilms, 1490 Eisenhower Place, P.O. Box 975, Ann Arbor, MI 48106, to whom the author has granted "the right to reproduce and sell (a) copies of the manuscript in microform and/or (b) printed copies of the manuscript made from microform."

Signature 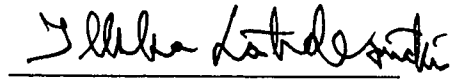

Date SEPT 23 1999

University of Washington
Graduate School

This is to certify that I have examined this copy of a doctoral dissertation by

Ilkka Johannes Lähdesmäki

and have found that it is complete and satisfactory in all respects,
and that any and all revisions required by the final
examining committee have been made.

Chairs of Supervisory Committee:

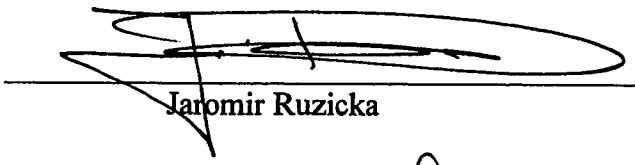

Jaromir Ruzicka

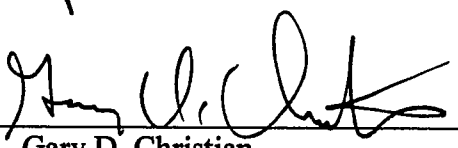

Gary D. Christian

Reading Committee:

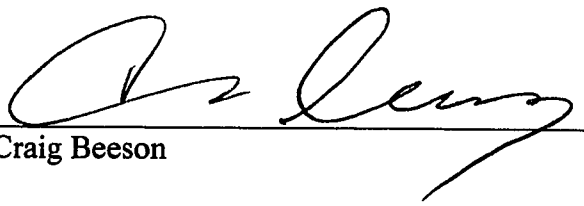

Craig Beeson

Date: SEPT 23 1999

University of Washington

Abstract

Flow injection methods for drug-receptor interaction studies, based on probing cell metabolism

Ilkka Johannes Lähdesmäki

Chairpersons of the Supervisory Committee:
Prof. Jaromir Ruzicka
Prof. Gary Christian
Department of Chemistry

The thesis describes the development of methods to study responses of living cells to chemical stimulation. To measure the responses, the developed methods utilize effects that the responses have on the rate of the cells' energy metabolism. The metabolic rate is probed either by measuring acid production or oxygen consumption. The technique of flow injection is used throughout the work to achieve swift and reproducible stimulant delivery and removal. Bead injection, a later variant of flow injection, is used to create optimal conditions for the detection of extracellular acidification and oxygen consumption. Detection of pH and $[O_2]$ is carried out by the appropriate fluorescent probes and a fluorescence microscope. The methods are validated by carbachol stimulation of Chinese Hamster Ovary M1 (CHO M1) cells.

TABLE OF CONTENTS

LIST OF FIGURES

LIST OF TABLES

ACKNOWLEDGEMENTS

I want to express my deep gratitude to my supervisors, Prof. Jaromir Ruzicka and Prof. Gary Christian at the University of Washington, and Prof. Ari Ivaska at Åbo Akademi University. This work would not have been possible without the help and guidance that they generously showed throughout my graduate career.

Prof. Craig Beeson has been a tremendous help and support in countless difficult issues involved with analytical measurements on live cells. Another invaluable source of biological information has been Dr. Bob Wiseman who guided me through the tough beginning with cellular pH measurements and also after that was always ready to offer his expertise in cell physiology to improve my work. Prof. Martin Gouterman is to be thanked for his expert advice on luminescent oxygen measurements, as well as for donation of the chemicals for the oxygen sensing work.

I am greatly indebted to Dr. Louis Scampavia for sharing his exceptional knowledge and abilities all across the field of physical sciences, ranging from chemistry to engineering. Pleasant and fruitful cooperation with Dr. Carmen Rehder in studying cellular pH regulation is gratefully acknowledged.

Zymogenetics Inc. (Seattle, WA) is acknowledged for lending facilities for tissue culture, as well as space for instrumentation. Special thanks go to the tissue culture staff at Zymogenetics for their friendliness and willingness to accommodate members of our group in their facilities. Further, I am grateful to Dr. Ole Thastrup and Dr. Kurt Scudder at BioImage (Copenhagen, Denmark) for showing interest in my work and arranging a visit in Copenhagen.

This work is based in many ways on research carried out by other, past and present, members of the flow injection group - their work and the pleasant working environment is acknowledged with great gratitude. In particular, I wish to thank Dr. Peter Hodder, Wendy Connors and Armando Herbelin.

Most of all, I want to thank my family for their unwavering support.

DEDICATION

To my parents

Chapter 1 Introduction

1.1 Scope of the thesis

The work described in the thesis has been aimed at designing new techniques for measuring cellular responses based on metabolic parameters. The techniques rely on the use of flow injection for fluidic handling and fluorescence microscopy for detection. The thesis is divided into seven chapters. Chapter 1 describes the concept of cell response and its link to energy metabolism, and provides an introduction to the instrumental techniques. Chapter 2 and Chapter 3 describe measurements based on a monolayer of cultured cells: the former focuses on concerted pH and Ca^{2+} measurements, the latter on pH measurements for characterizing the cellular pH control mechanisms. Chapter 4 and Chapter 5 describe extra- and intracellular pH measurements, respectively, based on cells cultured on microbeads. Chapter 6 describes oxygen consumption measurements, also based on cells cultured on microbeads. Finally, Chapter 7 presents the summary and future aspects of the work.

1.2 Cellular energy metabolism

1.2.1 Definition and purpose of energy metabolism

The term energy metabolism comprises the chemical reactions and processes that living cells are using to extract energy from nutrient molecules. In the case of animal cells, energy is derived from organic compounds, such as glucose and fatty acids. By subjecting these energy-rich source compounds to a series of metabolic reactions, they are transferred into energy-poor products. The released energy is captured in form of adenosine triphosphate (ATP), a compound formed from adenosine diphosphate (ADP) and pyrophosphate (P_i) in the following reaction:

$$ADP + P_i + energy \rightarrow ATP + H_2O$$

By including the reverse reaction, ATP hydrolysis, as a part of their overall reaction scheme, biosynthetic pathways can get the necessary energy to proceed. Consequently, ATP can be regarded as the cellular energy currency, generated from nutrients by one set of reactions and subsequently used for fueling a wide spectrum of other vital processes in the cell.

1.2.2 Pathways in energy metabolism

A cell can derive energy from proteins, polysaccharides/sugars or lipids [1]. For cultured cells, by far the most important source is glucose in the growth medium. The utilization of glucose for cellular energy production is shown in Figure 1-1. It begins by a nine-step pathway called *glycolysis* where one glucose molecule is converted to two molecules of pyruvate, yielding two ATP's. Whereas glycolysis occurs in nearly all living cells and in all conditions, further processing of the formed pyruvate will depend on cell type and the availability of oxygen. In the absence of oxygen, pyruvate is simply converted to lactic acid by the enzyme lactate dehydrogenase. Thus, the overall energy producing reaction will be:

$$glucose + 2\,ADP + 2\,P_i \rightarrow 2\,lactic\ acid + 2\,ATP + 2\,H_2O$$

The process is called *lactic acid fermentation* and cells employing it as their main route of energy supply are said to be *anaerobic*. Lactic acid fermentation commonly occurs in immortal cultured cells even in the presence of oxygen, to the extent where such cells usually are predominantly anaerobic under all circumstances.

In the presence of oxygen, pyruvate from glycolysis will be subjected to oxidation and decarboxylation in the *citric acid cycle*, an eight-step cyclic pathway. As a result, carbon dioxide is produced along with 2 ATP's. Also, several molecules of the dinucleo-

tide NAD^+ are converted into the reduced form NADH. The NADH molecules are subsequently re-oxidized on mitochondrial membranes through the processes of *electron transport chain* and *oxidative phosphorylation.* The oxidation of the NADH molecules is coupled to reduction of oxygen to water and, most importantly, to production of about 26 molecules of ATP. The overall reaction for this *aerobic* pathway of glucose oxidation (glycolysis, citric acid cycle, electron transport chain and oxidative phosphorylation) is:

$$\text{glucose} + 6\,O_2 + \sim 30\,\text{ADP} + \sim 30\,P_i \rightarrow 6\,CO_2 + \sim 30\,\text{ATP} + \sim 36\,H_2O$$

It is easy to see that the aerobic pathway makes much more efficient use of the chemical energy in glucose than the anaerobic pathway does. Therefore, it is not surprising that it is the preferred route of energy generation in all primary cells under sufficient supply of oxygen.

1.3 Cell response measurements

1.3.1 The concept of cell stimulation

In any multicellular organism, communication between different cells is needed for proper, controlled function of the organism [2]. Such intercellular communication is called cell signaling and is usually carried out by means of secreted signaling molecules, also referred to below as stimulants. A stimulant will recognize its target cells by binding to a specific receptor protein that the target cells carry on their membranes. Typically, binding of a stimulant to the extracellular part of the receptor protein will change the conformation of the intracellular end, which triggers off an intracellular cascade of biochemical reactions. This cascade will eventually result in the cell expressing the desired property or event that the stimulant was secreted to elicit. The steps in the cascade reaction (including the final event) are called the response of the

target cell to the stimulant in question. The binding of a stimulant to a receptor and the subsequent activation of a response cascade are described graphically in Figure 1-2.

Intracellular cascades are complicated processes, one cascade involving many different steps. The most commonly encountered kinds of steps include direct activation / deactivation of enzymes (e.g. by phosphorylation) and formation or release of small mediator species, such as Ca^{2+} and cyclic AMP, that will subsequently affect the activity of one or more enzymes or genetic effector molecules. These steps are used to relay and amplify the signal inside the cell to finally produce the desired event - that can be conversion of glucose into glucagon, contraction of a muscle or turning on a gene to produce a certain protein, to name a few. The mediator species are more usually called second messengers, reflecting their universal role as messengers that pick up the signal shortly after the primary event (stimulant binding) has occurred. They are of particular interest to cell biologist, due to their universality as signal carriers.

1.3.2 Quantification of cell response

It is clear from the above description that the response activated in a cell by stimulation is a complex process consisting of several phases: stimulant binding, signal transduction through the cell membrane, intracellular response cascade and the final event. The extent of the response triggered by a drug can be monitored at any of these levels. In addition, certain side effects or consequences of the response process can be utilized. The prime example of the latter approach is utilizing the effects of the response on the cell's energy metabolism. The work described in this thesis is primarily focused on measuring drug responses in terms of their metabolic consequences, and secondarily in terms of second messengers. Therefore, these two approaches are discussed more in detail below.

Monitoring the concentration of intracellular messengers is important for several reasons. First of all, the observations can be used to elucidate whether a messenger is at all

involved in the response cascade to a certain stimulant. Secondly, the time dependence of messenger concentration in response to a stimulant shows how fast the cell responds or at which point of the cascade the messenger is activated. Both of these are important issues in general cell physiology. Thirdly, the degree of change in messenger concentration provides an idea of how strongly the cell is stimulated by different stimulant levels, or by different stimulant species. Such information is very relevant for pharmacology, especially for drug discovery and screening.

1.3.3 Measurement of cell stimulation through metabolic acid generation

When a response cascade is activated, one of the general consequences will be altered consumption of energy in the cell. Since the energy metabolism generates acidic side products (lactic acid, CO_2), any changes in metabolic activity will be reflected in the rate of metabolic acid production, and subsequently in the rate of acid extrusion. The link between cell stimulation and acid extrusion is utilized in the Cytosensor Microphysiometer® (Figure 1-3), a commercial instrument that quantitates cell responses by measuring acid extrusion rates [3]. Cells are held in a small compartment that is continuously perfused by a flow of buffer solution. To measure the acid extrusion rate the flow is stopped, in which case acid produced by the cells accumulates in the compartment and changes the pH of the solution. A sensitive electrochemical pH sensor is used to detect the pH change, and acid extrusion rate is calculated as:

$$acid\ extrusion\ rate = \frac{\Delta pH}{\Delta t}$$

Since the rate correlates with the magnitude of cell response, the instrument can be used for quantitating cells' responses to stimuli. Exposure of cells to a stimulant is achieved by injecting a known volume of stimulant solution into the perfusion buffer stream – in other words, using flow injection. Based on the rather extensive microphysiometry literature, acid extrusion seems to be a very general response parameter

that can be used to study the responses of many cell lines and stimulant-receptor systems.

Altered activity of the energy metabolism should not only lead to changes in acid extrusion but also to changes in the cytosolic pH. That way, cytosolic pH monitoring could be used as a general means of following cellular stimulation, similarly to acid extrusion rate measurements. The relationship between cell stimulation, cellular acid generation and the different response parameters is shown in Figure 1-4.

1.3.4 Mathematical models of cell response

Cell stimulation is initiated by a stimulant (drug) binding to a receptor. The binding of a drug A to a receptor R can be described by the equation:

$$A + R \leftrightarrow A \cdot R$$

where $A \cdot R$ is the formed drug-receptor complex. Assuming that binding does not decrease $[A]$ to an observable degree and using the law of mass action, the following expression is obtained for $[A \cdot R]$:

$$\frac{[A \cdot R]}{[R_t]} = \frac{[A]}{[A] + K_A}$$

where $[R_t]$ is the total concentration of receptors and K_A is the dissociation constant of the drug-receptor complex. The above adsorption isotherm has been observed to adequately describe the binding of a drug to receptors on cell membranes. Further, there is wide agreement that the number of occupied receptors determines the extent of cellular response: in the absence of the drug, no receptors are occupied and no response is observed. When the drug is present in progressively larger quantities, an increasing portion of the receptors are occupied and an increasing response is observed. Finally, as

most or all of the receptors are occupied, the response reaches saturation. However, there is no absolute agreement regarding the exact relationship describing the dependence of the response on receptor occupation. Designating the observed response by E_A and the maximal response by E_M, we can write the following mathematical relationship between the response and receptor occupation:

$$\frac{E_A}{E_M} = f\left(\frac{[A \cdot R]}{[R_t]}\right)$$

The function f is unknown – its nature will depend on the drug, the cell type, the receptor and the response mechanism triggered off by the drug-receptor binding. Borrowing nomenclature from signal processing, one could say that f is the response function of a system to a stimulus. Since each combination of drug, receptor, cell type and response mechanism constitutes a unique system, the response functions can be very different.

Even though the cellular response functions could be substantially different, experimental observations have shown that in many cases the response and the *free* drug concentration are related by a hyperbolic function:

$$E_a = \frac{E_m[A]}{[A]+b}$$

where b is a fitting constant. Since b equals the concentration of free drug needed to produce half-maximal response, it is often called EC_{50} and the above relationship is written:

$$E = \frac{E_{\max} C}{C + EC_{50}}$$

A much more thorough discussion of the theory of cell responses is provided in refs. [4,5].

1.4 Flow injection techniques

1.4.1 Flow injection analysis

The flow injection analysis (FIA) technique was developed in the mid-1970's to automate wet chemistry assays [6]. Automation is achieved by carrying out analyses in a flow system where a peristaltic pump is used to continuously draw sample and reagent solutions into different lines or segments of plastic tubing, as well as push them forward through the system (see Figure 1-5). Precise aliquots of the sample solution are dispensed into the carrier stream by an injection valve. Bringing together solutions from different lines in mixing tees, or including a reagent in the carrier stream enables seamless, automated reagent addition. By connecting a detector at the end of the sample's flow path, automated detection of the processed sample is ensured. It is easy to see that compared to manual analyses, the tubing lines serve as solution containers and transfer vessels, the injection valve serves as a micropipet, and the pump replaces the lab technician using all this labware.

A central concept in flow injection analysis is that of dispersion. A prerequisite for understanding dispersion is to realize that in laminar flow conditions the radial flow profile in a tube is not uniform but parabolic (Figure 1-6a). The velocity of the fastest streamline (in the middle) is twice the average flow velocity in the tube, whereas the velocity close to tube walls is considerably less than the average flow. The non-uniform flow results in the fact that a plug introduced in the carrier stream will penetrate into the carrier and lose its original square concentration profile as it travels through the tube (Figure 1-6b). The resulting profile has a shape resembling a skewed Gaussian curve.

The degree of dispersion is defined as the ratio between the original concentration in the sample solution and the observed peak concentration after dispersion has taken place:

$$D_{\max} = \frac{C^0}{C'^{\max}}$$

It follows from this definition that D_{max} can only attain values >1. Further, the greater the value of D_{max}, the more drawn-out and depressed the concentration profile will be. Dispersion is determined by physical parameters of the FIA system, as explained by the following formula [7]:

$$D_{\max} = \frac{2\pi^{3/2} R^2 D_f^{1/2} L^{1/2}}{F^{1/2} S_v}$$

where R is the tube radius, D_f is the so-called axial dispersion coefficient, L is the tube length, F is the average linear flow velocity and S_v is the injected sample volume.

Dispersion exists in all flow injection systems. Therefore, in terms of signal processing, FIA could be described as a system that takes a square impulse (sample plug) as an input signal and returns a response (detector readout). The response is determined by the way that the system (dispersion) modulates the square input, as well as by how much analyte the sample contains. As FIA first was introduced, there were suspicions that the dispersion effects would mask the effects of analyte concentration and render the technique useless. As it turns out, the dispersion in a given FIA setup remains constant as long as no physical changes are made. Consequently, calibration of the setup corrects for all systemic effects and makes it possible to obtain analyte concentration from the signal just as in any other analytical instrument. It should be stressed, however, that although the systemic effects do not need to be considered when running a calibrated FIA system, they do become very important when designing one.

In its simplest form, a FIA analyzer consists of a single line containing the carrier/reagent stream (Figure 1-7a). When a sample plug is injected, the carrier stream propels it forward along the tube. As dispersion occurs along the way, the sample is mixed with the reagent in the carrier stream, giving rise to a detectable reaction product. The desired dispersion (= desired extent of dilution) can be achieved by including an extra length of tubing before the detector, called a reaction coil. In addition to promoting dispersion, the reaction coil allows adjustment of the time elapsed between reagent addition and detection. Figure 1-7b shows a more complex system, designed for an analytical assay requiring addition of several reagents. It also shows how labile reagents can be generated on-line by mixing the necessary ingredients in the FIA system. Many more types of analyses can be implemented by appropriate design of the plumbing and inclusion of components such as mixing chambers and gas-diffusion cells. A thorough description of the different possibilities is given in ref. [7].

FIA has been very successful in simplifying chemical assays. The main reasons for the success are the following advantages of FIA over conventional manual techniques:

1) reduced labor costs due to automation
2) greater precision due to mechanical performance of the assays
3) higher sample throughput due to mechanical performance of the assays
4) smaller sample and reagent consumption and waste generation due to smaller scale of the assays

1.4.2 Sequential injection analysis

Sequential injection analysis (SIA) evolved from FIA in the early 1990's [8, 9]. The typical FIA architecture of multiple lines driven by a peristaltic pump was replaced by a single line connected to a bidirectional pump (usually a syringe pump) and a multiport valve (Figure 1-8a). The continuous operation of a FIA analyzer changed to discontinuous aspiration of the sample and the reagent as finite zones through the multi-

port valve (Figure 1-8b). Once both zones are stacked in the holding coil, they are propelled into the detector. Due to dispersion occurring in the tubing, the sample and the reagent are mixed at their interface and the ensuing product can be detected. If necessary, dispersion can be enhanced by moving the stacked zones back and forth in the holding coil by repeated flow reversals. The pump and valve operations need to be carefully synchronized and precisely defined so that they are repeated exactly the same way from one assay to the next. Therefore, all the events in sequential injection assay protocols are run under computer control.

Sequential injection offers the following advantages over FIA:

1) Using a single valve and a single pump simplifies the system. The possibility of using a syringe pump makes the system mechanically more robust and the analyses more precise.
2) The sample volume is not fixed but can be freely changed through the control program.
3) Reagent consumption is decreased considerably since reagent solution is no longer continuously pumped through the system.
4) With a bidirectional pump and computer control, reaction time can be adjusted by stopping the flow for any desired period, rather than physically extending the line between the injection valve and the detector.
5) Tunable dispersion by flow reversals is readily achieved.

Using SIA instead of FIA does also have some disadvantages:

1) Sample throughput is lower since aspirating and dispensing the sample and the reagent consumes more time than the quick injection of the sample in FIA.
2) The need for computer control and a more sophisticated pump makes SIA more expensive.
3) Dispersion-mediated mixing of sample and reagent zones is not very efficient and as a result, the basic SIA system is normally restricted to chemistries involving a single reagent, although sandwiching the sample between two reagents is possi-

ble. Mixing the sample with more than one reagent usually necessitates the use of a mixing chamber.

1.4.3 Bead injection

Bead injection (BI) is the latest advancement of the flow injection techniques, developed as an extension of SIA. It features the use of microbeads to create a small, disposable sensing layer that can be renewed for each individual assay. A sequential injection setup designed for BI work is shown in Figure 1-9a. A suspension of indicator beads is connected to the multiport valve so that precise quantities of beads can be aspirated in the SI manifold. The heart of the BI technique is the jet ring cell (Figure 1-9b) that traps the beads and allows perfusion of the formed bead column with the carrier or with an injected zone of sample solution.

Due to the use of a solid reagent surface, BI enhances the sequential injection technique by eliminating the rather inefficient mixing of reactants during the loading process. Also, the ability to renew the bead column eliminates one of the greatest problems with solid state sensors, i.e. sensor fouling. Therefore, BI could be regarded as a hybrid approach that combines the advantages of solid state sensing and liquid reagent-based assays into one technique. A further advantage of BI is the fact that the bead column contains a large sensor area packed into a volume small enough to be viewed by many optical detection arrangements. As a result, the signal-to-noise ratio of many assays can be considerably improved by implementing them in a BI platform.

In its earliest phase, bead injection was mostly applied to inorganic analyses [10,11]. Later, the technique has been very successfully extended to bioligand interaction assays [12,13]. Its most recent applications have taken a step even further into the realm of biology by growing living cells on microcarrier beads and using BI to investigate cellular response to chemical stimulation [14]. A full account of bead injection and its applications can be found in a recent review [15].

1.5 Fluorescence microscopy

1.5.1 Fluorescence

Fluorescence refers to the ability of a molecule to absorb light in a certain wavelength region and subsequently re-emit light in a different (longer wavelength) region. The mechanism of fluorescence can be explained with the aid of the Jablonski diagram, i.e. a diagram showing a simplified view of the electronic and vibrational energy level structures of the fluorescent molecule (Figure 1-10). As shown in Figure 1-10, absorption of light is a fast process, occurring on a 10^{-15} s time scale. It promotes the molecule from its electronic ground state (S_0) to one of the vibrational levels of the excited electronic state (S_1). The molecule will not remain in the excited state but seeks to relax back to the ground state through one of several possible mechanisms. The mechanisms relevant to the present discussion are the following:

- In *non-radiative relaxation*, the energy released upon transition from S_1 to S_0 is transferred to neighboring molecules as heat. No light is given off in the UV-visible region.
- In *radiative relaxation*, the molecule first rapidly (10^{-11}-10^{-10} s) relaxes to the lowest vibrational level of S_1, followed by a slower (10^{-9}-10^{-7} s) transition from the bottom of S_1 to one of the vibrational levels of S_0. The latter transition leads to emission of a fluorescent photon.

Whether a molecule exhibits fluorescence will depend on the rate of the non-radiative relaxation relative to the radiative one: fluorescent species are those in which the latter is more rapid than or at least comparable to the former. The fluorescence emission spectrum will always be shifted to longer wavelengths compared to the absorption spectrum (see Figure 1-11). Part of the reason for the shift is the fact that vibrational relaxation is so fast that the molecule has practically always relaxed to the bottom of S_1 before the radiative transition from S_1 to S_0 occurs. The energy lost in vibrational re-

laxation will make the energy of the emitted photon less than the energy of the absorbed photon – hence a shift into longer wavelengths. Another contribution to the spectral shift arises from the difference in interaction energies between the ground state and the solvent, compared to the excited state and the solvent. However, a deeper discussion of the solute-solvent effects is beyond the scope of this chapter.

1.5.2 Fluorescence microscopy

When a microscope is used to study cells, it is common practice to use a dye to stain the part of the cell (e.g. an organelle) that is the object of the study. Staining creates a contrast between the object and the rest of the specimen, and thus facilitates visualization of the object. In fluorescence microscopy, a *fluorescent* dye is used to tag the area or component of interest. Because a fluorescent dye absorbs and emits light at different wavelengths, it is possible to isolate the emission from the illuminating light by using a special arrangement of optical filters. The resulting image has extremely high contrast since the fluorescence is viewed against a virtually black background.

Because of the need for efficient separation of the fluorescent signal from the intense illumination light, the optical train in a fluorescent microscope is different from that of a conventional light microscope. The most efficient design is the epi-illumination setup, which is shown in Figure 1-12. In epi-illumination, the microscope objective has a dual role: it is used both for focusing excitation light on and collecting light from the specimen. The dichroic mirror and the emission filter are used to selectively pick up the fluorescence emission from all the collected light (most of which is backscattered excitation light).

As a consequence of the high contrast of fluorescent images, very small quantities of the tag can be observed, resulting in superb image quality. The low limit of detection also guarantees a high dynamic range for the detected signal, enabling reliable extraction of quantitative information from the image/signal. These properties have made

fluorescence microscopy a powerful tool for several applications [16]: among the most usual applications are its use as a detection technique in immunofluorescent methods for visualization of cell and tissue components, as well as in fluorescence in situ hybridization (FISH) for quantitative localization and detection of specific DNA and RNA sequences. Recently, the discovery of the Green Fluorescent Protein has opened wide opportunities to use microscopy for extensive studies of protein trafficking and gene expression.

In all the above applications, fluorescence microscopy is used to detect the presence, location or distribution of an inactive fluorescent tag. Another, slightly different, area where the technique is used heavily is physiological and pharmacological studies of cells with the aid of fluorescent ion indicators and membrane potential indicators [17, 18]. These fluorescent dyes are actively responding to changes in ion concentrations or membrane potential by changing their fluorescence and, in that respect, are working analogously to traditional colorimetric ion indicators.

Just as for any other type of microscopy, the main use of fluorescence microscopy is in collecting images of the specimen. However, the technique can also be used for detecting the integrated intensity of sample fluorescence, without imaging. The instrumental difference between the two modes of operation is the choice of the detector: in the former case a CCD-camera, in the latter a photomultiplier tube or a photodiode. The light collection efficiency of a fluorescence microscope is determined by the *numerical aperture* (NA) and magnification (Mag) of the objective [19, 20]:

$$\textit{Light collection efficiency} \propto \left(\frac{NA}{Mag}\right)^2$$

Due to the excellent collection efficiency of high-NA objectives, microscopes equipped with them are powerful signal gathering devices for fluorescence detection.

Recently, the latter type of fluorescence microscope detection has been combined to a flow injection setup, creating the technique flow injection fluorescence microscopy (FIFM) [21]. FIFM has proven to be a powerful tool in cell response measurements due to the precise and reproducible stimulant delivery by means of flow injection, and the versatile and efficient signal collection by means of fluorescence microscopy.

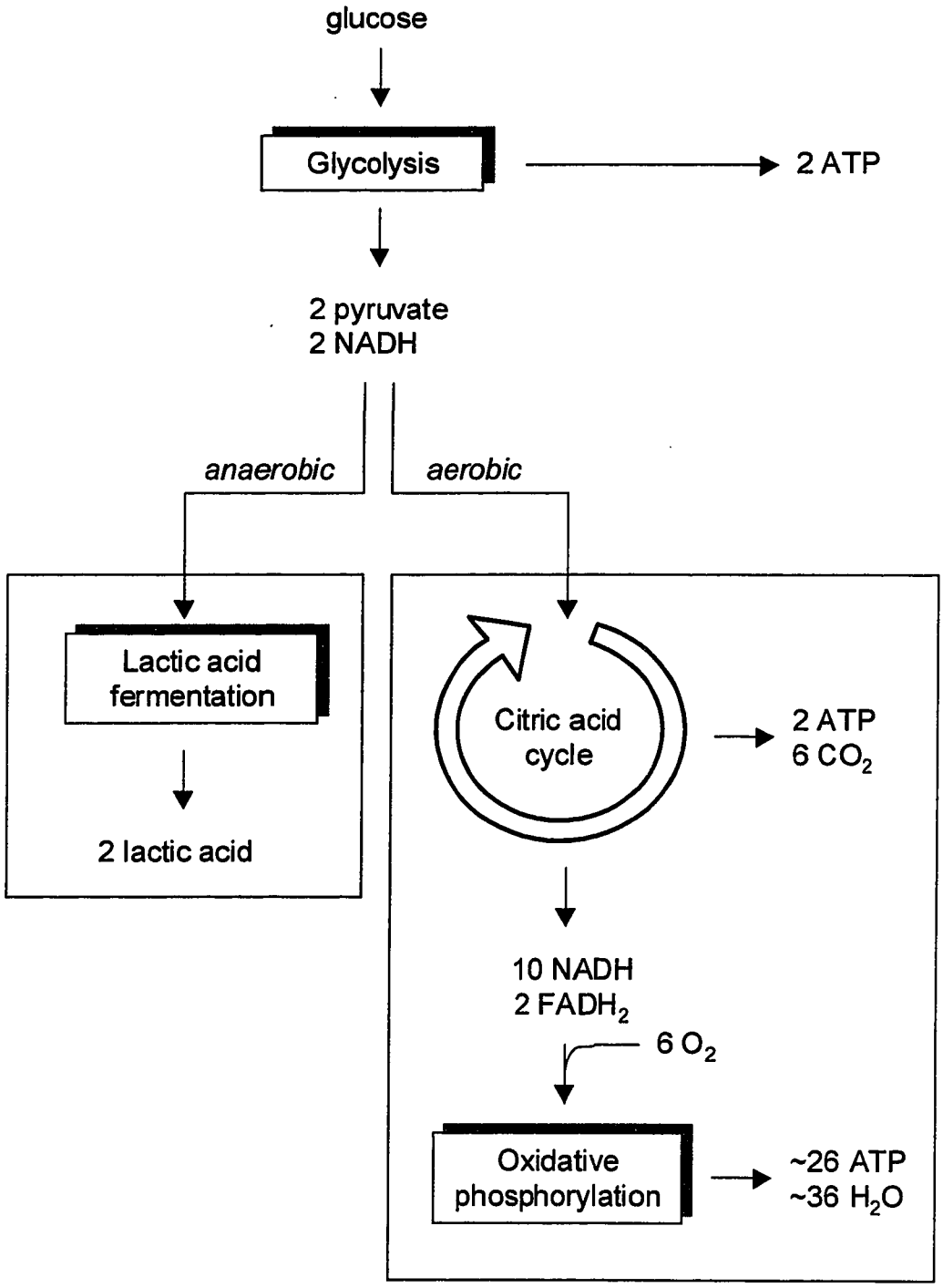

Figure 1-1 Metabolic processing of glucose for energy production.

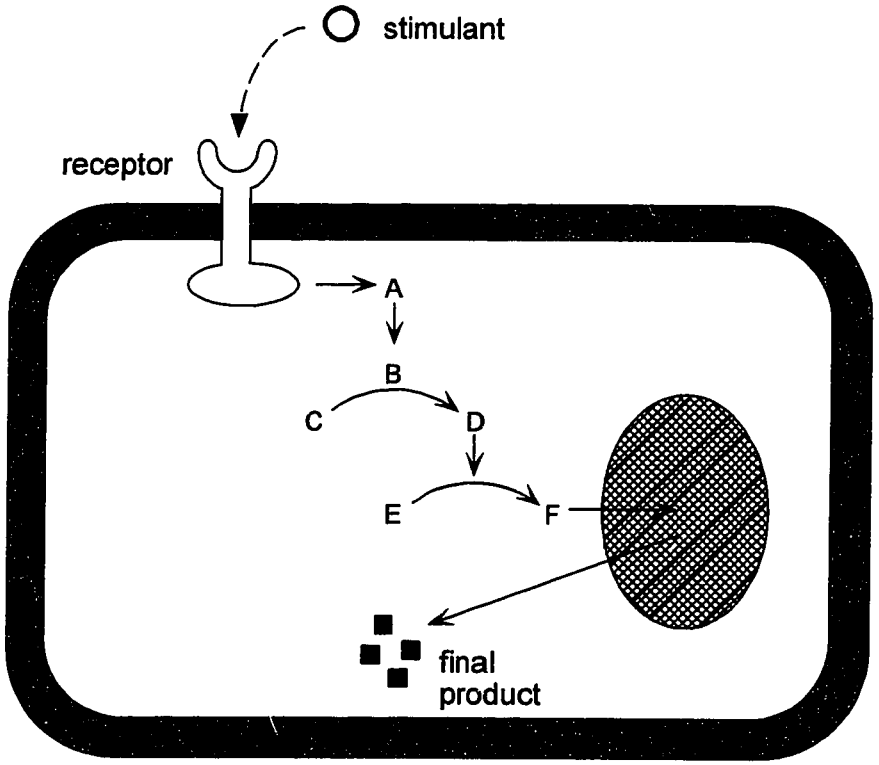

Figure 1-2 Cellular response induced by a stimulant binding to a receptor on the cell surface.

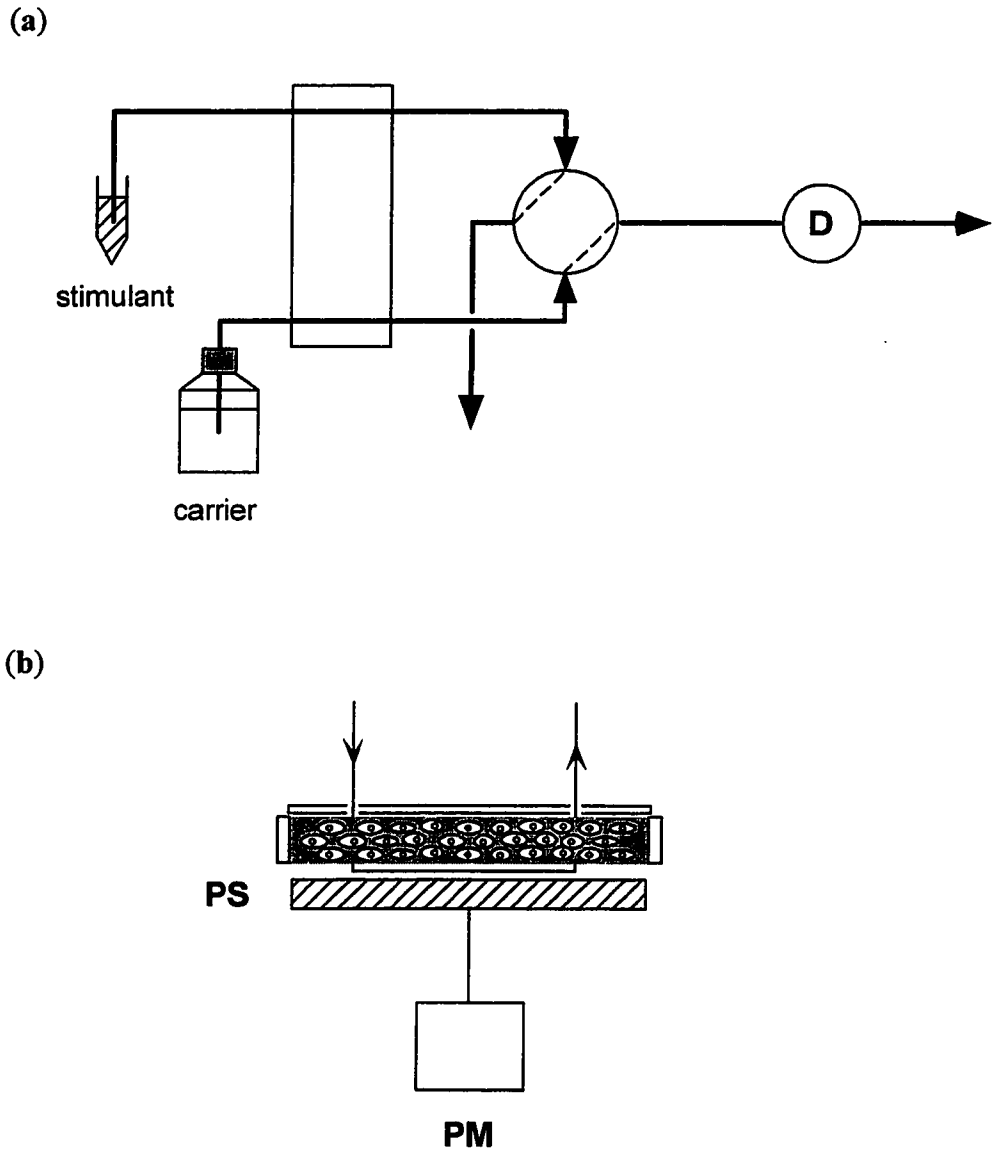

Figure 1-3 Cytosensor Microphysiometer. (**a**) The flow injection setup employed in the instrument. (**b**) The flow through chamber for detection of metabolic acidification. Cells are immobilized in an agarose matrix on top of the pH sensitive detector. **PS** – pH sensor, **PM** – potentiometer.

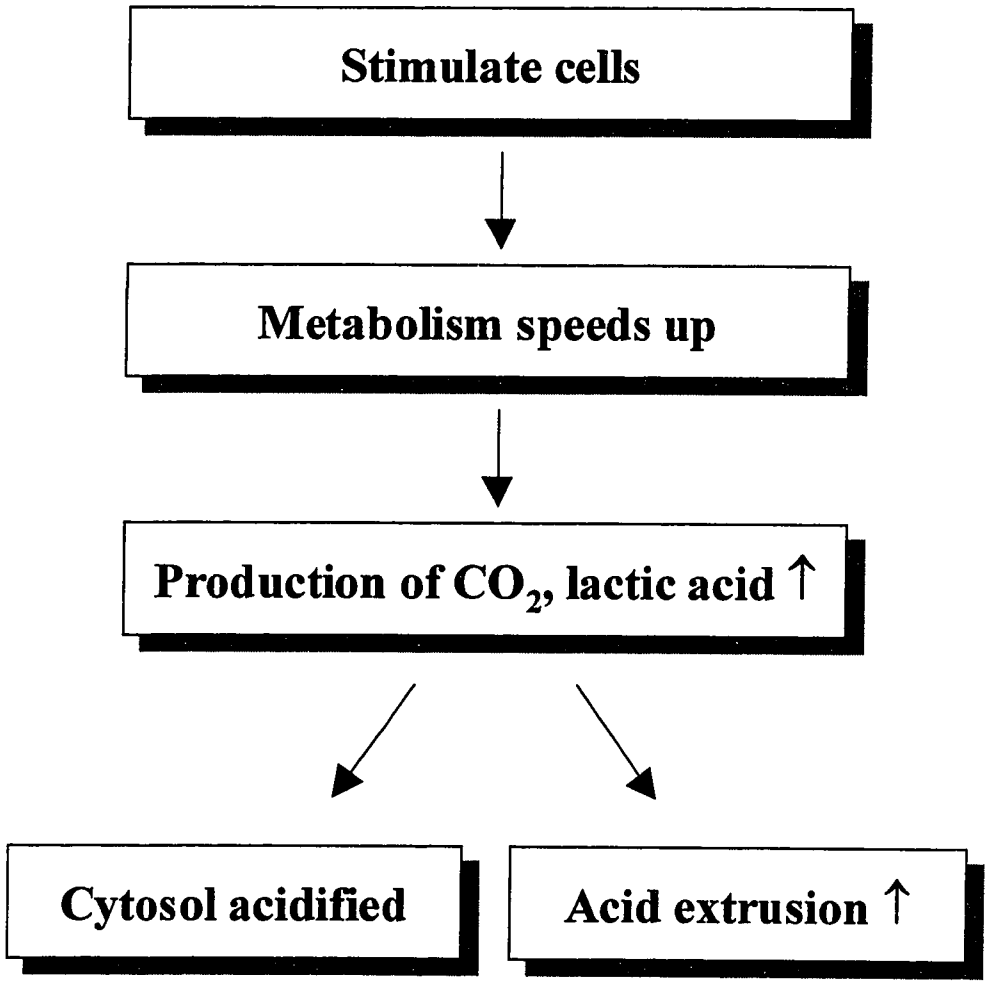

Figure 1-4 Relationship between cell stimulation, metabolic acid generation and the observable intra- and extracellular pH effects.

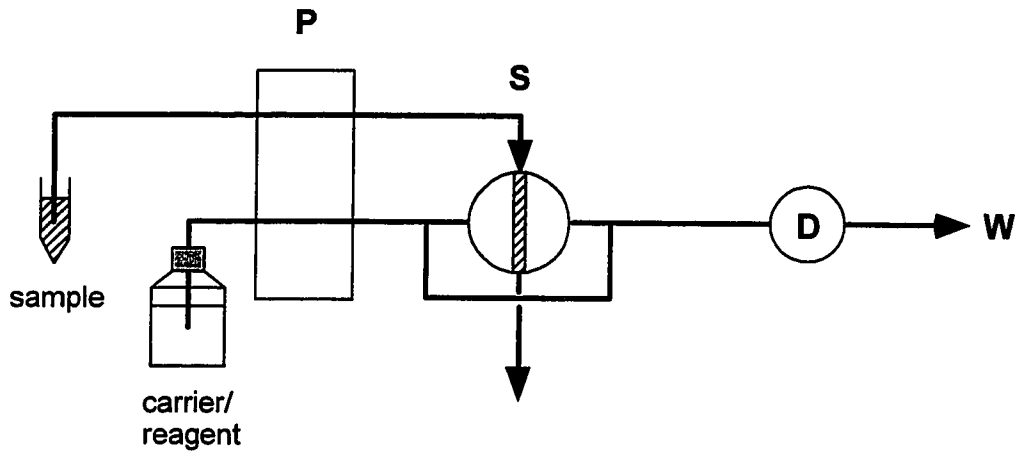

Figure 1-5 A basic FIA setup. **P** – pump, **S** – sample injection valve, **D** – detector, **W** – waste.

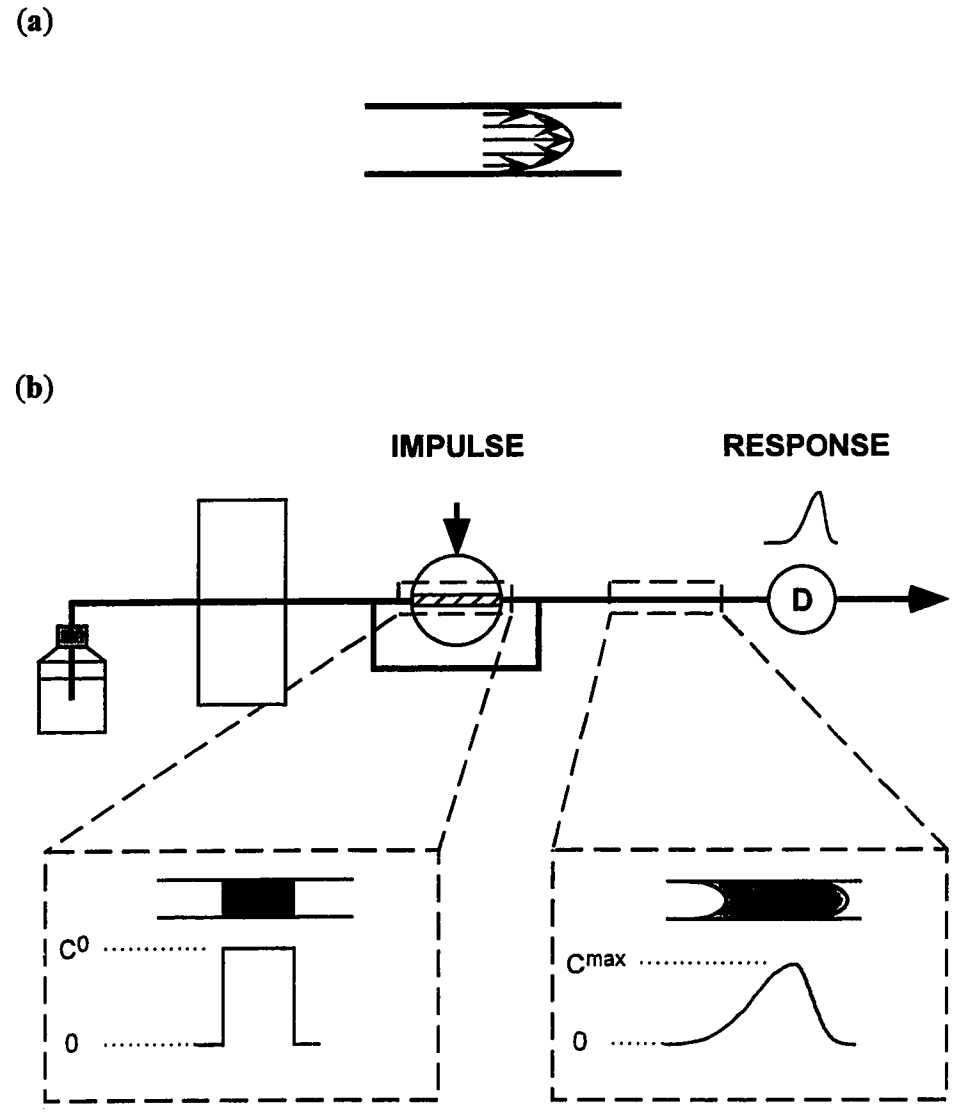

Figure 1-6 Dispersion in a flow injection system. (a) Parabolic flow profile in a tube under laminar flow conditions. (b) Dispersion-induced changes in the sample concentration profile: the originally square impulse is transformed into a stretched-out peak.

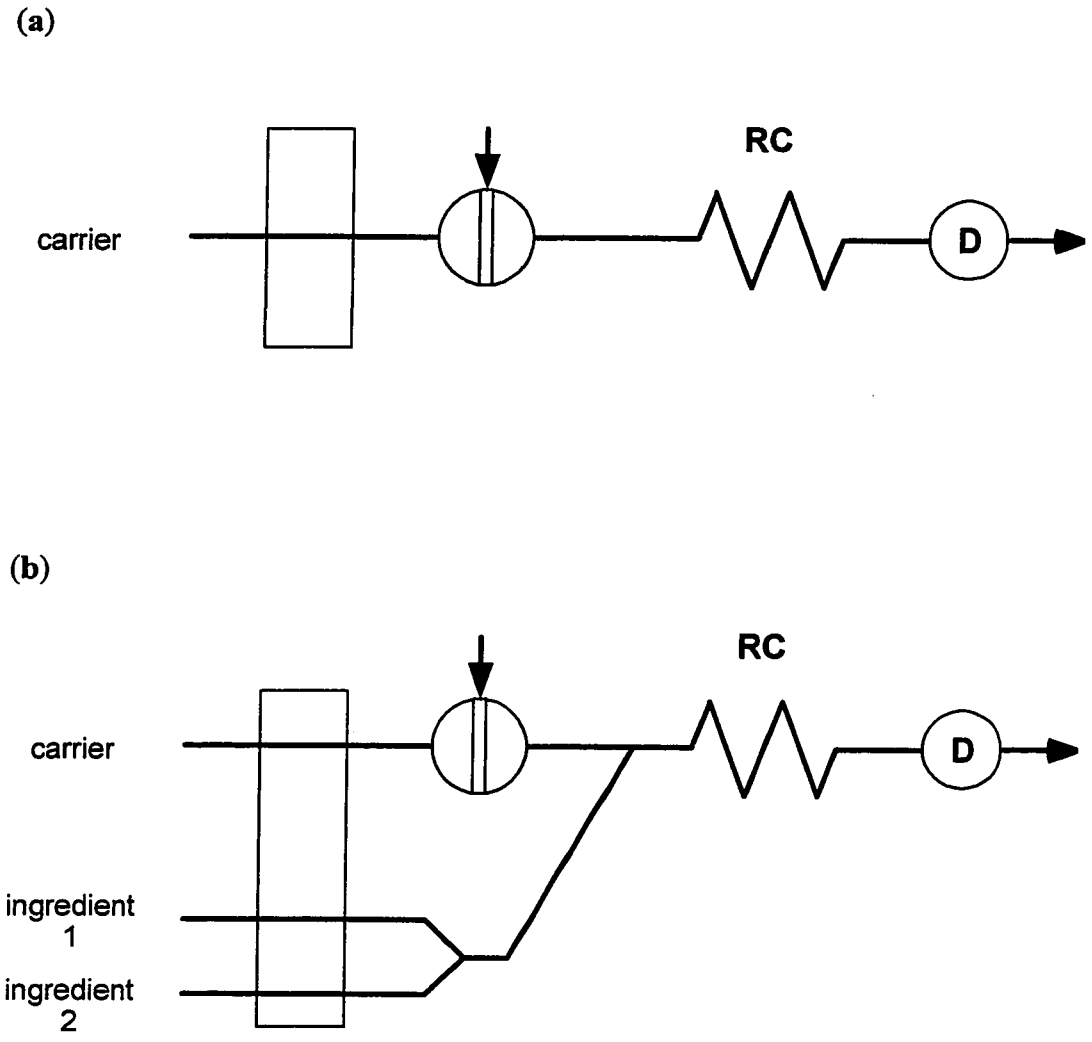

Figure 1-7 (a) A simple, single line FIA system. (b) A more complex variant featuring multiple flow lines. Two ingredients are mixed to form a labile reagent, which is immediately mixed on-line with the sample.

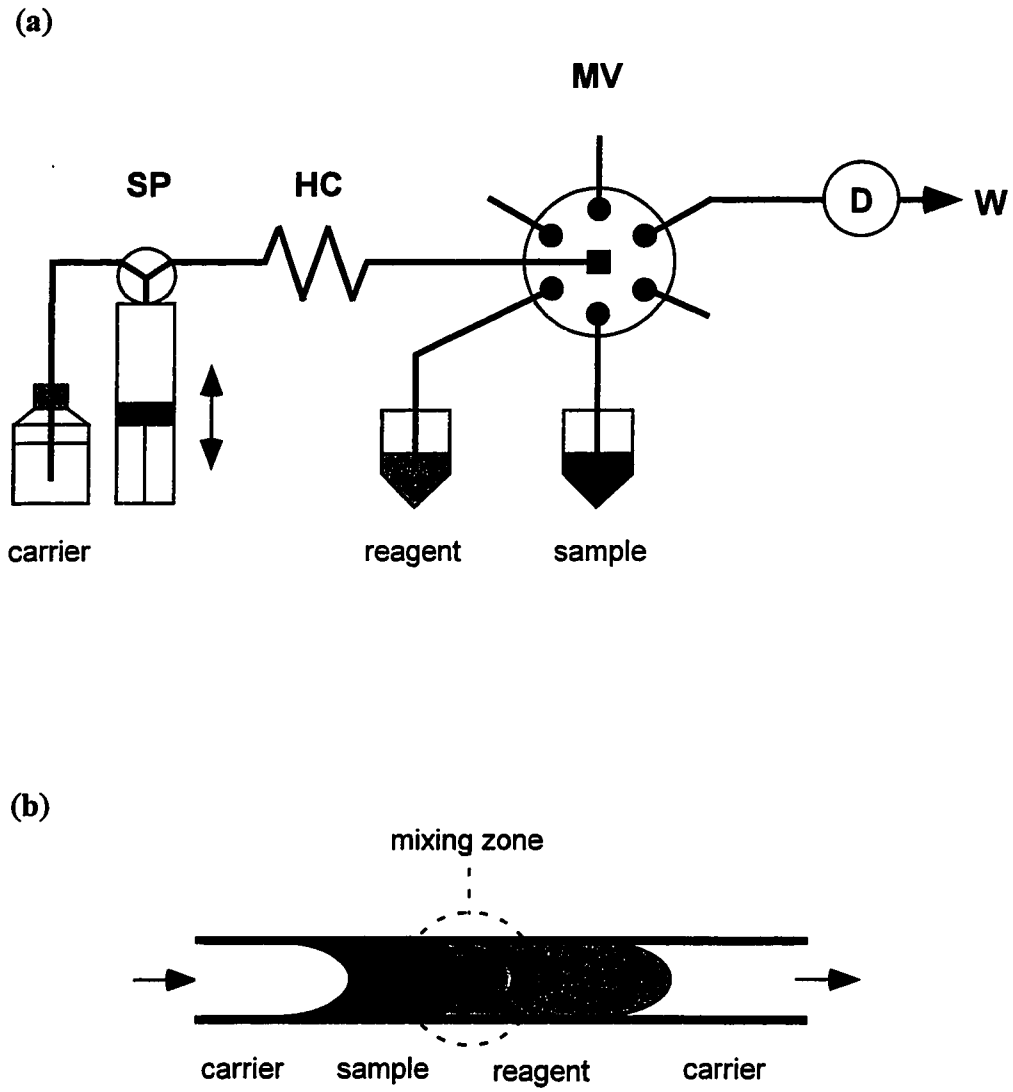

Figure 1-8 **(a)** Sequential injection setup. **(b)** Dispersion-mediated mixing of sample and reagent in SIA. **SP** – syringe pump, **HC** – holding coil, **MV** – multiport valve, **D** – detector, **W** – waste.

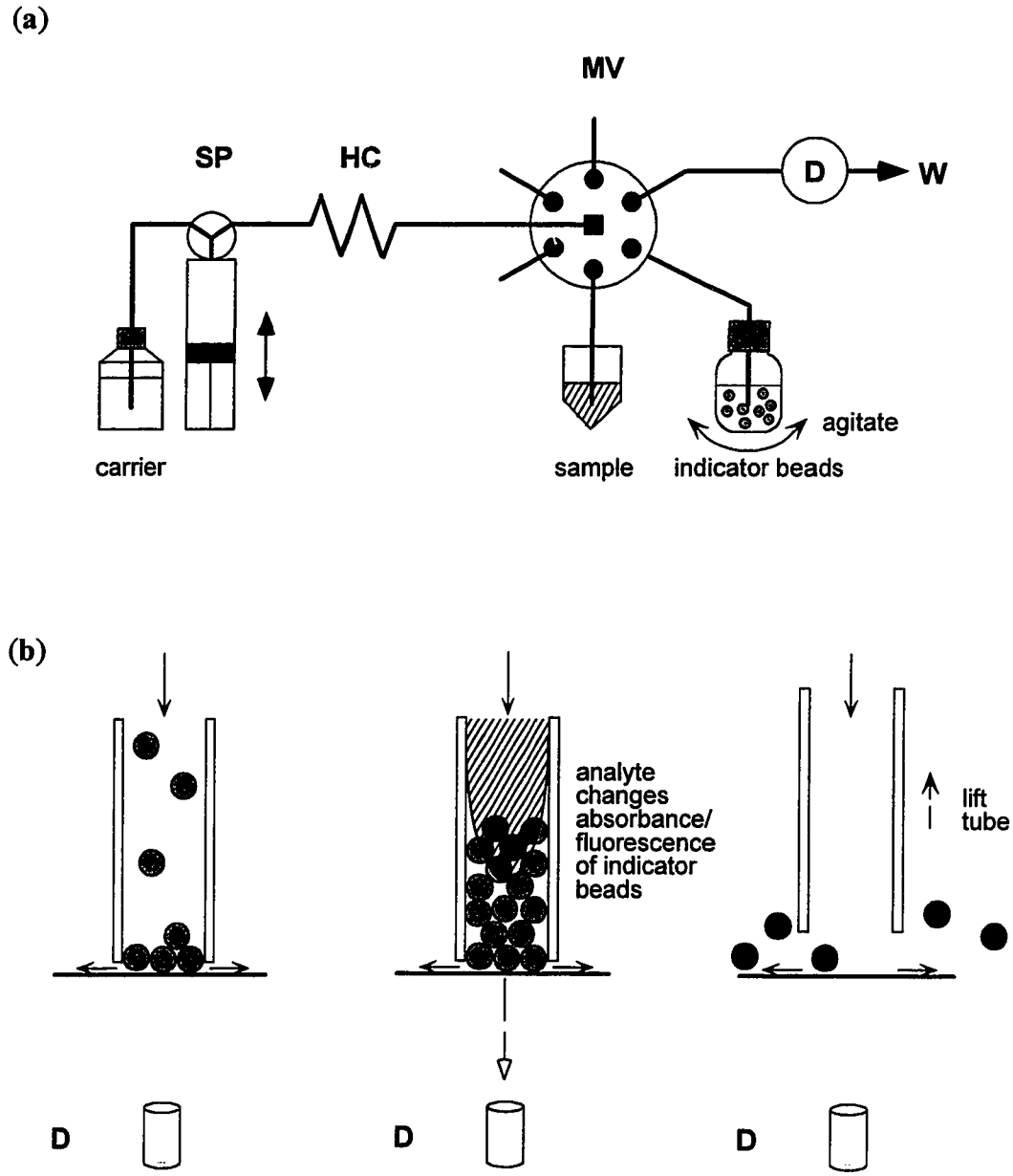

Figure 1-9 (a) Bead injection setup. (b) Operation of the jet ring flow-through cell (from left to right): bead loading, analysis, discarding spent beads. **D** - detector.

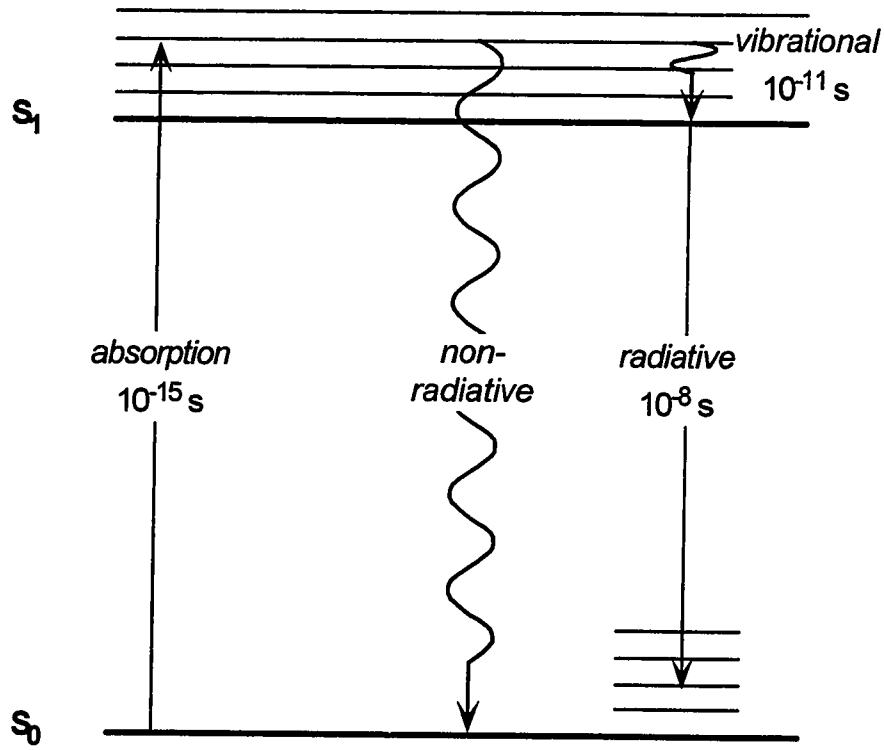

Figure 1-10 Jablonski diagram. S_0 – ground electronic state, S_1 – first excited electronic state.

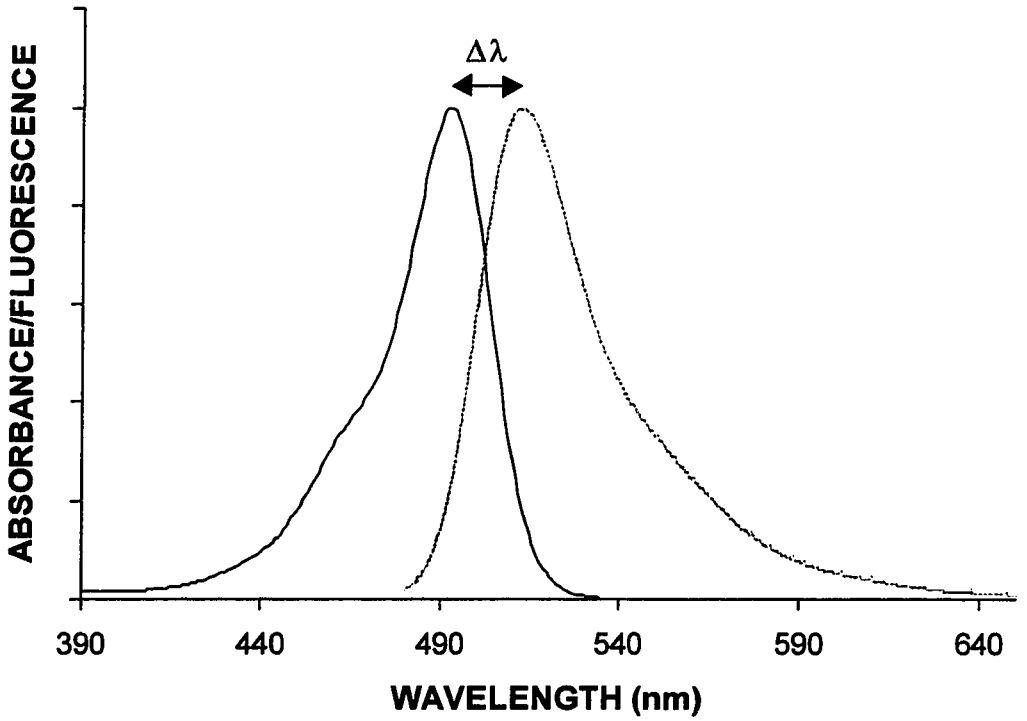

Figure 1-11 Absorption (black trace) and emission (grey trace) spectra of fluorescein, the most traditional and widely used fluorescent label. Δλ indicates the red shift of emission relative to absorption.

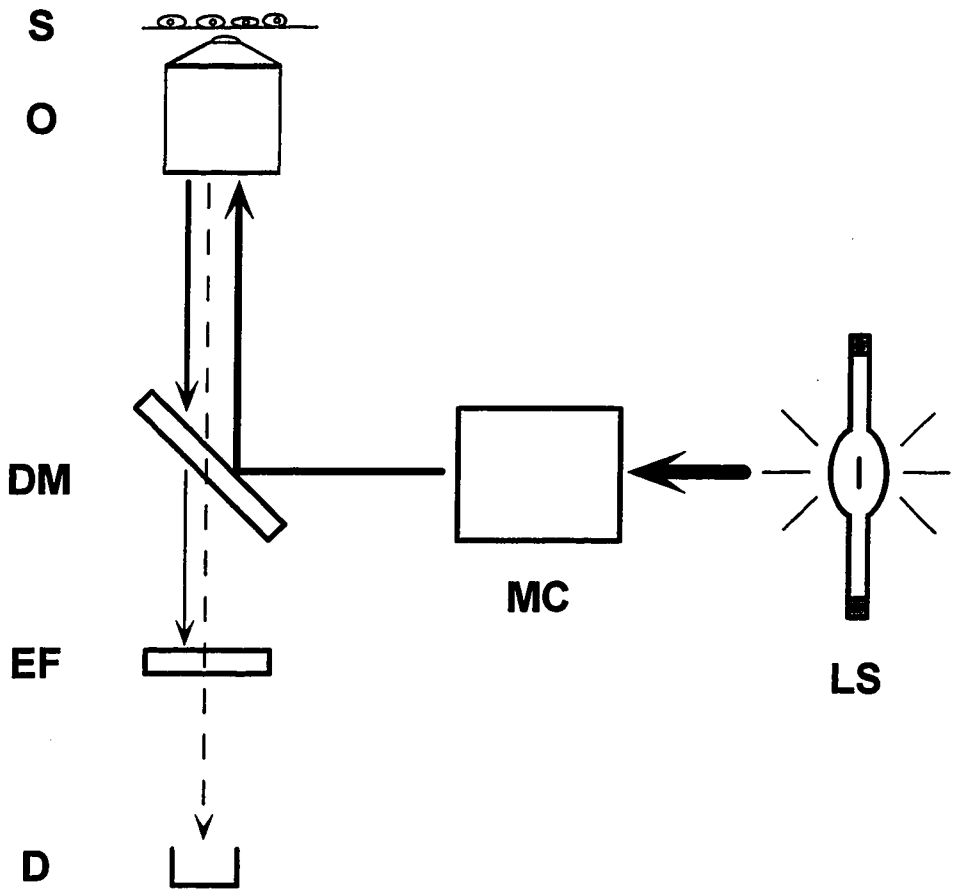

Figure 1-12 The components of an epifluorescence microscope. **LS** – light source, **MC** – monochromator, **DM** – dichroic mirror, **O** – objective, **S** – specimen, **EF** – emission filter, **D** – detector. The solid lines indicate excitation light, the dashed line indicates fluorescent emission light.

Notes to Chapter 1

[1] Garrett R.H., Grisham C.M. *Biochemistry*, Saunders College Publishing, Orlando, 1995, Chapter 17.

[2] Alberts B., Bray D., Lewis J., Raff M., Roberts K., Watson J.D. *Molecular Biology of the Cell*, Garland Publishing, New York, 3rd edn, 1994, Chapter 15.

[3] McConnell H.M., Owicki J.C., Parce J.W., Miller D.L., Baxter G.T., Wada H.G., Pitchford S. *Science,* **1992**, *257*, 1906-1912.

[4] Tallarida R.J., Jacob L.S. *The dose-response relation in pharmacology*, Springer Verlag, New York, 1979, Chapter 3.

[5] Kenakin, T. *Pharmacologic analysis of drug-receptor interaction*, Lippincott-Raven, Philadelphia, 1997, Chapters 1 and 5.

[6] Ruzicka J., Hansen E.H. *Anal. Chim. Acta*, **1975**, *78*, 145-157.

[7] Ruzicka J., Hansen E.H. *Flow injection analysis*, Wiley, New York, 1988.

[8] Ruzicka J., Marshall G.D. *Anal. Chim. Acta* **1990**, *237*, 329-343.

[9] Ruzicka J., Gübeli T. *Anal. Chem.* **1991**, *63*, 1680-1685.

[10] Egorov O., Ruzicka J. *Analyst* **1995**, *120*, 1959-1962.

[11] Holman D.A., Christian G.D., Ruzicka J. *Anal. Chem.* **1997**, *69*, 1763-1765.

[12] Ruzicka J., Ivaska A. *Anal. Chem.* **1997**, *69*, 5024-5030.

[13] Ruzicka J. *Analyst* **1998**, *123*, 1617-1623.

[14] Hodder P.S., Ruzicka J. *Anal. Chem.* **1999**, *71*, 1160-1166.

[15] Ruzicka J., Scampavia L.D. *Anal. Chem.*, **1999**, *71*, 257A-263A.

[16] Herman, B. *Fluorescence microscopy*, Springer, New York, 1998, Chapter 4.

[17] Herman, B. *Fluorescence microscopy*, Springer, New York, 1998, Chapter 6.

[18] Haugland, R.P. *Handbook of fluorescent probes and research chemicals*, 6th ed., Molecular Probes, Eugene, OR, 1996.

[19] Herman, B. *Fluorescence microscopy*, Springer, New York, 1998, Chapter 2.

[20] Inoué, S. *Video Microscopy*, Plenum Press, New York, 1986, Chapter 5.

[21] Ruzicka J., Baxter P.J., Thastrup O., Scudder K. *Analyst*, **1996**, *121*, 945-950.

Chapter 2 Comparison of response parameters measured by FIFM

2.1 Background

2.1.1 Cellular response parameters

As described in section 1.3.2, cellular responses can be followed by monitoring levels of second messenger molecules. Of all the different second messengers, intracellular Ca^{2+} is a particularly good target for monitoring since it is a very common messenger and reliable, easy-to-use fluorescent methods have been developed for measuring it. It is further stated in section 1.3.2 that an alternative approach to monitoring cellular responses is measuring the pH changes caused by altered turnover rates of the energy metabolism. Since intracellular pH can be measured conveniently by fluorescence microscopy, it is a suitable parameter to follow together with $[Ca^{2+}]_i$.

In order not to oversimplify the roles of pH_i and $[Ca^{2+}]_i$, it should be stressed that pH changes are not necessarily just a consequence of altered metabolism. Changes in pH can be an integral part of the response cascade [1,2], and in cases like this the role of pH is roughly analogous to that of Ca^{2+} as a second messenger. In fact, it has been observed that changes in pH are sometimes accompanied by changes in $[Ca^{2+}]$. Clarification of such interrelation is one reason why it is important to be able to monitor both parameters. Finally, cytosolic pH is a crucial physiological parameter and any observed changes are of interest in themselves, not just as a manifestation of the stimulation event.

Studying the cellular response through several parameters gives considerably more information about the response process than one-parameter studies do. Fluorescent probes are well-suited for multiparametric studies due to their molecular scale size and

mildly invasive or nearly non-invasive nature (depending on the probe type). Still, designing multiparameter measurements is not necessarily a simple task if exact quantitation of all parameters is desired. This has been shown by Martínez-Zaguilán *et al.* [3,4] who carried out extensive studies on different aspects of simultaneous intracellular pH and Ca^{2+} measurements, including interaction of fluorescent pH and Ca^{2+} probes. Interestingly enough, their results also showed that the fluorescence characteristics of most Ca^{2+} indicators are pH dependent, meaning that exact Ca^{2+} quantitation *requires* accompanying pH measurements.

Considering the utility of $[Ca^{2+}]_i$ and pH_i as cell response parameters, their possible interdependence and the ease of monitoring both of them by fluorescence microscopy, it is easy to see that they make an excellent combination for multiparametric measurements. Indeed, this approach has been used for studies of cell physiology [5-7].

2.1.2 Fluorescent measurement of intracellular pH

Fluorescent pH indicators are weak acids or bases that exhibit different spectral properties in protonated (HIn) and deprotonated (In^-) form. Since the ratio $[HIn]/[In^-]$ changes with pH according to

$$\frac{[In^-]}{[HIn]} = 10^{pH-pK_a}$$

the observed spectral properties of an indicator solution will also change in a pH dependent manner. At $pH << pK_a$, the [HIn] form is dominant and the observed fluorescence resembles that of HIn. At $pH >> pK_a$, the $[In^-]$ form is dominant and the observed fluorescence resembles that of In^-. The intervening region, $pK_a-1 < pH < pK_a+1$, shows a gradual transition between the two extremes, and it is in this region that the indicator has the greatest pH-sensitivity.

One can distinguish three fundamental ways in which the fluorescence spectrum can change with pH:

1) One of the forms (HIn or In^-) is strongly fluorescent, the other is poorly fluorescent on non-fluorescent (i.e. pH induces a change in overall spectral intensity).
2) Both forms are fluorescent, but they absorb at different wavelengths (i.e. pH induces a spectral shift in the excitation spectrum).
3) Both forms are fluorescent, but they emit at different wavelengths (i.e. pH induces a spectral shift in the emission spectrum).

It should be pointed out, however, that this division cannot be rigorously used for classification of the indicators, since many of them exhibit at least two of the above types of behavior.

In discussing the fluorescent properties of the indicators, one detail is particularly worth mentioning: some indicators exhibit an *isosbestic point*, i.e. a wavelength where the HIn and In^- forms show equal excitation (isoexcitation) or emission (isoemission) properties. The existence of an isosbestic point allows one to conduct the measurements in the *ratiometric mode*, where fluorescence is monitored at two different wavelengths on the opposite sides of the isosbestic point. Subsequently, the ratio of the recorded intensities is calculated as $R(t_i)=F_{\lambda 1}/F_{\lambda 2}$. This has the advantage that R will still be pH-dependent, but relatively insensitive to artifacts such as dye leaching and photobleaching [8,9] that often deteriorate the quality of fluorescent signals.

The most popular fluorescent indicator for intracellular pH measurements is 2',7'-bis-(2-carboxyethyl)-5-(and-6)-carboxyfluorescein (BCECF, Figure 2-1a). It has several desirable properties, including a high extinction coefficient and quantum yield, a suitable pK_a for physiological pH measurements and an isosbestic point in the excitation spectrum (Figure 2-1b). Its most marked downside is the weakness of the isosbestic behavior. BCECF can be conveniently loaded into cells as the acetoxymethyl ester derivative. The ester derivative is uncharged and can readily pass the lipophilic cell mem-

brane. Once the dye molecules enter the cell the ester bonds are cleaved by intracellular esterases, converting the dye into charged form and thus rendering it membrane impermeable. As a result, the cells become stained with the fluorescent indicator for a time long enough to carry out the measurements. Reviews of BCECF and other fluorescent pH indicators are provided in refs. [9, 10].

2.1.3 Utility of tracer curves in cell response measurements

Flow injection fluorescence microscopy (FIFM, see section 1.5.2) was first applied to cell stimulation measurements by Baxter *et al.* [11] who studied Ca^{2+} release in Baby Hamster Kidney cells as a result of carbachol stimulation. One of the main conclusions from their work was the importance of tracer curves in elucidating the kinetic relationship between stimulant exposure and observation of response from the cells. A tracer curve, in this case, is an injection of a fluorescent tracer chemical in place of the stimulant. The fluorescent chemical is delivered onto cells exactly as the stimulant would be and therefore the fluorescent signal from the tracer yields the precise stimulant exposure profile.

2.2 Experimental

2.2.1 Cells and reagents

Chinese Hamster Ovary cells transfected with the rat m1 muscarinic receptor (CHO M1 cells) were chosen as a target for the two-parametric stimulus-response studies. Carbachol, a stimulant binding specifically to the muscarinic receptors, was chosen to stimulate the cells. This should make a good model system since carbachol has been shown to trigger both [Ca^{2+}] and acid extrusion responses in CHO M1 cells [12].

The cell line was maintained in Ham's F-12 medium, supplemented with 10% fetal bovine serum and 50 μg/ml G418. The working buffer used in cell preparation and in the

measurements was a phosphate buffered balanced salt solution (0.3 mM $CaCl_2$, 0.6 mM $MgCl_2$, 0.5 mM KH_2PO_4, 0.5 mM Na_2HPO_4, 3 mM KCl, 0.13 M NaCl) with 1 g/l bovine serum albumin and 10 mM glucose, adjusted to pH 7.4.

One to three days prior to the experiments, cells from a culture dish were transferred to LabTek coverglass bottom chambers (LabTek, Naperville, IL). The cells were prepared for the experiments by first rinsing them with the working buffer and then incubating them 0.5 h in a solution of 2 μM BCECF-AM and 1 μM fura-2-AM (Molecular Probes, OR, USA) at 37 °C. BCECF and fura-2 are fluorescent pH- and Ca-sensitive indicators, respectively, and AM stands for acetoxy methyl ester derivative. The ester derivatives are uncharged and can readily pass the lipophilic cell membrane. Once the dye molecules enter the cell the ester bonds are cleaved by intracellular esterases, converting the dyes into charged form and thus rendering them membrane impermeable. As a result, the cells become stained with the ion-sensitive fluorescent dyes for a time long enough to carry out the measurements. BCECF-AM was stored as 2 mM and fura-2-AM as 1 mM solution in DMSO at -20 °C.

2.2.2 Instrumentation

The work was carried out using a FIAlab-3000 sequential injection system with the inverted radial flow chamber (Figure 2-2, ref. [11]) detector configuration. The sequential injection apparatus was used to deliver a 500 μL dose of carbachol or a tracer chemical onto the cells and the resulting changes in intracellular pH or [Ca^{2+}] were recorded by the fluorescent microscope. Since fura-2 and BCECF have very different spectra, different excitation wavelengths and filter sets had to be used in Ca^{2+} and pH measurements. Ca^{2+} measurements were performed with the excitation channels set at 340 and 380 nm, with a 415 nm dichroic beamsplitter and a 510/40 nm emission filter. pH measurements were performed with the excitation channels at 428.5 and 490 nm, with a 505 nm dichroic and a 545/40 nm emission filter.

The stimulation protocol consisted of aspirating working buffer followed by 500 µL of 13 µM carbachol, then delivering the carbachol onto the cells, stopping it on the cells for 3 min and rinsing it out. The protocol was concluded by an additional buffer aspiration and rinse. A graphical representation of the events is included in the figures. A flow rate of 50 µL/s was used for both stimulant delivery and rinsing. The 13 µM carbachol concentration was chosen to yield a concentration of 10 µM after dispersion in the sequential injection tubing. A recovery time of approximately 30 min was allowed between subsequent carbachol stimulations - a procedure that has been shown to minimize desensitization of the m1 receptors [12].

2.2.3 Data processing

The obtained raw data was processed by calculating, for each point of time, the ratio between emission detected after excitation from channel 1 and emission detected after excitation from channel 2, $R(t_i)=F_{\lambda 1}(t_i)/F_{\lambda 2}(t_i)$.

In the case of pH measurements, the ratiometric data was further converted to pH units after calibrating the fluorescence ratio and pH by a procedure described in [13]. Briefly, the fluorescence intensities were recorded with the cells immersed in pH 6.8, 7.2, 7.6 and 8.0 standard solutions, in the presence of 120 mM K^+ and 10 µM nigericin. In these conditions the intracellular pH will be equal to the extracellular pH and thus pH and fluorescence ratio can easily be related. The calibration was carried out manually by pipetting the various pH standards into the LabTek chamber. For each standard, the intracellular pH was allowed to equilibrate 4-5 min before recording the fluorescence intensities.

The calibration equation could be constructed simply by linear regression of pH vs. fluorescence ratio. For best results, however, a more complicated equation should be used for relating the ratiometric signal to the quantity of interest [8]. In the case of pH measurements, that equation is [14]:

$$pH = pK_a + \log\left[\frac{R - R_A}{R_B - R}\right] \times \frac{F_{A(\lambda 2)}}{F_{B(\lambda 2)}}$$

where $F_{\lambda i}$ is fluorescence emission intensity from excitation at λ_i and R is the fluorescence ratio as described above. The subscripts A and B represent the limiting values, obtained at pH values where all of the indicator dye is in the acidic (protonated) or basic (deprotonated) form, respectively. For BCECF, an indicator with $pK_a \approx 7$, the limiting values can be obtained by recording fluorescence intensities at pH 4 and pH 10.

2.3 Results

2.3.1 Development of functional tracers

Some concerns have been voiced about the reliability of tracer curves in cell response measurements by FIFM [15]: it has been suggested that although a tracer curve reports the delivered concentration profile in the bulk solution, there might be a more or less stagnant diffusion layer right next to cell surfaces where the concentration changes in a different way than it does in the bulk.

To address these concerns, a concept of functional tracer curve was devised based on injecting a bolus of a weak acid (NH_4Cl) on cells and monitoring the intracellular pH. The idea was borrowed from physiological cell pH measurements where injections of a weak acid or a weak base are routinely used to create an artificial alkali or acid load in the cell [16]. As the injected plug of NH_4Cl comes in contact with the cells, the lipophilic cell membrane will repel the charged NH_4^+ ions whereas the neutral NH_3 molecules (roughly 1% of the total concentration at pH 7.4) can easily permeate it. As a consequence, the intracellular space receives an injection of NH_3, which makes the in-

tracellular fluid more alkaline. The alkalization is detected as a change in the fluorescence intensity of the pH indicator. Since a signal can only be observed once NH_3 has been "extracted" into the cell, the time-dependence of the functional tracer must include diffusion through the assumed stagnant surface layer, as well as diffusion through the cell membrane.

Comparison of a regular fluorescein tracer curve and an NH_4Cl functional tracer curve in Figure 2-3 reveals that there is no noticeable time difference between their leading edges. Based on this observation, it can be concluded that the concentrations in the bulk solution and the solution-cell membrane interfaces are the same at all times and that a regular tracer curve gives flawless information about the stimulant exposure profile.

Another functional tracer curve was developed to characterize the rates of cross-membrane transport processes and the pathways of energy metabolism. Prior to recording the curve, the cells were perfused with glucose-deficient buffer. This slows down their metabolism and considerably reduces metabolic acid production. When a plug of normal glucose containing buffer is then injected on the cells, acid production should increase as a result of the more intense metabolic activity. The ensuing decrease in intracellular pH will be detected as a change in the fluorescence intensity of the pH indicator. When the glucose containing plug is removed, an opposite change should be seen. The method was adopted to sequential injection from microphysiometry [3] where glucose starving is routinely used as a kind of instrument calibration procedure.

The results are shown in Figure 2-4. Comparison of the regular tracer curve and the functional tracer now shows clear kinetic differences: the onset of the functional tracer is lagging slightly behind the regular tracer. Also, the leading edge of the functional tracer develops more sluggishly than that of the regular tracer. One reason for these differences is that in contrast to ammonia, glucose does not enter cells by diffusion through the cell membrane but by the action of carrier proteins located on the membrane [17]. Another reason is that in order to see a change in cytosolic pH, glucose not

only needs to enter the cell but also go through glycolysis to produce lactic acid. Consequently, the observed kinetic differences give an idea about the rates of these two processes. Since glucose intake and lactic acid/CO_2 production is a common feature in all animal cells, this experiment can be used as a universal tracer curve for metabolic responses.

2.3.2 Comparison of pH_i and $[Ca^{2+}]_i$ responses

The latter part of this work involved repetitive stimulation of the CHO M1 cells with carbachol and alternate observation of the response in terms of intracellular pH and $[Ca^{2+}]$ changes.

Figure 2-5 shows pH and Ca^{2+} responses to stimulation with 10 μM carbachol, as well as the stimulant exposure profile. It can be seen that the kinetics of the two responses are clearly different. Once past the delay, intracellular $[Ca^{2+}]$ rises very rapidly, reaching a maximum within 5-10 s. The pH response on the other hand takes considerably longer - around 65-80 s - to peak. The observed behavior could be explained by looking at the mechanisms behind the responses: Ca^{2+} release is the result of a single, well defined step in the signal transduction pathway. It can occur easily and fast since the release only requires opening the Ca^{2+} channels in the endoplasmic reticulum membrane. The pH response is different: first of all, at least part of the observed acidification is a metabolic consequence of several events in the signal transduction pathway. Contributions from several such temporally distinct events could be thought to broaden the pH response. Secondly, an increase in metabolic acid production is ultimately brought about by accelerating complex processes, i.e. glycolysis and respiration. It is clear that such heavily regulated pathways cannot be stepped up instantaneously but their acceleration - and consequently the intracellular pH change - must be gradual. Finally, there are separate control mechanisms for restoring $[Ca^{2+}]$ and pH back to their resting levels. The different control mechanisms also contribute to differences in the observed Ca^{2+} and pH responses.

2.4 Conclusions

As a continuation of prior work [11], it has been shown that FIFM is a useful tool for multiparametric monitoring of cellular responses. The ability to remove the stimulant allows repetitive stimulation of the same group of cells. Further, owing to the excellent reproducibility and exact knowledge of the stimulant exposure, data from different experiments can be reliably compared. This makes it possible to carry out multiparametric measurements by alternating the monitored parameter in subsequent experiments, rather than modifying the instrument hardware to allow simultaneous monitoring of several parameters in one experiment. Of course, it should be pointed out that carrying out the measurements in a sequential fashion on the same group of cells has the disadvantage that several runs are needed to obtain the data. This takes more time and makes the latter runs susceptible to receptor desensitization effects.

The role of Ca^{2+} as a messenger in many intracellular response processes is well-known [2] but there are also many response pathways that do not involve Ca^{2+} at all. In contrast, Microphysiometer measurements have proved acid extrusion to be a general phenomenon linked to cellular stimulation. The universality makes pH measurements the more widely applicable method for detection of cellular stimulation. The downside of the universality is that pH measurements give little information about the type of signal transduction pathway and thus are not so well-suited for elucidating transduction mechanisms for newly discovered stimulants. Further, in cases where one stimulant triggers several distinct intracellular cascades, pH measurements can only tell the compound effect although it is usually just one of the cascades that is of interest in a given situation.

pH changes are the result of the events in the whole signaling cascade and changes in important metabolic cycles, whereas Ca^{2+} release is normally a single, relatively early

step or one of the middle steps in a signaling cascade. Therefore, pH monitoring probably gives more reliable information about the completion of the entire signaling cascade, as well as about the overall physiological condition of the cells. On the other hand, whenever just the stimulant-receptor binding is studied, Ca^{2+} release should be a more reliable indicator since it is dependent on much fewer factors than the pH response. Viewed from a purely instrumental angle, Ca^{2+} measurements have the advantage that stimulation usually changes $[Ca^{2+}]_i$ by at least an order of magnitude whereas pH changes typically remain within $\pm$ 0.1 pH units from the resting pH. This translates into better signal-to-noise ratio in Ca^{2+} measurements.

The discussion can be summarized by stating that both methods - pH and Ca^{2+} monitoring - have their merits and weaknesses, and the method of choice depends on what aspect of the cellular response one wants to study. Clearly, the most complete picture is obtained by using both approaches.

(a)

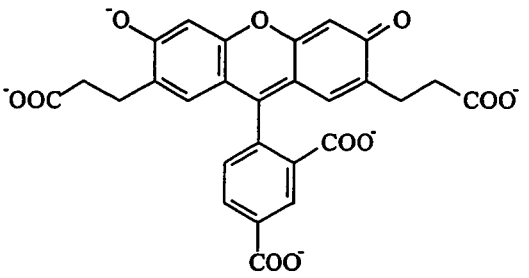

(b)

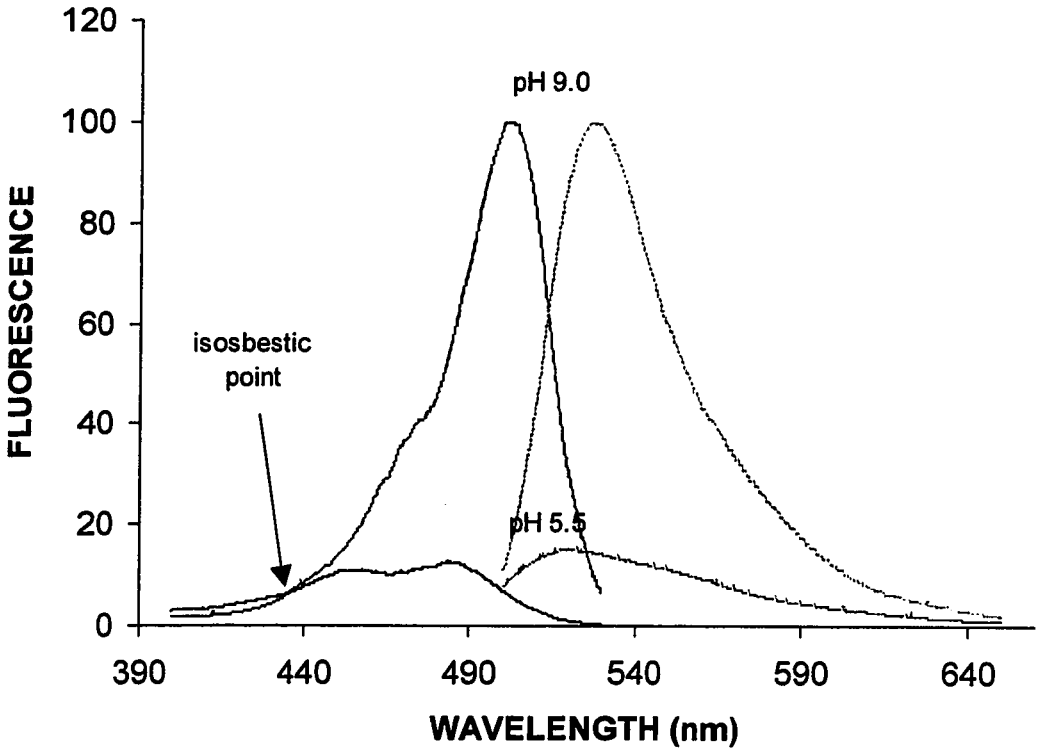

Figure 2-1 (a) Molecular structure of BCECF. (b) Excitation (black trace) and emission (grey trace) spectra of BCECF.

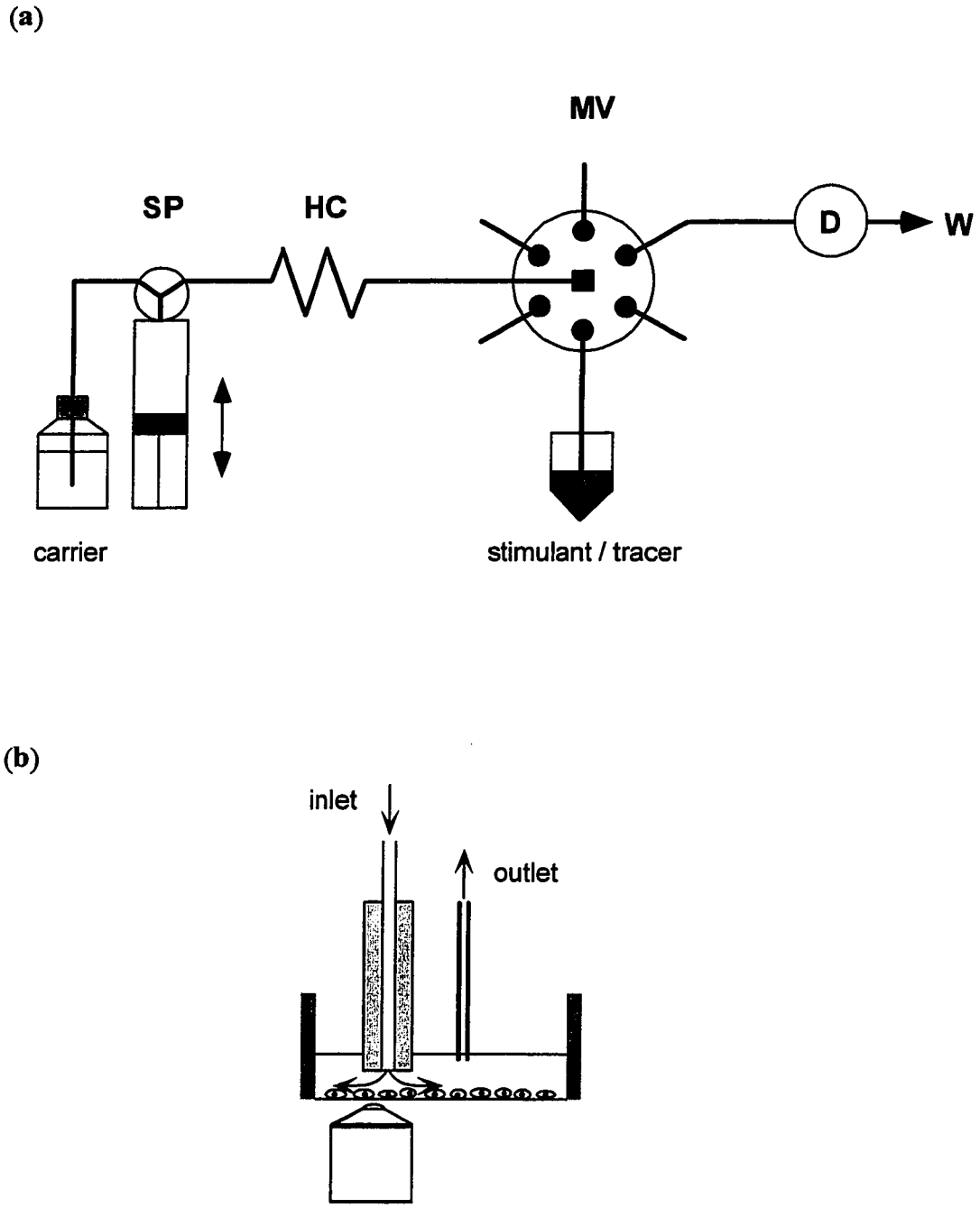

Figure 2-2 (a) Sequential injection setup used in the experiments. (b) An expanded view of the inverted radial flow chamber.

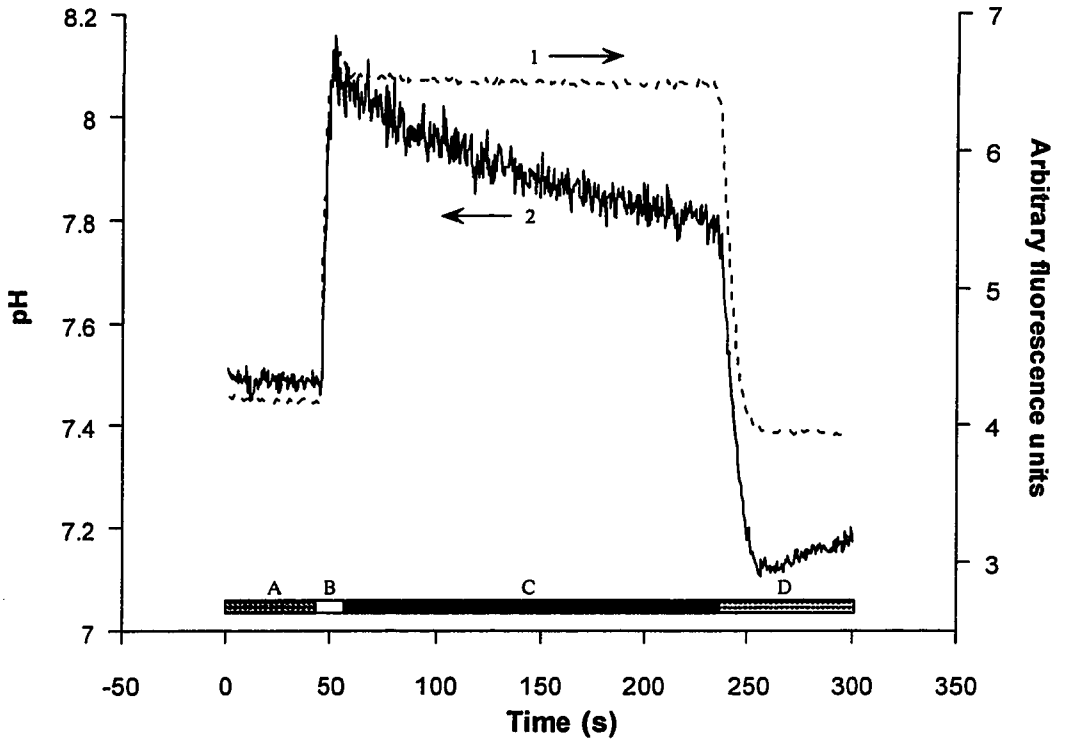

Figure 2-3 Tracer curve 1: injection of 50 µg/l fluorescein. Functional tracer curve 2: injection of 10 mM $(NH_4)_2SO_4$, monitoring internal pH. Events in injection protocol: A - aspirate buffer and tracer into the flow injection manifold; B - deliver tracer onto cells; C - stop tracer on cells for 3 min; D - flush out tracer with buffer. Cells are grown as a monolayer on a LabTek microscope chamber.

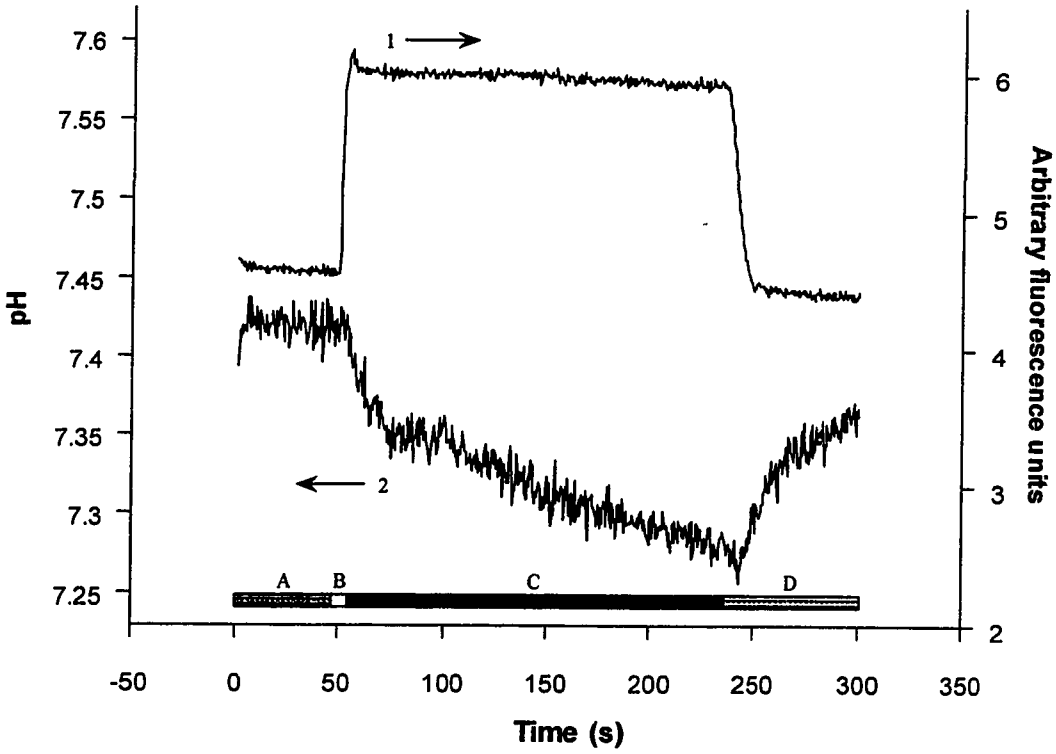

Figure 2-4 Tracer curve 1: injection of 50 µg/l fluorescein. Functional tracer curve 2: injection of buffer containing 10 mM glucose (normal working buffer), after starving the cells for 30 min in glucose-free buffer. Events in injection protocol: A - aspirate buffer and tracer into the flow injection manifold; B - deliver tracer onto cells; C - stop tracer on cells for 3 min; D - flush out tracer with buffer.

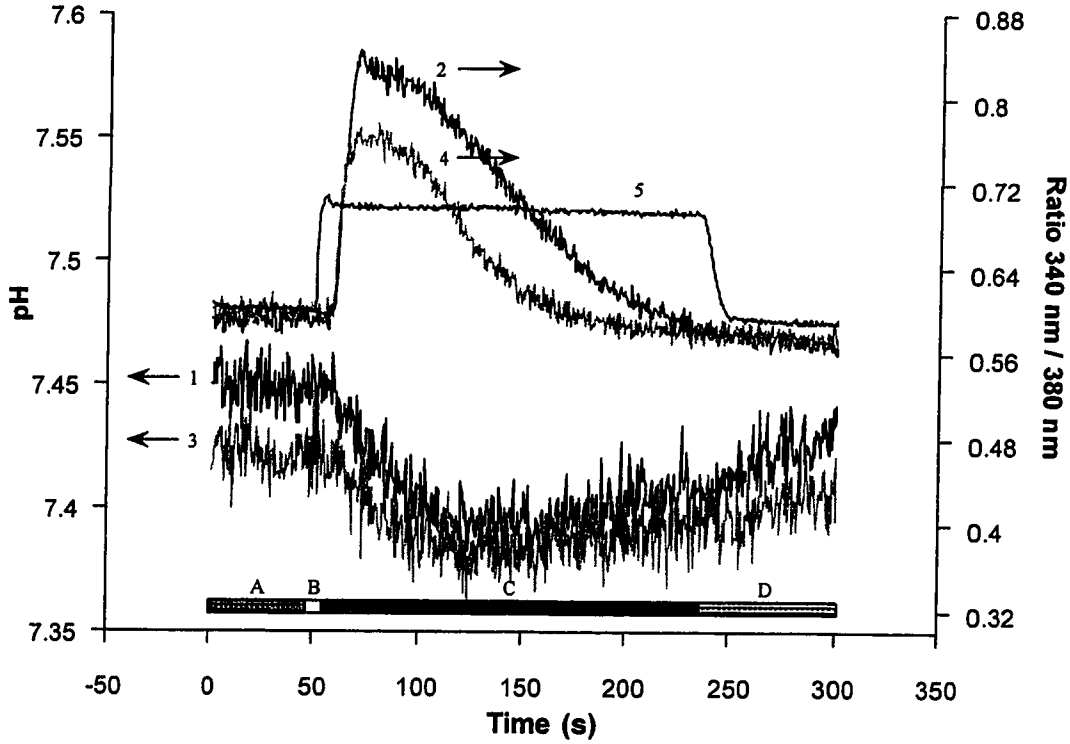

Figure 2-5 Runs 1 and 3: injection of 13 μM carbachol, monitoring internal pH. Runs 2 and 4: injection of 13 μM carbachol, monitoring internal [Ca^{2+}]. Run 5: injection of 50 μg/l fluorescein. The runs are numbered in the order that they were performed. Events in injection protocol: A - aspirate buffer and stimulant into the flow injection manifold; B - deliver stimulant onto cells; C - stop stimulant on cells for 3 min; D - flush out stimulant with buffer.

Notes to Chapter 2

[1] Busa W.B. *Ann. Rev. Physiol.*, **1986**, *48*, 389-402.

[2] Vicentini L.M., Villereal M.L. *Life Sciences*, **1986**, *38*, 2269-2276.

[3] Martínez-Zaguilán R., Martínez G.M., Lattanzio F., Gillies R. *Am. J. Physiol.*, **1991**, *260*, C297-C307.

[4] Martínez-Zaguilán R., Parnami G., Lynch R.M. *Cell Calcium*, **1996**, *19*, 337-349.

[5] Austin C., Dilly K., Eisner D., Wray S. *Biochem. Biophys. Res. Commun.* **1996**, *222*, 537-540.

[6] Yoshizaki K., Ohtomo K., Fukuhara K., Kawaguchi T., Kawaguchi J. *Adv. Exp. Med. Biol.* **1996**, *410*, 221-226

[7] Wiegmann T.B., Vamos S., Welling L.W., Beatty D.M., Morris S.J. *Int. Rev. Exp. Pathol.* **1996**, *36*, 175-196.

[8] Grynkiewicz G., Poenie M., Tsien R.Y. *J. Biol. Chem.*, **1985**, *260*, 3440-3450.

[9] Haugland R.P. *Handbook of Fluorescent Probes and Research Chemicals*, Molecular Probes, Eugene, OR, USA, 6th ed., 1996.

[10] Tsien R.Y. *Meth. Cell Biol.*, **1989**, *30*, 127-156.

[11] Ruzicka J., Baxter P.J., Thastrup O., Scudder K. *Analyst*, **1996**, *121*, 945-950.

[12] Baxter G.T., Young M.-L., Miller D., Owicki J.C. *Life Sciences*, **1994**, *55*, 573-583.

[13] Negulescu P.A., Machen T.A. Meth. Enzymol., **1990**, *192*, 38-81.

[14] Graber M.L., DiLillo D.C., Friedman B.L., Pastoriza-Munoz E. *Anal. Biochem.*, **1986**, *156*, 202-212.

[15] Ruzicka J., personal communication.

[16] Roos A., Boron W.F. *Physiol. Rev.*, **1981**, *61*, 296-434.

[17] Alberts B., Bray D., Lewis J., Raff M., Roberts K., Watson J.D. *Molecular Biology of the Cell*, Garland Publishing, New York, 3rd ed., 1994, Chapter 11.

Chapter 3 Characterization of pH control mechanisms in CHO M1 cells

3.1 Background

3.1.1 pH control mechanisms in cells

Almost all cellular processes are sensitive to pH. It is therefore critical that a cell has mechanisms to regulate its pH against various acid and alkali loads. Most of the time these processes are designed to neutralize an acid load due to two ubiquitous phenomena [1]: first of all, the electrochemical gradient across the cell membrane favors influx of H^+ ions. Second, the two major pathways in the cellular energy metabolism – the aerobic path and the anaerobic path - both produce acidic side products (section 1.2.2, ref. [2]):

Anaerobic: $\text{glucose} \rightarrow 2\ \text{lactate}^- + 2\ H^+$

Aerobic: $\text{glucose} + 6\ O_2 \rightarrow 6\ HCO_3^- + 6\ H^+$

As a result, the pH control mechanisms are mainly designed for extruding acid from (or bringing base into) the cell. An obvious, passive control mechanism is the chemical buffering capacity of the cytosol. Chemical buffering is an extremely fast means of maintaining a constant pH in the cell but is limited in its capacity to counteract acid production. In order to maintain a long-term pH homeostasis, active control mechanisms are needed. The most important and most universal of these is the Na^+/H^+ antiport that relieves acid load by exchanging intracellular H^+ for extracellular Na^+ (see Figure 3-1). The second most universal acid transporter is the Cl-HCO_3 exchanger. Its operation can be described as exchanging intracellular, neutral Cl^- for extracellular, al-

kaline HCO_3^- (Figure 3-1). Other, less frequently encountered active mechanisms are the ATP-driven H^+-pump and monocarboxylic acid transporters (e.g. the lactic acid transporter).

The operation of the pH control machinery is traditionally studied by intracellular pH (pH_i) measurements. An acid or alkali flux is generated into the cell and measuring the extent and the rate of pH recovery characterizes the efficiency of the control mechanisms. By using chemical blocking agents to inactivate specific acid transporters, the importance of each transporter in the pH control of a certain cell type can be elucidated. Both the operation of the transporters and techniques to study them have been reviewed extensively in several articles and books [1,3,4].

3.1.2 Potential of microphysiometry for pH regulation studies

Acid release measurements by the Microphysiometer have been successfully used for drug screening for several years now [3]. However, its significant potential for studying the mechanisms that generate and regulate acid release has remained unused, with a few exceptions [5]. Although there is a significant body of knowledge about acid release mechanisms, it has all been obtained as a kind of side product from intracellular pH regulation studies. That is to say, the information has been acquired by measuring pH *inside* the cell, which only probes acid release indirectly.

3.1.3 Combination of pH_i and acid release studies

Chemical stimulation was used to perturb the energy metabolism of cells, leading to altered rate of metabolic acid production. The general reaction of the cellular pH control mechanisms to the altered acid production was studied in parallel measurements by *two* techniques:

1) intracellular pH measurements
2) direct acid release measurements

The studies were further extended to investigate the importance of the Na^+/H^+ antiport and the Cl-HCO_3 exchanger in controlling pH_i and acid release rate. The respective importance of the two control systems were resolved by stimulating the cells in the presence of chemical blocking agents that specifically inactivate one or the other system.

The work was carried out as a joint project where pH_i measurements were performed by the author and acid release measurements by Dr. Carmen Rehder (University of Washington, Department of Chemistry).

3.2 Experimental

3.2.1 Cells and reagents

CHO M1 cells were grown as described in section 2.2.1. One day prior to an experiment the cells were placed in cell culture medium in which the serum concentration was reduced to 5%. This was done to reduce the basal metabolic activity of the cells. The buffer solution used in the experiments was phosphate buffered balanced salt solution (0.3 mM $CaCl_2$, 0.6 mM $MgCl_2$, 0.5 mM KH_2PO_4, 0.5 mM Na_2HPO_4, 3 mM KCl, 0.13 M NaCl with 1 g/l bovine serum albumin and 10 mM glucose, adjusted to pH 7.4).

Intracellular pH and acid release measurements were conducted on different groups of cells from the same parent culture. For pH_i measurements, cells in a LabTek chamber were stained with BCECF-AM and the LabTek chamber was assembled into the inverted radial flow cell of the FIFM setup (see section 2.2.2) . For acid release measurements, a pellet of approximately $1x10^5$ cells was resuspended in 60 µL of buffer and mixed with 15 µL of melted low temperature-melting agarose at 37 °C. The agarose mixture (7 µL) was then spotted onto a cell capsule membrane and allowed to solidify

for about 10 minutes at 25 °C. The cell capsules were then placed into the sensor chambers of the Microphysiometer.

3.2.2 Instrumental setup

Two experimental setups were used (see Figure 3-2):

1) Intracellular pH was monitored using the FIFM setup, with cells grown as a monolayer in LabTek chambers. The setup was operated exactly as described in Chapter 2.
2) Acid release was monitored using the Cytosensor Microphysiometer®, set to operate in a 90 second measurement cycle: for the first 60 s of each cycle, the cells are perfused with buffer. The pump is then stopped for 30 seconds and the acid extrusion rate is measured as the rate of acidification of the stagnant solution. The typical drop in pH during the pump-off cycle is 0.05 pH units.

Since both instruments employ flow injection as the stimulant delivery technique, similar stimulant exposure profiles could easily be created. A stimulant exposure time of 180 s was selected for all experiments.

3.3 Results and discussion

3.3.1 Comparison of changes in pH_i and acid release rate

An example of how the two responses compare independent of signaling pathways is provided by a glucose deprivation experiment. For pH_i measurements, cells in a LabTek chamber were incubated in glucose-free buffer for fifteen minutes and the chamber was then mounted in the FIFM instrument. The cells were first perfused with glucose-free buffer, followed by exposure to 10 mM glucose containing buffer (Figure 3-3). The pH_i decreased immediately (<20 s) upon exposure to glucose and continued to drop slowly during the three minute period of observation. In the acid extrusion ex-

periment, cells in a Microphysiometer chamber were perfused with glucose-free buffer until the cells reached a stable basal rate of extracellular acid release. Following exposure to 10 mM glucose, an increase in acid extrusion was detectable already after the first 90 s rate measurement cycle. By the time of the second rate measurement (180 s), the acid release rate had reached a stable level that was 5-fold higher than the basal rate in glucose-free buffer. The results show that both techniques possess the kind of signal-to-noise ratio and kinetic resolution that are necessary for studying changes in acid generation and release by the CHO M1 cells. Further, it is evident that the use of flow injection in stimulant delivery makes comparison of pH_i and acid release data easy.

Shown in Figure 3-4 are the changes in pH_i and the rate of acid release for CHO-M1 cells exposed to carbachol, a muscarinic receptor agonist. In both measurements, cells were exposed to 100 μM carbachol for 180 s, and then the drug was removed by perfusion with buffer. The pH_i initially decreases (7.46 ± 0.04 to 7.37 ± 0.03; n=6) after 30 s of exposure to carbachol and then recovers reaching a new steady state pH_i that is more basic than prior to stimulation (7.58 ± 0.05; n=3). The rate of acid release increases from 21.6 ± 2.0 $nmol \cdot min^{-1} \cdot 10^{-6}$ reaching a maximum of 30.7 ± 1.9 $nmol \cdot min^{-1} \cdot 10^{-6}$ within 180 s and then returns to the basal rate. The specificity of the carbachol response was confirmed by the inhibition of this response with 100 μM atropine, a competitive inhibitor of carbachol. Not surprisingly, the two different measurements provide complementary data. For example, the kinetics of the acid release and pH_i are quite similar: both perturbations are over in about 4 minutes.

The responses to ATP, PMA, and insulin were also studied. ATP presumably activates an endogenous purinergic receptor, PMA is a phorbol ester that activates protein kinase C, and insulin activates an endogenous insulin receptor. In all measurements, cells were exposed to stimulant for 180 s and then stimulant was removed by perfusion with buffer. The pH_i and acid release responses for ATP and PMA stimulations were similar to those seen in Figure 3-4. One notable difference in both the ATP and PMA stimulation cases was that the recovery of pH_i did not begin until the drug was washed out.

The longer time required for recovery of the pH_i was also observed in the recovery of the acid release response. After stimulation with ATP, the recovered pH_i was partly elevated (7.46 ± 0.04 to 7.53 ± 0.04; n=6 and n=7,respectively). After stimulation with PMA the recovered pH_i was slightly lowered (7.46 ± 0.04 to 7.44 ± 0.05; n=6 for both). We were surprised to find that insulin did not cause a change in pH_i given that it produces a dramatic sustained increase in the rate of acid release. One difference between the conditions used for microphysiometry and FIFM is that the latter is done at room temperature. It was found that the acid release response observed for insulin was not observed when the temperature in the microphysiometer chambers was lowered to ambient (Figure 3-5a). The acid release responses to all other stimuli were essentially the same at the lower temperature (Figure 3-5b). The data suggests that some step in the insulin signal transduction pathway is uniquely temperature sensitive.

3.3.2 Regulation of pH_i

Transporter inhibitors were used to study the roles of the Na^+/H^+ antiport and bicarbonate transporters in the regulation of pH_i in response to changes induced by chemical stimuli. In these experiments, an acid transporter was selectively inactivated by continuous perfusion with buffer containing a specific inhibitor of the transporter. The cells were subsequently stimulated with a drug for 180 s, followed by wash-out. The inhibitor was included even in the stimulation and wash-out steps to keep the transporter inactivated throughout the whole experiment.

When cells are exposed to carbachol in the absence of any inhibitors, the pH_i decreases to 7.37 ± 0.03 (n=3) within 1 min (Figure 3-6a). The pH_i starts to recover already during stimulation and finally (after 4 min) settles to a new steady state that is more alkaline (7.58 ± 0.05; n=6) than the original resting pH. In the presence of a specific Na^+/H^+ antiport inhibitor, hexamethylamiloride [4,6,7], the initial pH_i decrease is more dramatic (7.27 ± 0.03; n=4) and there is no recovery during drug exposure (Figure 3-6b). Following removal of drug, the pH_i shows a slow recovery that finally settles to

a value more acidic than the original resting pH. In the presence of a bicarbonate transporter inhibitor, 4,4'-diisothiocyanato-stilbene-2,2'-disulfonic acid (DIDS) [8,9], the initial pH_i decrease is even more dramatic (7.22 ± 0.03; n=4) than observed with hexamethylamiloride (Figure 3-6c). Again there is no recovery during drug exposure but immediately following removal of drug there is a rapid recovery to a pH_i value above the resting pH_i (7.52 ± 0.04; n=4). The data suggest that the initial phase of recovery from acidification is due to both activation of the sodium-proton antiport and the bicarbonate-dependent transporters. The recovery phase observed after drug removal, however, appears to be largely dependent on the Na^+/H^+ antiport.

The effects of hexamethylamiloride and DIDS on the pH_i response observed for stimulation with ATP are essentially the same as those observed for carbachol stimulation. In the presence of hexamethylamiloride the acidification was slightly more pronounced (7.23 ± 0.03 vs. 7.27 ± 0.03; n=6 and n=4, respectively), and there was little recovery. In the presence of DIDS, the initial acidification also was pronounced (7.17 ± 0.03; n=6) but the final recovery was rapid and slightly elevated (7.58 ± 0.04; n=6). Our data suggest that the pH_i response to ATP is regulated in a manner similar to the carbachol response. The similar pH_i regulation confirms that the regulation of the response to the transfected M1-muscarinic receptor is not artifactual. PMA directly activates protein kinase C which is known to regulate the Na^+/H^+ antiport in many cells. The normal response of CHO cells to PMA, an initial acidification and subsequent partial recovery, was affected by hexamethylamiloride only in the respect that the recovered pH_i was slightly lower than in the absence of hexamethylamiloride. The PMA response was not affected by DIDS.

3.3.3 Regulation of acid release rate

The effects of the transporter inhibitors on the acid release responses were substantially different than those observed for the pH_i responses. The burst of increased rate of acid release stimulated by carbachol (Figure 3-7a) was completely blocked by hex-

amethylamiloride (Figure 3-7b). This would suggest that the acid release response to carbachol is dominated by Na^+/H^+ antiport activity. Indeed, the bicarbonate transporter inhibitor DIDS had no effect on the acid release response (Figure 3-7c). The acid release responses to ATP and PMA were also completely blocked by hexamethylamiloride and entirely unaffected by DIDS. Because the microphysiometer measures the rate of extracellular acidification, it is unable to discriminate between protons released by the Na^+/H^+ antiport, protons released by bicarbonate dependent transporters, or protons generated from the hydration of CO_2 released from the cell (the latter arises from either respiration or cellular uptake of bicarbonate that neutralizes intracellular acid to form CO_2). Since all mechanisms of acid release are measured by the microphysiometer response, the hexamethylamiloride blockade indicates that the stimuli induced changes in the rate of acid release in these cells is regulated almost exclusively by the Na^+/H^+ antiport.

It could be argued that the low concentration of bicarbonate used in these experiments (0.5 mM) had disabled the bicarbonate transporters. However, it is evident that the bicarbonate transporters are sufficiently active at this concentration to participate in the pH_i response, and DIDS does cause a decrease in pH_i upon stimulation with carbachol (Figure 3-6c). The choice of 0.5 mM bicarbonate was dictated by the FIFM experiments which were done at ambient temperatures in an open atmosphere. The 0.5 mM bicarbonate eliminates any drift in pH due to atmospheric carbon dioxide. Traditionally bicarbonate is not added to the buffers used in the microphysiometer which utilizes a membrane degassing unit to minimize the introduction of bubbles into the sensor chamber. In these experiments the degassing unit was disabled and 0.5 mM bicarbonate was used in the buffer to better compare the acid release rates results to the pH_i results measured with FIFM. The acid release response observed under these conditions was identical to that observed with no bicarbonate in the buffer. For further proof, the operation of the microphysiometer was modified such that a buffer with 30 mM bicarbonate and a 5% carbon dioxide atmosphere can be used. Even under these conditions the acid release response to carbachol is identical to that observed with no bicarbonate

(Figure 3-8). The acid release responses to ATP and PMA are also independent of the presence of bicarbonate in the buffer. Clearly, the acid release response in these cells is not regulated by bicarbonate transporters.

3.4 Conclusions

It was found that the increased rate of acid release in response to cell stimulation was solely dependent upon the function of the Na^+/H^+ antiport. The recovery of the acidified pH_i after stimulation was also found to be solely dependent upon the Na^+/H^+ antiport. Our results suggest that the bicarbonate dependent transporters are not strictly required in the long-term recovery of the pH_i after an acid load in CHO cells. Our observation does not, however, suggest that the bicarbonate dependent transporters are not involved in the homeostatic maintenance of pH_i since it was found that DIDS did induce a lower pH_i (Figure 3-6c). It is well understood that bicarbonate is required for normal functioning of a cell [9] and it has even been stated that "He who works in bicarbonate-free media risks studying cellular and molecular pathology rather than physiology."[10] The importance of bicarbonate for cellular homeostasis also arises from its role in chloride ion balance and, thus, cell volume. We conclude that the primary role of bicarbonate for CHO cells is maintenance of cell volume, a role that affects the homeostatic pH_i but not its dynamic regulation.

During stimulation the Na^+/H^+ antiport is activated and, thus, the rate of acid release increases. In the absence of any change in energy metabolism, the upregulated antiport activity would lead to a more alkaline cytoplasm. It was found that during stimulation the cytoplasm initially acidified despite the increased antiport activity, suggesting that the flux of energy metabolism was rapidly increased. The acid load was eventually countered by increased antiport activity and, ultimately, the pH_i stabilized at a more alkaline pH after stimulation. If one were to have observed only the pH_i drops before and after stimulation, it would have been concluded that stimulation activated the so-

dium proton Na^+/H^+ antiport causing a more efficient extrusion of acid and, thus, more alkaline pH_i. The rate of acid release after stimulation, however, was the same as prior to stimulation. The more alkaline pH_i could be due to a decrease in the basal energy metabolism following the initial metabolic burst and not a long-term change in Na^+/H^+ antiport activity.

In summary, the concurrent monitoring of both pH_i and acid release, such as reported here, provides a more comprehensive view of acid regulation that includes the contribution of metabolic flux, a component not frequently included in such studies. Reliable comparison of pH_i and acid release responses is made possible by the well-defined and reproducible exposure of receptors to drugs, as well as the swift and efficient removal of the drug from the medium surrounding the cells. These tasks are achieved by the use of flow injection.

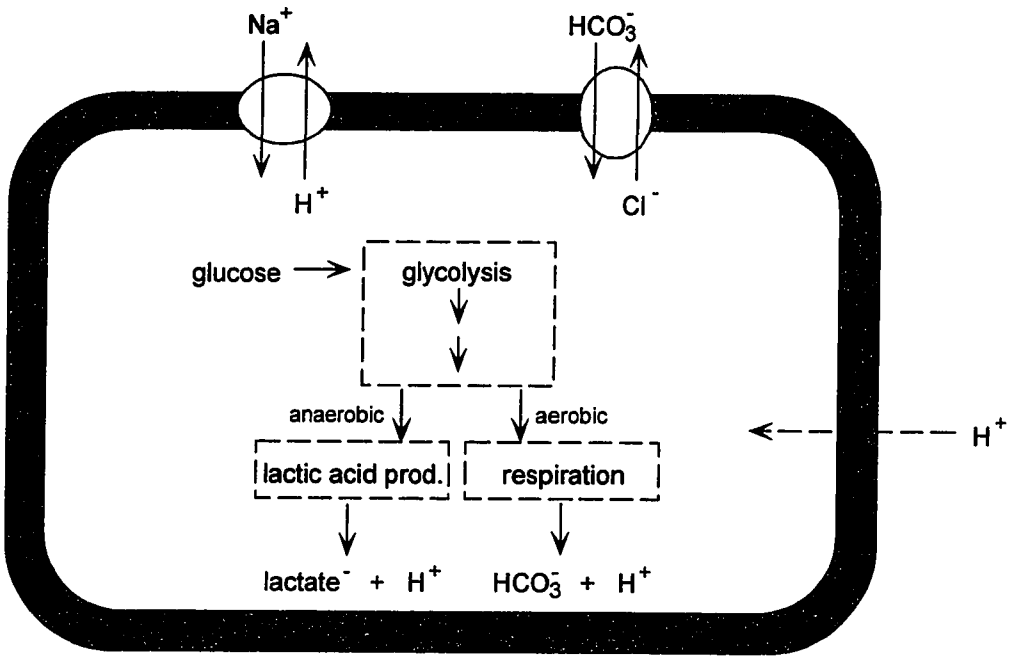

Figure 3-1 Mechanisms of acid generation and pH control in a living cell.

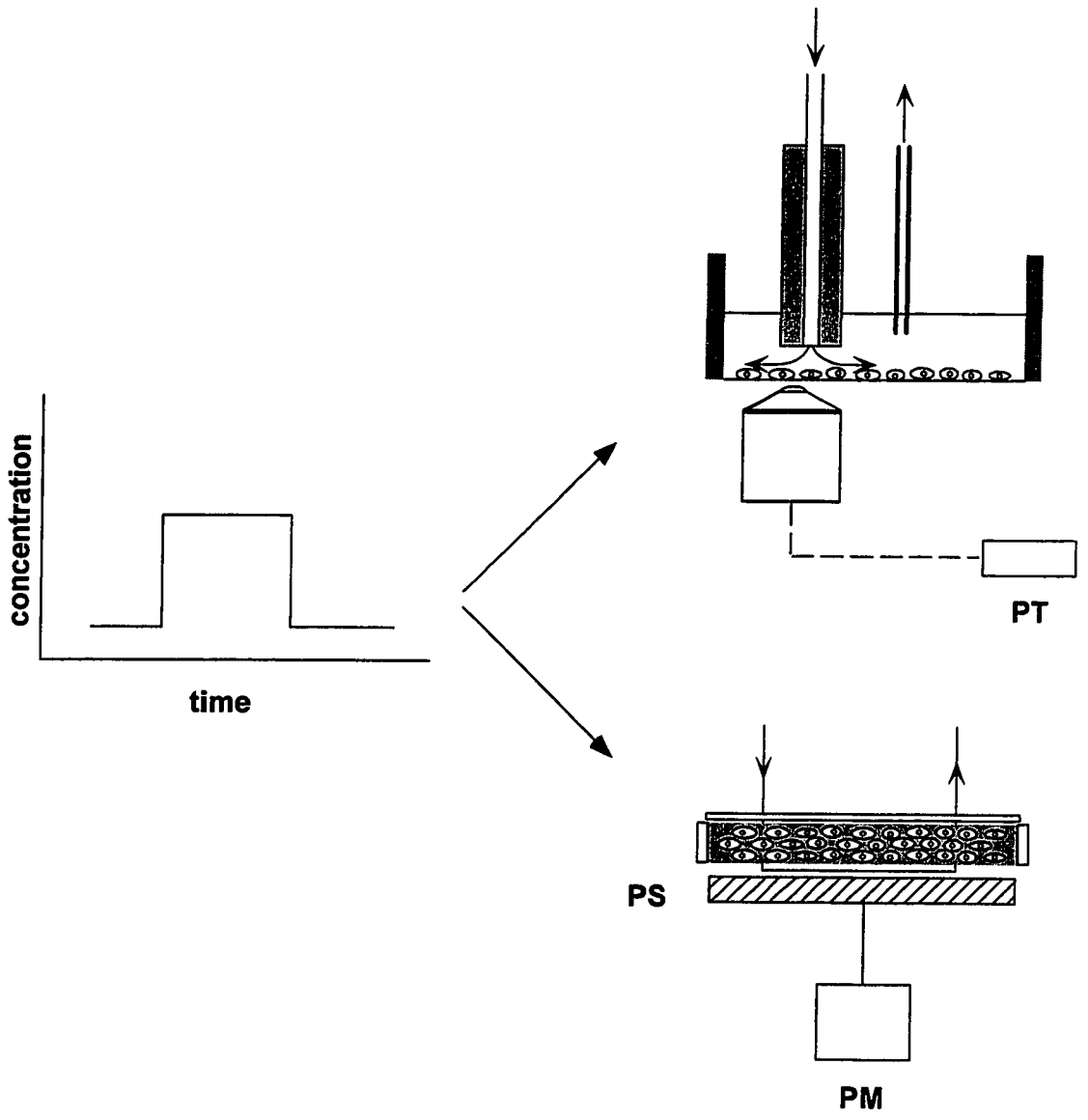

Figure 3-2 Experimental arrangement in concerted pH_i and acid release measurements, using FIFM and the Microphysiometer, respectively. **PS** – pH sensor, **PM** – potentiometer, **PT** – photomultiplier tube.

(a)

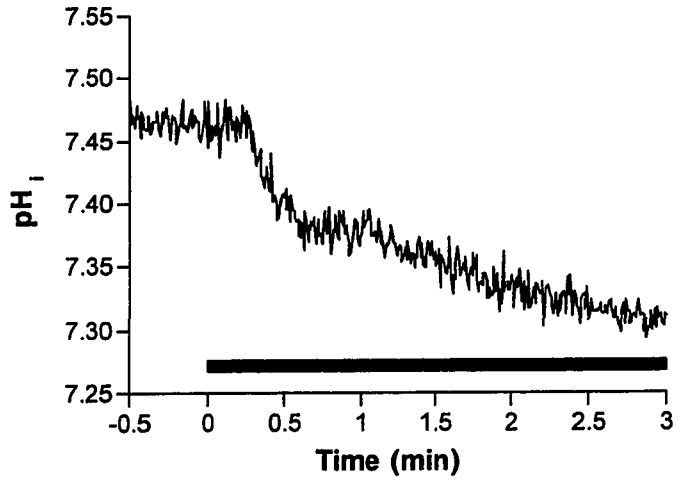

(b)

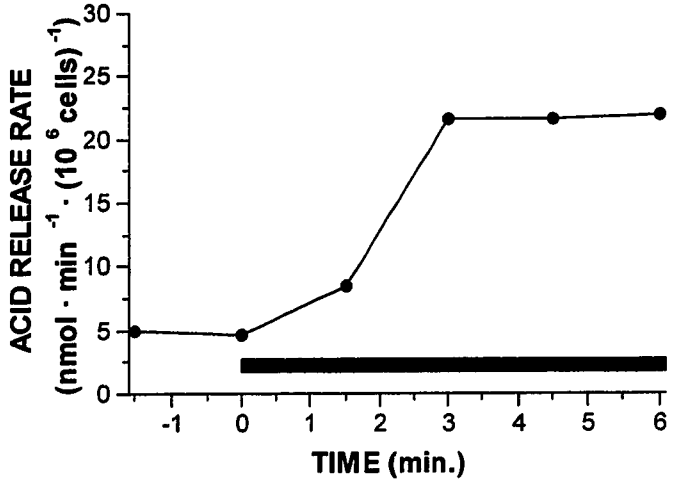

Figure 3-3 Glucose deprivation experiments. (a) Intracellular pH. Cells are grown as a monolayer on a LabTek microscope chamber. (b) Acid release rate. Cells are immobilized in agarose. The black bar indicates exposure to glucose after starvation.

(a)

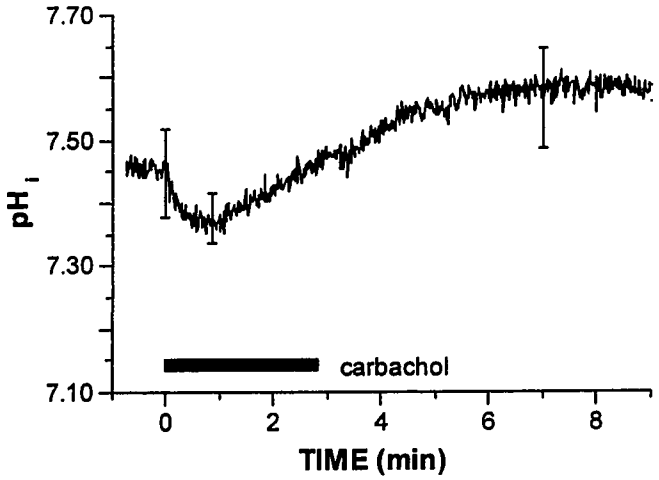

(b)

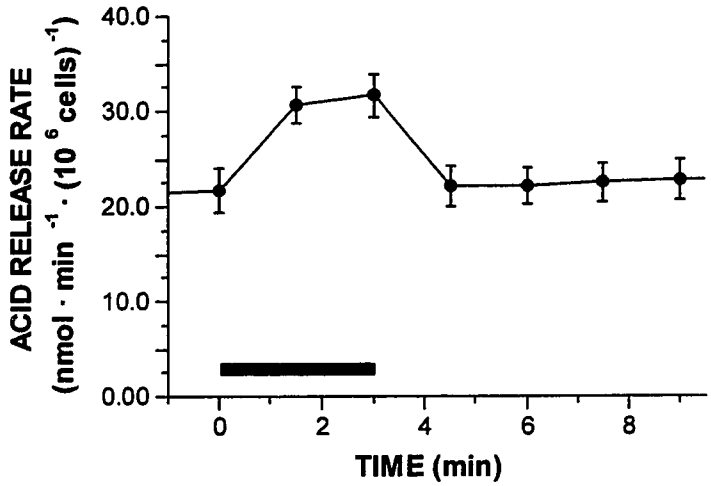

Figure 3-4 Changes in (**a**) pH_i and (**b**) acid release rate as a result of exposure to carbachol. The cells were exposed to 100 μM carbachol for 180 s.

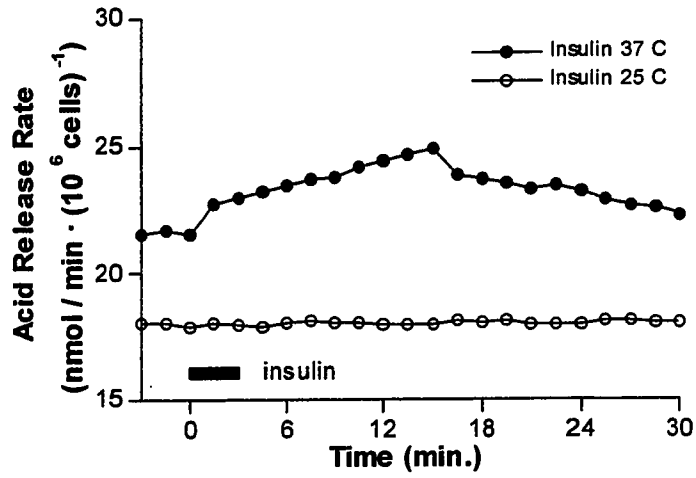

Figure 3-5 Acid release responses to insulin at 37 °C (●) and 25 °C (○).

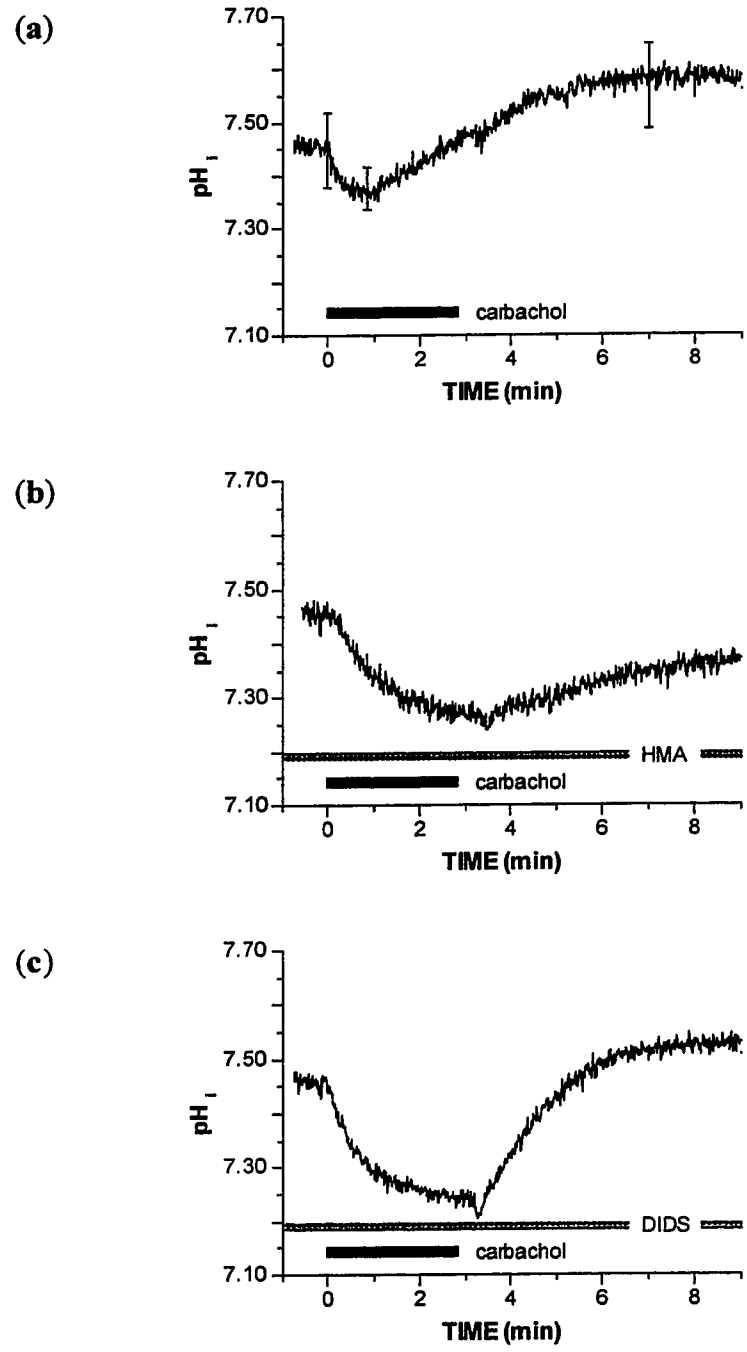

Figure 3-6 Carbachol-induced changes in pH_i in the absence and presence of acid transport inhibitors. (**a**) No inhibitors present. (**b**) 10 μM hexamethylamiloride. (**c**) 10 μM DIDS. The concentration of carbachol was 100 μM.

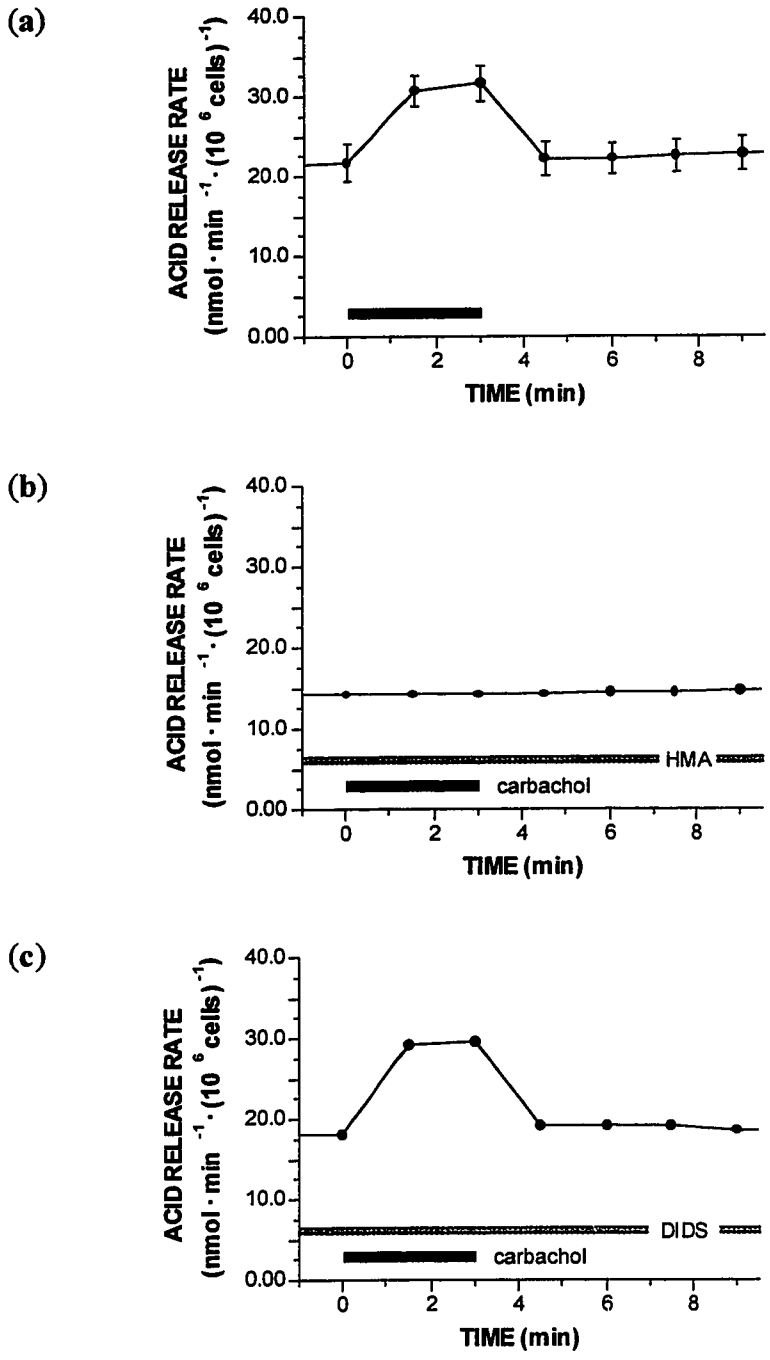

Figure 3-7 Carbachol-induced changes in acid release rate in the absence and presence of acid transport inhibitors. (**a**) No inhibitors present. (**b**) 10 μM hexamethylamiloride. (**c**) 10 μM DIDS. The concentration of carbachol was 100 μM.

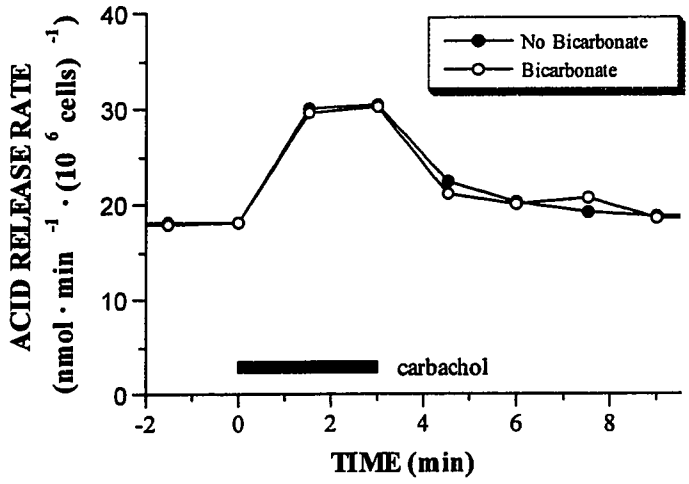

Figure 3-8 Acid release response to carbachol in the absence and presence of bicarbonate. The cells were exposed to 100 μM carbachol for 6 min.

Notes to Chapter 3

[1] Boron W.F. in Seldin D.W., Giebisch G. (eds) *The Regulation of Acid-Base Balance*, Raven Press, New York, 1989, Chapter 2.

[2] McConnell H.M., Owicki J.C., Parce J.W., Miller D.L., Baxter G.T., Wada H.G., Pitchford S. *Science*, **1992**, *257*, 1906-1912.

[3] Roos A., Boron W.F. *Physiol. Rev.*, **1981**, *61*, 296-434.

[4] Frelin C., Vigne P., Ladoux A., Lazdunski M. *Eur. J. Biochem.*, **1988**, *174*, 3-14.

[5] Wada H.G., Indelicato S.R., Meyer L., Kitamura T., Miyajima A., Kirk G., Muir V.C., Parce J.W. *J. Cell. Physiol.*, **1993**, *154*, 129-138.

[6] Grinstein S., Cohen S., Rothstein A. *J. Gen. Physiol.*, **1984**, *83*, 341-369.

[7] Bianchini L., Pouyssegur J. *J. Exp. Biol.*, **1994**, *196*, 337-344.

[8] Chaillet J.R., Amsler K., Boron W.F. *Proc. Natl. Acad. Sci. USA*, **1986**, *83*, 522-526.

[9] L'Allemain G., Paris S., Pouyssegur J. *J. Biol. Chem.*, **1985**, *260*, 4877-4883.

[10] Thomas R.C. *Nature*, **1989**, *337*, 601-601.

Chapter 4 Acid release measurements by fluorescence

4.1 Background

4.1.1 Cell response measurements

The study of responses of living cells to different chemical or physical stimuli is central to cell biology and pharmacology (section 1.3). Several different instrumental methods are used for such studies, the most common ones being radioactive labeling and scintillation, fluorescence spectroscopy and potentiometry. During the past decade, fluorescence microscopy and flow cytometry have achieved a dominant position among these methods, owing to the recent development of many reliable and easy-to-use fluorescent indicators [1]. Response studies are typically carried out by following an intracellular parameter, such as [Ca^{2+}], [cyclic AMP] or pH, that is a part of the biochemical response mechanism and therefore will change in the course of the response. The response mechanisms – and consequently the available parameters – are different, depending on the given cell type and the type of stimulant. Therefore, there is a need to develop an instrumental approach that will allow the same methodology to be used for measurement of cell stimulation – regardless of its manifestation. Due to the availability of a wide array of available fluorescent indicators, fluorescence microscopy and flow cytometry are emerging as such universal platforms.

4.1.2 Acid release measurements

The concept of acid release measurements and its utility for cell response quantitation have been demonstrated by the development and success of the Cytosensor Microphysiometer® (see section 1.3.3), where metabolic acid production is quantified by measuring electrochemically the rate at which the extracellular medium acidifies as

cells secrete acid [2]. The greatest strength of this technique is that it measures a parameter – metabolic turnover - which occurs in all animal cells. And although there are some signal transduction pathways that do not alter energy metabolism, the method has proved to be applicable to an extremely wide range of cells and stimulants [2].

Rather than carrying out acid release measurements with a special electrochemical instrument, it would be desirable to implement the technique into the more universal platform, such as fluorescence microscopy. However, the implementation is complicated by a fundamental difference between traditional measurement of cell response and measurement of acid release: the former involves measurement of *intracellular* phenomena whereas the latter involves an *extracellular* quantity. The complication with extracellular measurements arises from the difficulty of detecting effects of a modest cellular acid generation on the large volume of buffered solution surrounding the cells. In order to be able to measure the acidification, the following requirements need to be met:

1) The buffering capacity of the bathing solution must be low, or at most intermediate level (10 mM or less). Otherwise the secreted acid will not produce observable pH changes.
2) The volume of solution around the cells should be as small as possible in order to prevent excessive dilution of the secreted acid. Also, the movement of the solution needs to be restricted to prevent dilution.
3) The pH sensing element needs to be brought as close to the cells as possible.

The Microphysiometer achieves all the above by immobilizing a large number of cells in an agarose matrix and sandwiching the agarose "sheet" between a physical support and the surface of an electrochemical pH sensor [2]. For construction of an analogous fluorescent technique, the obvious solution would be to place cells in a thin-layer flow through chamber and include a fluorescent pH indicator in the bathing solution. The approach does indeed work but suffers from the problems of a limited signal-to-noise

ratio (due to the thin layer of fluorescent indicator) and the necessity to include the fluorescent indicator in the carrier solution as well as in all stimulant solutions [3]. Clearly, a different method is needed to achieve convenient and reliable measurements. The bead injection technique (section 1.4.3, ref. [4]) was chosen as the approach to address the above problems and develop a viable method for fluorescent acid release detection.

4.2 Experimental

4.2.1 Cells and reagents

The working buffer used in the measurements was a phosphate buffered balanced salt solution (0.3 mM $CaCl_2$, 0.6 mM $MgCl_2$, 0.5 mM KH_2PO_4, 0.5 mM Na_2HPO_4, 3 mM KCl, 0.13 M NaCl) with 1 g/l bovine serum albumin and 10 mM glucose.

Cytodex-2 microcarrier beads were prepared by letting dry bead powder swell overnight in balanced salt solution. The beads were then sterilized by soaking in 95% ethanol for 2-3 h, washed repeatedly with balanced salt solution and finally suspended in cell culture medium. The fluorescent pH indicator BCECF-AM was immobilized on the beads as follows: a wet bead volume of 0.7 mL was suspended in 2 mL of a 10 μM solution of BCECF-AM and left to sit for two days. The stained beads were washed with the cell growth medium and cells were then grown on them as described below. Immediately prior to the experiments, 1.3 mL of the bead suspension was diluted to 10 mL with the working buffer. A 100 μL aliquot of the diluted suspension was aspirated into the sequential injection manifold to pack a column of beads and cells.

The cells used in the experiments were Chinese Hamster Ovary cells (CHO M1 WT3, American Type Culture Collection), transfected with the gene for the rat m1 muscarinic receptor. The growth medium was Ham's F-12 nutrient medium supplemented with 10% fetal bovine serum and 50 μg/mL G418. A wet volume of 0.3 mL of BCECF-la-

beled Cytodex-2 beads was suspended in 3.7 mL growth medium and inoculated with ca. $5 \cdot 10^5$ cells. The cells were then allowed to grow to full confluence. One day prior to experiments, the nutrient medium was switched to Ham's F-12 + 5% fetal bovine serum + 50 μg/mL G418. The lower serum content helps quiet down the cellular metabolism, thus creating a more suitable background for acid extrusion measurements.

4.2.2 Instrumentation

The instrumental setup is shown in Figure 4-1. It consisted of a FIAlab-3000 sequential injection system (Alitea USA, Medina, WA) for manipulation of solutions, a jet ring flow cell for trapping beads and a fluorescence microscope for detecting fluorescent signals from the trapped beads and cells.

The fluorescence detection system consisted of a Zeiss Axiovert 100 inverted microscope equipped with a 20×/0.75 N.A. objective (Carl Zeiss, Oberkochen, Germany) and a SE-510 photometer head (Photon Technology International, South Brunswick, NJ). The microscope was connected to a dual wavelength Delta Scan illuminator (Photon Technology International) to provide the excitation of fluorescent indicator dyes. All measurements were performed with the excitation wavelengths set at 497.5 nm for channel 1, and 430.5 nm for channel 2. The fluorescence filter system consisted of a 505 nm dichroic mirror and a 545/40 nm emission filter.

4.2.3 Experimental protocol for BIS technique

The bead injection analysis protocol consisted of four main steps: 1) packing beads into a column, 2) stopping the flow and recording signal in the absence of carbachol, 3) exposing the cells to carbachol, stopping the flow and recording the signal, 4) discarding the spent beads. A typical series of experiments comprised nine runs: exposure to 0 (blank), 0.1, 0.3, 1, 3, 10, 30, 100 and 300 μM carbachol. It should be stressed that since the beads were discarded after every run, each analysis was performed on a fresh set of

cells. The carbachol concentrations were selected so that the whole response range of CHO M1 WT3 cells could be observed. Further, the above concentrations are equally spaced when plotted on a logarithmic scale – a property that makes dose-response data optimal for visual inspection.

4.2.4 Calibration of pH measurements

A column of indicator beads was perfused with the minimally buffered balanced salt solution, into which pH standards of 7.10, 7.20, 7.30 and 7.40 were injected. The standards were prepared in a solution that was more strongly (10 mM HEPES) buffered than the carrier in order to keep pH at the nominal value despite dispersion in the flow injection system.

4.2.5 Data processing

The raw data were converted to the ratiometric form: $R(t_i)=F_{\lambda 1}(t_i)/F_{\lambda 2}(t_i)$, where $F_{\lambda 1}(t_i)$ is the emission detected after excitation from channel 1 and $F_{\lambda 2}(t_i)$ the emission detected after excitation from channel 2.

The cellular response (i.e. the acidification rate) from an individual run was determined from the slope of the acidification profile (described in more detail in section 4.3.2). The obtained data was then normalized by dividing each value by the maximum value of the data series. In other words, the cellular responses to different carbachol concentrations were now presented in terms of fractions relative to the maximal response. This enables easy comparison of data from different analysis series.

Normalized data from a total of four analysis series were combined by calculating the average response to each carbachol concentration. Finally, the average responses were fitted to the classical stimulus-response equation [5]

$$E = \frac{E_{max} C}{C + EC_{50}} + K$$

where E = cell response, E_{max} = maximal response, C = stimulant concentration, EC_{50} = stimulant concentration corresponding to half-maximal response, K = offset from zero.

The above data processing allowed useful information to be extracted from a noisy signal. The most obvious example is Figure 4-3 where the slopes of monitored responses in the absence and presence of stimulant appear similar by visual observation. However, when the collected data are treated as described above, the obtained dose-response curves show a well-defined inflection point along with acceptable error bars.

4.3 Results and discussion

4.3.1 Verification of pH response

The pH-sensitivity of the BCECF-treated Cytodex-2 beads was verified by calibration with pH standard solutions. Linear regression using the known pH values and the obtained fluorescence data yielded a calibration curve $pH = 1.61 \cdot R + 5.63$, with $r^2 = 0.997$.

The fact that the extracellular pH change is related to cell metabolism was verified with glucose depletion experiments that are routinely used for stimulation-independent acid release calibration in microphysiometry [2]. First, the bead column was packed and perfused using glucose free buffer. A blank injection of the same glucose-free buffer shows little acidification, even when the flow is stopped (Figure 4-2). This is to be expected since in the absence of glucose the cells have considerably less metabolic fuel so the turnover rates of glycolysis as well as respiration are significantly lower. Consequently, the cells produce noticeably smaller amounts of lactic acid and CO_2. An injec-

tion of 10 mM glucose-containing buffer, on the other hand, shows significant acidification during the stop flow period – just as it should since now the cells have ample fuel supplies for their metabolism and are producing much larger quantities of acid.

The glucose depletion experiments also demonstrate the necessity to stop the flow in order to properly detect the acidification. If the cells are being perfused continuously, even at the very low flow rate of 1 μL/s, the flow is removing acid almost as fast as it is produced, and only very slight acidification is noticed as the cells come into contact with glucose (end of part B in the flow protocol in Figure 4-2). Once the flow is stopped (part C in Figure 4-2) the extruded acid can accumulate and a steady, pronounced decrease in pH is observed.

The crucial role of the bead injection technique in the success of the above results should be stressed. Our previous attempts to detect cellular acid release from cells grown in conventional single layer configuration on a planar surface of a microscope slide all failed or worked very poorly because the amount of secreted acid was too small to significantly alter the pH of the relatively large volume of solution covering the cell layer [3]. Being able to pack indicator beads with cells into a column is an excellent configuration for detection of acid release, since the bead column minimizes the extracellular solution volume that cells extrude their acid into. Futhermore, since the beads form a multilayer structure, approximately 30 times thicker than a monolayer of cells, the fluorescent microscopy signal is correspondingly enhanced, which translates into more sensitive measurements and acceptable signal-to-noise ratio [6].

4.3.2 Stimulation results

Acidification rates in the absence and presence of carbachol were evaluated by determining the slope of the fluorescence ratio signal during the stop flow periods (see Figure 4-3). Taking the ratio [acidification(in X μM carbachol)]/[acidification(in plain buffer)] yielded a measure for the degree to which the cells responded to a particular

level of carbachol. After subtracting the blank response, the data was normalized. Normalized data from four different dose-response series were averaged to yield one data set. The processed response data are shown in Figure 4-4, together with a fit into the stimulus-response equation. The numerical results from the fit can be used to characterize the effect of carbachol on the CHO M1 WT3 cells: the EC_{50} value describes the potency of carbachol to stimulate the cells. In this case, an EC_{50} value of 1 μM is obtained, which is in good agreement with the pEC_{50} of 5.5 (EC_{50}=3 μM) obtained by Baxter *et al.* [7] using the microphysiometer.

4.4 Conclusions

This work introduces successful combination of a versatile detection method (fluorescence microscopy) with a biologically universal cellular response parameter (acid release). The link that enables joining the two together is the bead injection technique for sensor assembly and drug delivery. The BI approach is able to overcome, in the following manner, the limitations of excessive buffering/dilution and limited signal caused by measuring pH changes in the extracellular solution:

1) A relatively large number of cells (on the order of 10^3-10^4) can be packed in a small (ca. 2 μL) volume.
2) The BCECF-labeled beads provide a solid, renewable pH sensing surface and therefore obviate the need to include fluorescent indicator in the aqueous phase.
3) Immobilization of the BCECF pH indicator on the beads brings the pH sensor as close to the cells as possible.

In comparison to the established technique, the Cytosensor Microphysiometer, the noise level in the presented BI method is greater and repeatability of the results (comparing error bars of our stimulus-response data to those in [8]) is poorer. This is most probably due to the fact that the Microphysiometer carries out pH measurements by electrochemical titration, which is an inherently more precise method than optical

sensing of indicator equilibrium. Further, the ratio of (cell count)/(chamber volume) can be made higher in the Microphysiometer. However, the BI technique has unique advantages: first, it allows the measurement of acid release response using the universal fluorescence microscopy platform, rather than an instrument limited to measuring acid release only. Secondly, it automates the process of loading and discharging spent cells, an operation that requires skill and time when running the Microphysiometer.

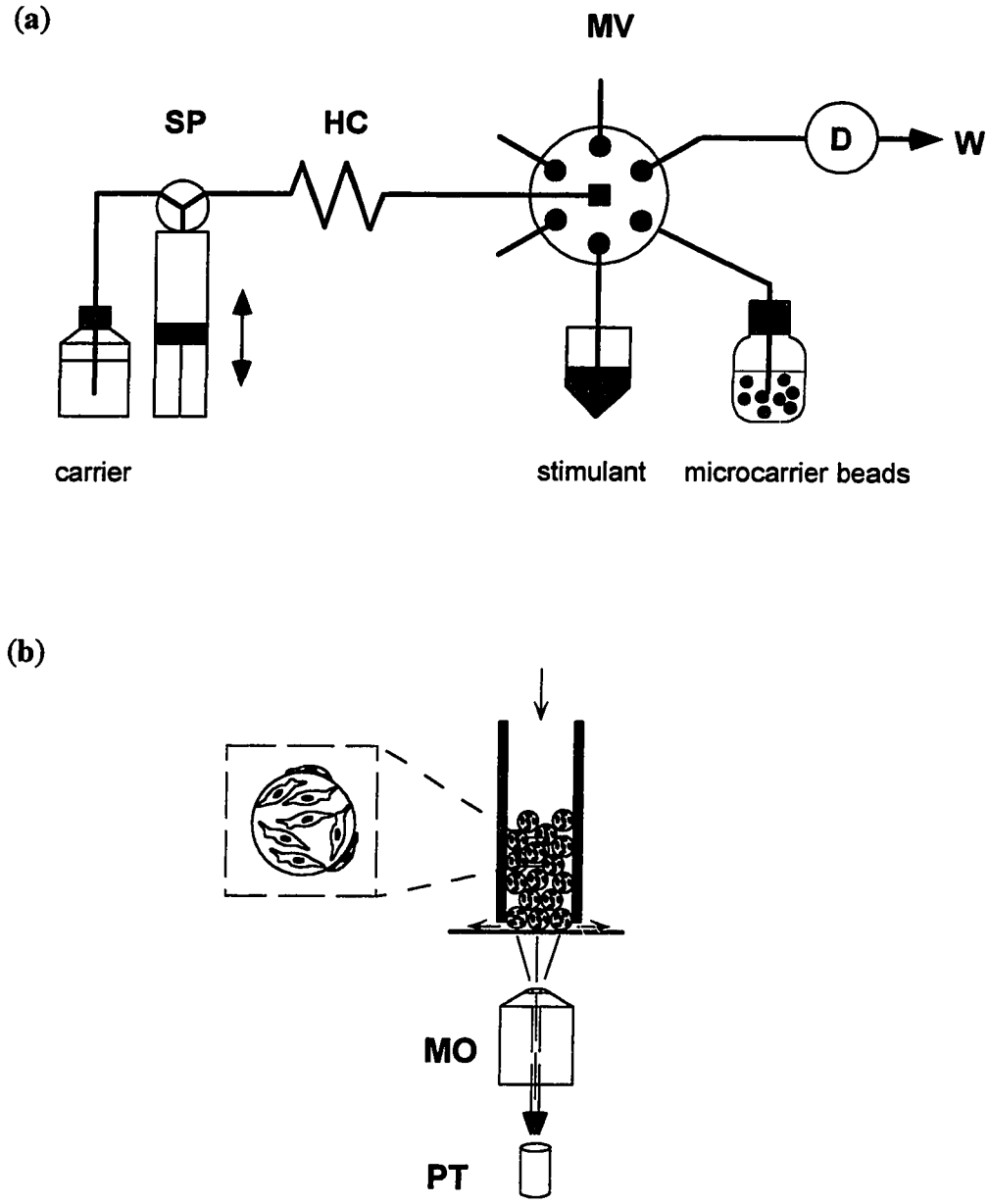

Figure 4-1 (**a**) Bead injection setup used in the experiments. (**b**) Jet ring flow-through chamber. The enlarged part shows cells attached to microcarrier beads. **SP** – syringe pump, **HC** – holding coil, **MV** – multiport valve, **D** – detector, **MO** – microscope objective, **PT** – photomultiplier tube.

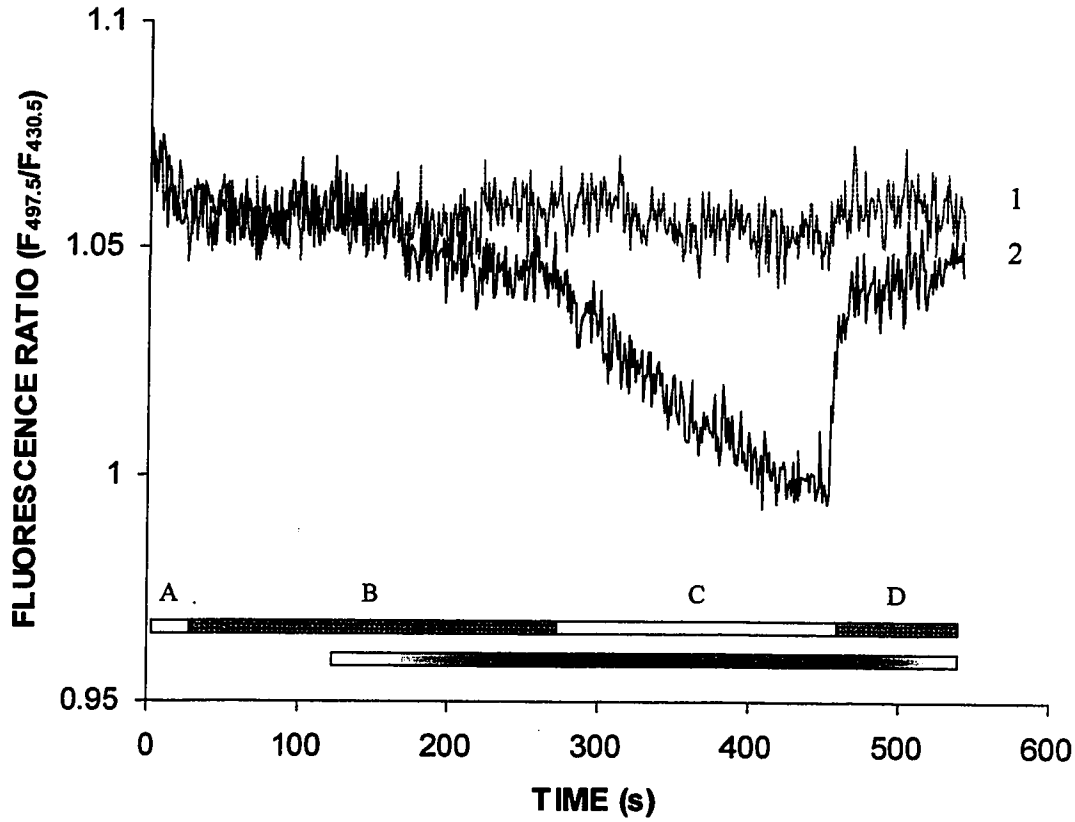

Figure 4-2 Extracellular acidification in the absence and presence of glucose. 1- blank injection of glucose-free buffer; 2 – injection of 10 mM glucose. Top bar, sequential injection protocol: **A** - aspirate sample solution into sequential injection manifold; **B** – deliver aspirated sample onto cells; **C** - stop the sample onto cells for 3 min; **D** - wash out. Bottom bar, exposure to injected sample. Cells were grown on Cytodex-2 microcarrier beads.

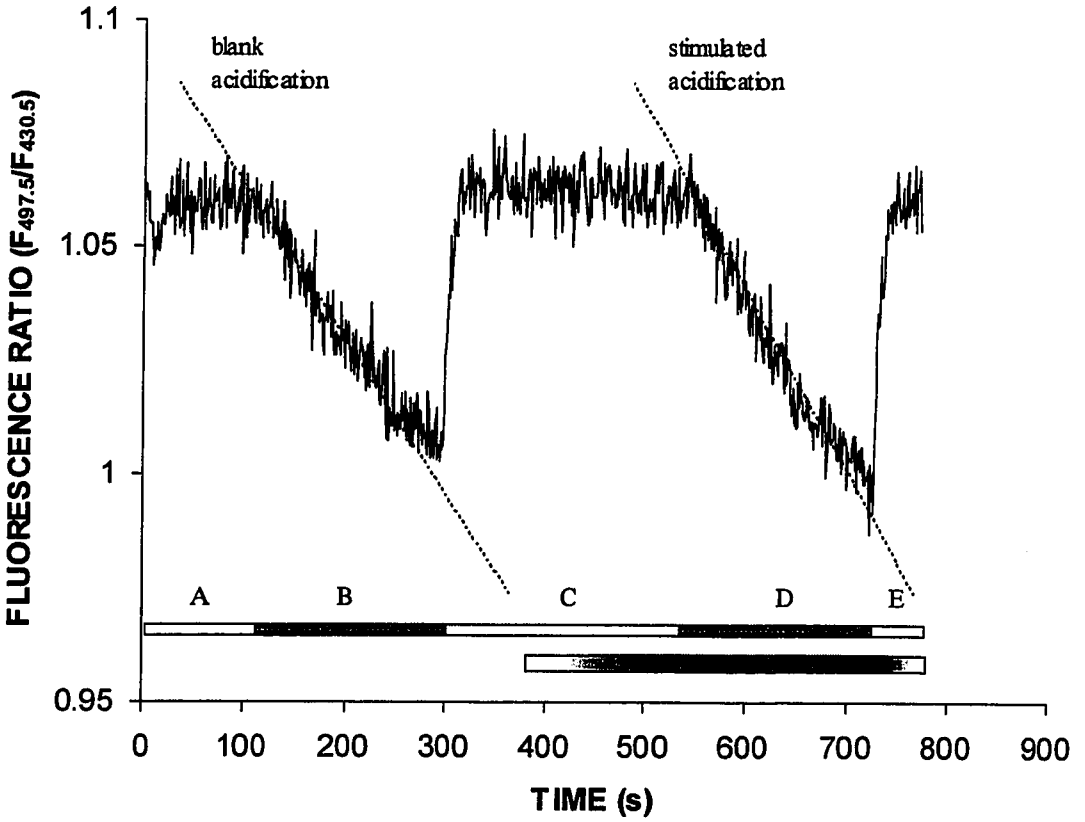

Figure 4-3 Response quantitation based on extracellular acidification. Acidification in response to the blank and the stimulant is measured during the stop periods as indicated. Top bar, sequential injection protocol: **A** - aspirate buffer and deliver it onto cells; **B** - stop the buffer onto cells for 3 min; **C** - aspirate stimulant and deliver it onto cells; **D** - stop the stimulant onto cells for 3 min; **E** - wash out. Bottom bar, exposure to carbachol.

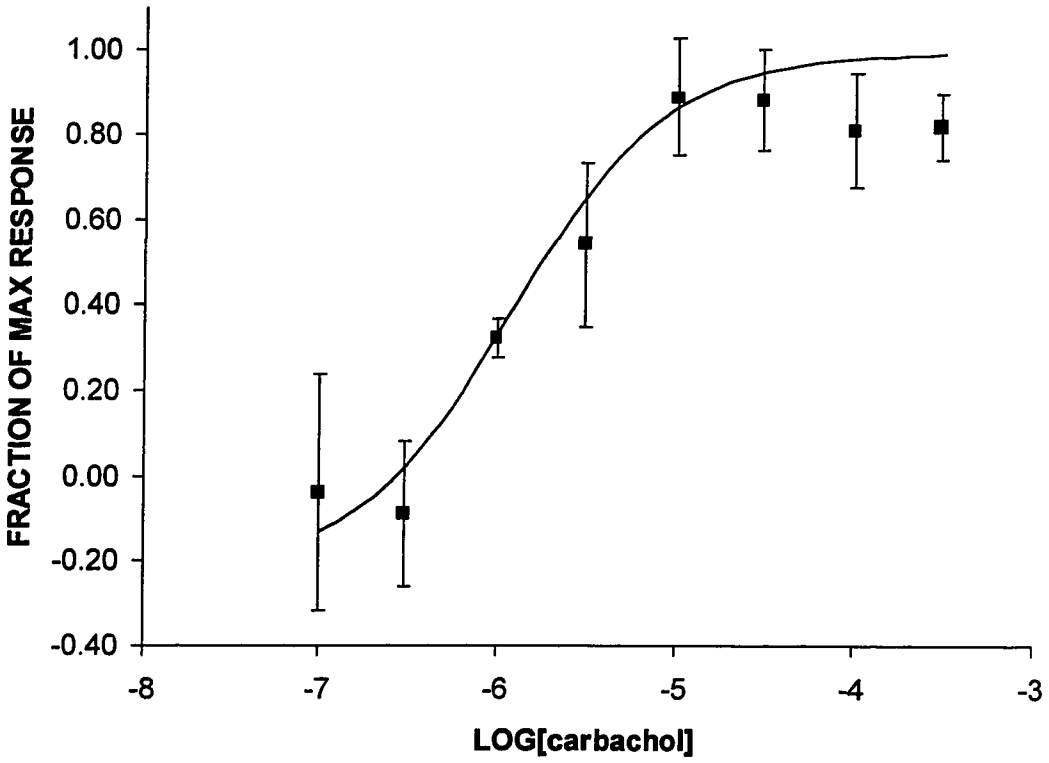

Figure 4-4 Extracellular acidification response data and a fit to the theoretical stimulus-response model. Each data point is an average of four independent measurements.

Notes to Chapter 4

[1] Haugland R.P. *Handbook of fluorescent probes and research chemicals*, 6th ed., Molecular Probes, Eugene, OR, 1996.

[2] McConnell H.M., Owicki J.C., Parce J.W., Miller D.L., Baxter G.T., Wada H.G., Pitchford S. *Science*, **1992**, *257*, 1906-1912.

[3] Lähdesmäki I., Beeson C., Ruzicka J. unpublished results

[4] Ruzicka J., Scampavia L.D. *Anal. Chem.*, **1999**, *71*, 257A-263A.

[5] Katzung B.G. *Basic and clinical pharmacology*, 7th ed., Appleton & Lange, Stamford, CT, 1998, Chapter 1.

[6] Hodder P.S., Ruzicka J. *Anal. Chem.* **1999**, *71*, 1160-1166.

[7] Baxter G.T., Young M.-L., Miller D., Owicki J.C. *Life Sciences*, **1994**, *55*, 573-583.

[8] Pitchford S., Hirst M. *J. NIH Res.*, **1994**, *6*, 84.

Chapter 5 Intracellular pH as a metabolic response indicator

5.1 Background

5.1.1 Possibility of using pH_i for measuring metabolic acid production

It is obvious to raise a question of whether *intracellular* pH measurements could be used to quantitate metabolic acid production. What makes intracellular pH so attractive as a stimulation parameter is the fact that the detection volume is restricted by the cell membrane to the volume inside a single cell, or, rather, to multiple separate volumes corresponding to the number of cells in the field of view of the detector. All acid generated by the cellular metabolism is, naturally, produced and confined within the cell. Since the cell membrane shields the generated acid against dilution by diffusion and convection, only very small amounts of acid should be needed to create observable changes in pH.

It was shown earlier (Chapter 2 and Chapter 3) that perturbations caused by stimulation of CHO M1 cells are manifested as changes in intracellular pH. The remaining question is whether the observed changes show dose-dependent variation that would allow the use of pH_i to quantitatively characterize the cells' response to drugs.

5.1.2 Earlier uses of pH_i

Intracellular pH measurements – potentiometric or fluorescent – in themselves are anything but new. They have been used extensively for studies of cell pH in different physiological conditions, particularly to study pH regulation mechanisms in cells [1,2]. Even the idea of using intracellular pH as a quantitative dose-response indicator is not new. However, most of its previous uses in dose-response quantitation have been re-

stricted to cases where the stimulant modulates the activity of the Na^+/H^+ exchanger protein on the cell membrane either directly or indirectly, which usually results in dose-dependent intracellular alkalization (e.g. [3-5]). There are also reports of dose-dependent intracellular acidification [6-8] and mixed responses (acidification followed by alkalization) [9,10]. In the latter two cases, alkalization is again due to modulation of the Na^+/H^+ exchanger but the exact mechanism of acidification does not seem to have been resolved. One could argue, though, that any event that changes cellular acid extrusion should at least to some extent be manifested in intracellular pH as well. If this were true, intracellular pH could be used as a general stimulation indicator in the same way acid extrusion measurements are used at the moment – not just in cases where stimulation is coupled to modulation of a H^+ antiport, but in any event where the cellular metabolism is accelerated.

5.1.3 Bead injection techniques for intracellular measurements

Bead injection has been used very successfully for measuring cell stimulation based on fluorescent detection of intracellular Ca^{2+} mobilization in CHO M1 cells [11]. The technique was shown to provide a signal-to-noise ratio clearly superior to traditional Ca^{2+} assays where cells are observed as a monolayer on a microscope coverslip. Further, it allows quick renewal of the observed cells, so that each assay can be performed on a fresh set of cells. Due to the close similarity of the use of intracellular Ca^{2+} and pH indicators, the bead injection methodology developed for Ca^{2+} measurements should be easily applicable intracellular pH measurements.

5.2 Experimental

5.2.1 Cells and reagents

The working buffer used in the measurements was a phosphate buffered balanced salt solution (0.3 mM $CaCl_2$, 0.6 mM $MgCl_2$, 0.5 mM KH_2PO_4, 0.5 mM Na_2HPO_4, 3 mM

KCl, 0.13 M NaCl) with 1 g/l bovine serum albumin, 10 mM glucose and 10 mM HEPES. pH was adjusted to 7.3.

Cytodex-2 beads were prepared as described in section 4.2.1, except that they were left unlabeled. CHO M1 cells were grown on the beads in exactly the same manner as in section 4.2.1. Immediately prior to the experiments, 1.3 mL of the bead suspension was transferred into a 15 mL conical tube. The beads were allowed to settle and the supernatant was aspirated out. The beads were re-suspended in 2 mL of 2 μM BCECF-AM in the working buffer and left in the incubator (at 37 °C) for 30 min, which caused the cells on the beads to become stained with BCECF. The beads were washed twice with the working buffer and finally suspended in 10 mL. A 100 μL aliquot of the diluted suspension was aspirated into the sequential injection manifold to pack a column of beads and cells for each assay.

5.2.2 Data processing

The raw data were converted to the ratiometric form: $R(t_i)=F_{\lambda 1}(t_i)/F_{\lambda 2}(t_i)$, where $F_{\lambda 1}(t_i)$ is the emission detected after excitation from channel 1 and $F_{\lambda 2}(t_i)$ the emission detected after excitation from channel 2.

5.2.3 Instrumentation

The instrumental arrangement was as described in section 4.2.2, except that the excitation wavelength on channel 1 was set at 490 nm instead of 497.5 nm.

5.2.4 Experimental protocol for BIS technique

The protocol was the same as described in section 4.2.3.

5.3 Results and discussion

In contrast to the acid extrusion response, the changes in intracellular pH of the CHO M1 WT3 cells during carbachol stimulation are complex (see Figure 5-1). Instead of simple acidification or alkalization, the response is a combination of both: an initial phase of acidification is followed by gradual alkalization that brings the pH back towards the original level (the pH recovery phase). Therefore, it is not immediately evident how the degree of stimulation should be measured. Some choices for a stimulation indicator are acidification rate, maximum acidification, pH recovery rate, total pH recovery and the net pH change (see Figure 5-2). The stimulus-response curves constructed based on these parameters are shown in Figure 5-3.

A clear distinction of stimulation parameters is evident both from Figure 5-1 and Figure 5-3: the acidification response develops mainly at $c_{carbachol} \leq 1$ μM, whereas the pH recovery (i.e. the alkalization) response only becomes observable at $c_{carbachol} \geq 1$ μM. This is not surprising since the two phenomena reflect two different domains in the cellular acid-base balance. Acidification is mainly linked to the acid generating processes (glycolysis, respiration), whereas pH recovery reflects the acid extrusion processes: Na^+/H^+ antiport, Cl-HCO_3^- transporter.

The suitability of each parameter as an indicator of cell stimulation was judged based on the following criteria: 1) the EC_{50} value obtained from the best fit should be the same order of magnitude as the literature value 3 μM, 2) the fit to the theoretical model should be reasonably good, 3) the data should show little scatter. Total pH recovery satisfies the criteria the best; choosing it as the stimulation parameter yields an EC_{50} of 4 μM and a good fit to the theoretical equation with r^2=0.996 (Fig. 8). This value compares well to the 1 μM obtained by acid extrusion measurements above.

5.4 Conclusions

The complexity of the intracellular pH response is a disadvantage in that the responses are more difficult to interpret, but it offers a valuable insight into the acid generation and pH regulation processes, whereas external pH measurements either only sense the effects of pH regulation or a compound effect where acid generation and extrusion remain unresolved. Indeed, intracellular pH measurements reveal differences in cell responses that remain hidden when acid extrusion measurements (see sections 3.3.2 and 3.3.3) are carried out.

Thus, intracellular pH can serve as a versatile indicator of cellular responses since both intracellular acidification and pH recovery of the CHO M1 cells are proportionally dependent on the concentration of carbachol they are exposed to. The total pH recovery (parameter 4 in Figure 5-2, see also Figure 5-4) turns out to be most useful since it gives the best fit to the classical model and shows the least scatter.

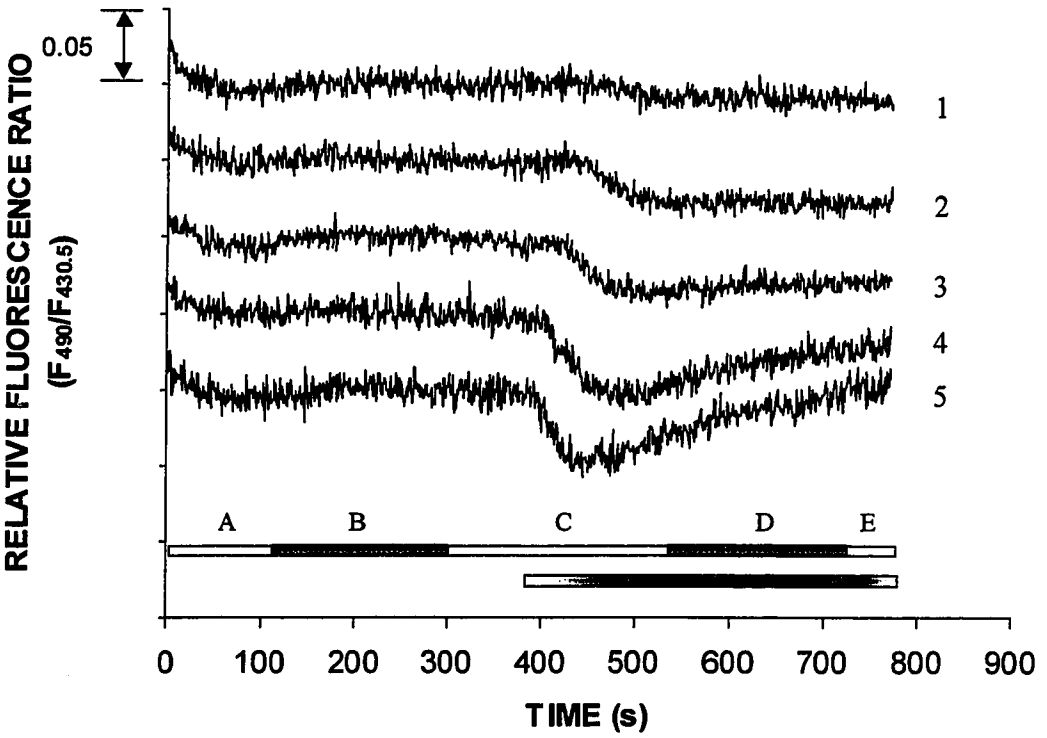

Figure 5-1 Response to carbachol in terms of intracellular pH. **1**- (0.1 μM); **2** – (0.3 μM); **3** – (1 μM); **4** – (10 μM); **5** – (100 μM) carbachol. Top bar, sequential injection protocol: **A** - aspirate buffer and deliver it onto cells; **B** - stop the buffer onto cells for 3 min; **C** - aspirate stimulant and deliver it onto cells; **D** - stop the stimulant onto cells for 3 min; **E** - wash out. Bottom bar, exposure to carbachol. The curves have been offset by 0.05 ratio units for visual clarity. Cells were grown on Cytodex-2 microcarrier beads.

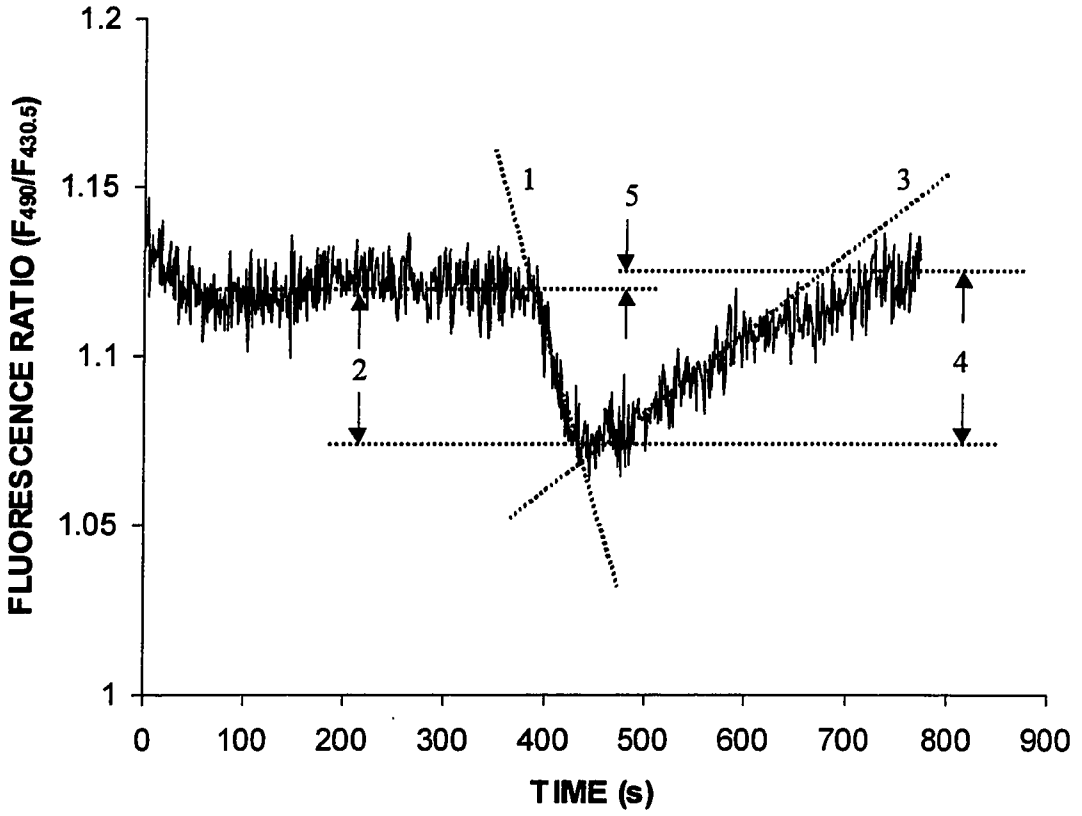

Figure 5-2 Possible parameters for response evaluation based on intracellular pH measurements. **1** – acidification rate, **2** – maximum acidification, **3** – initial pH recovery rate, **4** – total pH recovery, **5** – net pH change ($pH_{\text{after stimulation}} - pH_{\text{before stimulation}}$).

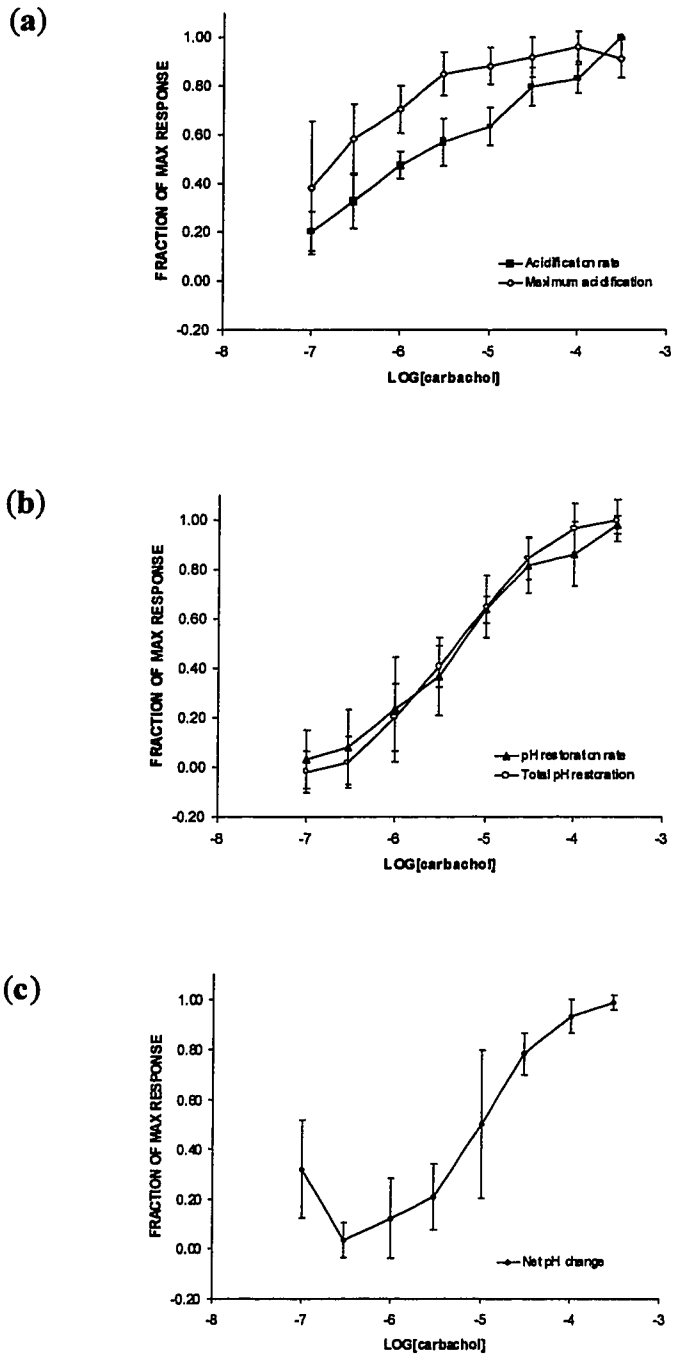

Figure 5-3 Intracellular pH response data, evaluated by different parameters. Each data point is an average of four independent measurements.

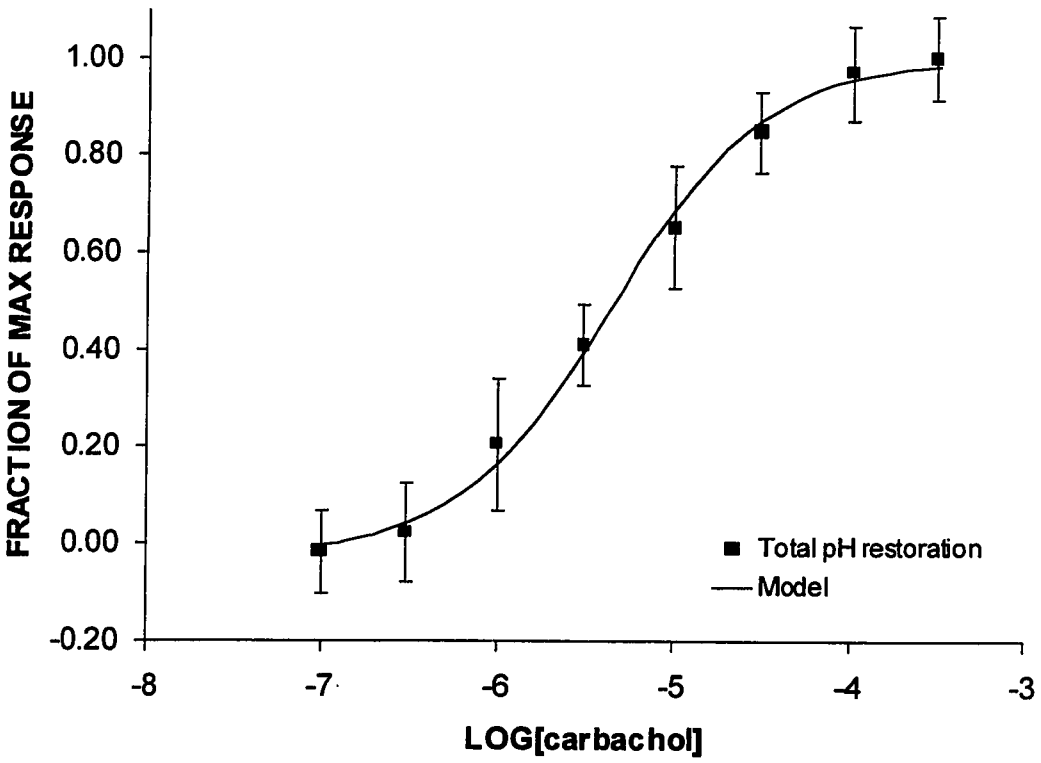

Figure 5-4 A fit of the classical dose-response model into intracellular pH response data, as evaluated by the total pH recovery.

Notes to Chapter 5

[1] Boyer M.J., Hedley D.W. *Meth. Cell. Biol.*, **1994**, *41*, 135-148.

[2] Haugland R.P. *Handbook of fluorescent probes and research chemicals*, 6th ed., Molecular Probes, Eugene, OR, 1996, p. 554.

[3] Incerpi S., Rizvi S.I., DeVito P., Luly P. *J. Cell Physiol.*, **1997**, *171*, 235-242.

[4] Touyz R.M., Schiffrin E.L. *Hypertension*, **1997**, *30*, 1440-1447.

[5] Poch E., Botey A., Gaya J., Cases A., Rivera F., Revert L. *Biochem. J.*, **1993**, *290*, 617-622.

[6] Ekokoski E., Törnquist K. *Biochim. Biophys. Acta*, **1994**, *1223*, 274-278.

[7] Staub F., Winkler A., Peters J., Kempski O., Kachel V., Baethmann A. *J. Cereb. Blood Flow Metab.*, **1994**, *14*, 1030-1039.

[8] Bidet M., Tauc M., Gastineau M., Poujeol P. *Pflugers Arch.*, **1992**, *421*, 523-529.

[9] Azuma E.K., You A., Matsushima K., Kasahara T., Mizoguchi H., Saito M., Takaku F., Kitagawa S. *Exp. Hematol.*, **1996**, *24*, 169-175.

[10] Ohara T., Takeda K., Asano Y. *Jpn. Circ. J.*, **1992**, *56*, 133-141.

[11] Hodder P.S., Ruzicka J. *Anal. Chem.* **1999**, *71*, 1160-1166.

Chapter 6 Detection of oxygen consumption of cultured adherent cells

6.1 Background

6.1.1 Role of oxygen in the energy metabolism

In the aerobic metabolism, oxygen is constantly being consumed for energy production (see section 1.2.2). More precisely, oxygen is used as electron acceptor at the end of the pathway of glucose oxidation. This is a conjugate pathway consisting of glycolysis, citric acid cycle, electron transport and oxidative phosphorylation; the net stoichiometric equation for the overall process is[1]:

$$\text{glucose} + 6\,O_2 + \sim 30\,\text{ADP} + \sim 30\,P_i \rightarrow 6\,CO_2 + \sim 30\,\text{ATP} + \sim 36\,H_2O$$

where ADP stands for adenosine diphosphate, ATP for adenosine triphosphate and P_i for PO_4^{3-}.

6.1.2 Measurement of cellular oxygen consumption

Since oxygen plays such a crucial role in the aerobic energy metabolism, oxygen consumption measurements can be used to study biochemical events where some part of the aerobic pathway is affected [2,3]. There are several good methods for measuring oxygen consumption of cultured cells in suspension. These methods include the amperometric Clark electrode [4,5], the use of a phosphorescent oxygen indicator in the cell suspension [3,6] and electron paramagnetic resonance spectroscopy [2]. The phosphorescent method has also been successfully used to map oxygen consumption in a tissue sample [7]. However, there does not seem to be reports on using any of these

methods on adherent cell cultures. This may be due to the fact that adherent cells are most commonly cultured as monolayers on flat solid substrates. The limited number of cells in a monolayer will be small compared to the volume of the bathing solution, which makes it difficult to detect oxygen consumption within reasonable time periods.

Since many cell types are naturally adherent, such cultures lend themselves well to studies of cellular responses to biochemical effector molecules and drugs. As described in section 1.3.2, this is typically done by following a relevant cellular parameter, such as intracellular Ca^{2+} (or other second messenger concentration), pH, acid extrusion rate or membrane potential, while exposing cells to the effector agent. The lack of a convenient oxygen consumption assay means that oxygen consumption cannot easily be included among the monitored parameters. This is a significant deficiency since all primary cells are aerobic and thus there is a wide range of cases where oxygen measurements could potentially be applied.

6.1.3 Luminescent oxygen sensing

Luminescent O_2 sensing is based on the ability of O_2 to quench the fluorescence or the phosphorescence of certain fluorophores and phosphors, respectively, in a concentration dependent manner. Viewed on the molecular level, the mechanism of the process is that of dynamic quenching, meaning that quenching is brought about by collisions between O_2 and the excited luminescent indicator molecules. Viewed on the electronic level, different quenching mechanisms exist depending on the multiplicity and the energy level structure of the excited indicator molecule [8]. For the most usual luminescent O_2 indicators, the predominant path seems to be energy transfer between the excited indicator molecule (X*) and ground state triplet oxygen, leading to formation of ground state indicator and singlet oxygen [9-11]:

$$X^* + {}^3O_2 \rightarrow X + {}^1O_2$$

The dependence of the observed luminescent intensity on oxygen concentration can be understood by considering some of the pathways by which the excited indicator molecule can relax (Table 6-1).

Detected luminescent intensity will depend on the rate of the radiative decay relative to the rates of non-radiative decay and quenching. The fraction of excited molecules undergoing luminescence emission can be expressed in terms of the decay rates:

$$\frac{k_r[X]}{k_r[X]+k_{nr}[X]+k_q[X][O_2]} = \frac{k_r}{k_r+k_{nr}+k_q[O_2]}$$

In the absence of O_2, the luminescent fraction of excited molecules will be:

$$\frac{k_r}{k_r+k_{nr}+k_q\cdot 0} = \frac{k_r}{k_r+k_{nr}}$$

The observed luminescence intensity is directly proportional to the luminescent fraction of excited molecules. Denoting the observed intensity in the absence of oxygen by I_0 and the intensity in the presence of a certain O_2 concentration by I, we can write:

$$\frac{I_0}{I} = \frac{k_r}{k_r+k_{nr}} \cdot \frac{k_r+k_{nr}+k_q\cdot[O_2]}{k_r} = 1+K_{SV}[O_2]$$

The above expression is the so-called Stern-Volmer equation ([12]), and $K_{SV} = k_q/(k_r + k_{nr})$ is the Stern-Volmer quenching constant. The equation shows that the detected signal (I) is in inverse proportion to the O_2 concentration. This is in contrast to the Clark oxygen electrode where the signal (reduction current) is directly proportional to $[O_2]$.

A variety of different indicators have been applied to luminescent O_2 sensing [13]. Polycyclic aromatic hydrocarbons (e.g. pyrene, diphenylanthracene) are fairly photostable and efficiently quenched by oxygen, but have the disadvantage of requiring excitation deep in the UV range. Certain transition metal complexes, on the other hand, display strong absorptive transitions in the visible region, combined with chemical stability and strong oxygen sensitivity of the luminescence emission. The most popular of them are the Ru(II)-bipyridine and Ru(II)-phenylphenantroline complexes, whose properties and some applications are described in ref. [14]. Another class of popular luminescent O_2 indicators are Pt- and Pd-complexes of different porphyrin derivatives [11, 15]. Oxygen-dependent quenching of Pt-porphyrin phosphorescence has been widely utilized in pressure-sensitive paints [16]. A recent review on luminescent pressure-sensitive paints provides an excellent overview of both the theory and the practical aspects of phosphorescent oxygen sensing [11].

6.1.4 Choice of detector configuration for O_2 consumption measurements

Detection of cellular oxygen consumption is achieved through measurement of the extracellular oxygen concentration, i.e. by probing a quantity of the bulk solution surrounding the cells. In other words, the situation is similar to the acid release measurements that were carried out by probing the extracellular pH. For this reason, the requirements for the O_2 detector configuration are much the same as the requirements for acid release detection listed in section 4.1.2.: the main concerns are restriction of the volume and movement of the extracellular solution, as well as the proximity of the sensing element to the cells. Since the bead injection technique has already been shown to satisfy these requirements, it is the natural choice as the technique for cellular O_2 measurements.

6.2 Experimental

6.2.1 Preparation of oxygen sensor beads

Pt-tetra(paracarboxy-phenyl)porphyrin tetraethyl ester (Pt-(p-COOEt)$_4$PP) was provided by prof. Martin Gouterman (University of Washington, Dept. of Chemistry). It was converted to free acid form as described in literature [17]. Briefly, 5.5 mg Pt-(p-COOEt)$_4$PP was added to 10 mL of dimethylformamide and refluxed under stirring until all the solid was dissolved. Addition of 0.8 mL aqueous 1 M NaOH under reduced heat resulted in formation of the free acid (Pt-(p-COOH)$_4$PP) as a precipitate. Further addition of water dissolved most of the precipitate, and the resulting solution was kept on gentle heat for 2 h to ensure complete reaction. The solvent was removed using a rotovap and the obtained solid was redissolved in water. Pt-(p-COOH)$_4$PP was re-precipitated by addition of 1.5 mL 2 M HCl. Again, the solvent was removed by a rotovap and the solid Pt-(p-COOH)$_4$PP was finally dissolved in 6 mL 0.010 M aqueous NaOH to yield the Pt-(p-COOH)$_4$PP stock solution used for preparing the oxygen indicator beads.

Cytodex-3 microcarrier beads were prepared by letting dry bead powder swell overnight in balanced salt solution. The beads were then sterilized by soaking in 95% ethanol for 2-3 h, washed repeatedly with balanced salt solution and finally suspended in cell culture medium. The phosphorescent oxygen probe was attached to Cytodex-3 microcarrier beads non-covalently by adding 40 µL Pt-(p-COOH)$_4$PP stock solution to a (wet) volume of 80 µL Cytodex-3 beads suspended in 1 mL phosphate buffer. The suspension was gently shaken periodically, and all the Pt-(p-COOH)$_4$PP was taken up by the beads in a matter of minutes.

6.2.2 Instrumentation

The instrumental setup was identical to that described in section 4.2.2. The only alterations were the different spectral regions for excitation and emission, required by the different luminescent probe. The measurements were performed with the excitation wavelength set at 509 nm. The optical filter system consisted of a 560 nm dichroic mirror and a 550 nm longpass emission filter.

6.2.3 Experimental protocol for BIS technique

The bead injection protocol for drug assays is described in Table 6-2. Each assay was repeated four times. Each assay was followed by measurement of the sensor signal in a deoxygenated solution. This was done to improve the reliability of sensor output, as discussed in section 6.2.4.

The sensor response was calibrated by perfusing the sensor with buffer solutions containing different levels of dissolved O_2. The O_2 concentrations were adjusted by purging the solutions with air and N_2 at controlled flow rates. VCD-1000 flow controllers (Porter Instrument Co., Hatfield, PA) were used to achieve steady gas flow rates. Dissolved O_2 was expressed as the partial O_2 pressure in the purging gas (taking partial O_2 pressure in air to be 0.21 atm).

6.2.4 Data processing

The Stern-Volmer equation can be rearranged to obtain an expression that is directly proportional to O_2 concentration:

$$\frac{I_0}{I} - 1 = K_{SV}[O_2]$$

Raw luminescence intensity data (I) from all experiments were converted into (I_0/I)-1 for further data analysis and/or presentation. In addition to achieving direct proportionality to O_2 concentration, the transformation also makes the data independent of indicator concentration on the beads and the number of beads seen by the detector in any particular experiment.

In order to evaluate the effect of a drug on the cellular aerobic metabolism, the O_2 consumption in the presence of a drug (step 7 in Table 6-2) was divided by the O_2 consumption of the same cells in the absence of the drug (step 4 in Table 6-2):

$$\text{Relative O}_2\text{ cons.} = \frac{\Delta O_2(\text{drug})}{\Delta O_2(\text{no drug})} = \frac{[(I_0/I)-1]_{drug}}{[(I_0/I)-1]_{no\ drug}}$$

This treatment makes the data independent of the number of cells packed into the flow cell in any particular experiment. Thus, it allows reliable comparison of data from different runs.

6.3 Results

6.3.1 Detection optimization

In order for the cellular metabolism to consume oxygen to a detectable degree, it was necessary to stop the flow. It was observed, however, that the sensing mechanism alone also consumed oxygen at a high enough rate to significantly decrease the O_2 concentration in the monitored volume in stopped flow conditions. Such effects have been observed earlier (the so-called induction effect in pressure-sensitive paints) and can most likely be attributed to the singlet oxygen produced in the sensing event.[10] Since singlet oxygen is very reactive, it will react with components of the surrounding matrix or

solution, thus removing itself from the O_2 pool. The behavior is analogous to O_2 consumption by the amperometric Clark electrode.

The sensing-related decrease in O_2 was strongly dependent on illumination intensity and choosing the minimal intensity that still yielded a good signal-to-noise ratio helped bring down this undesired effect considerably. The magnitude of the effect in optimal conditions is shown in Figure 6-1a: the decrease in (I_0/I)-1 with illumination off is purely due to cellular oxygen consumption, whereas the decrease observed with illumination on represents oxygen consumption by the cells and the sensing. It can be seen that even in optimized conditions the sensing-related consumption is comparable to the cellular consumption. Therefore, it was necessary to keep illumination switched off for most of the stopped flow period. Illumination was only switched on for the last 6 s of the stopped flow period to record the final level of O_2 around the cells. Oxygen consumption (ΔO_2) was measured as shown in Figure 6-1b.

6.3.2 Sensor calibration

The sensor response showed good agreement with the Stern-Volmer equation in the range 0-0.17 atm O_2, and some deviation from it in the range 0.17-0.21 atm. Fitting five data points in the 0-0.17 atm range to the Stern-Volmer equation yielded a calibration equation $I_0/I = 0.87 + 23 \cdot p(O_2)$, with r^2=0.998.

6.3.3 Drug responses

The effects of exposing the cells to different drugs are shown in Figure 6-2. Relative O_2 consumption values of >1 and <1 indicate increased and decreased consumption, respectively, induced by the drug. Amobarbital, an agent that blocks a step (Complex 1) in the aerobic electron transport chain [1,18], is seen to strongly diminish the cellular

O_2 consumption when administered to the cells in a 1.5 mM dose. This can be taken as proof that the sensor is truly probing the aerobic O_2 consumption of the cells.

Exposing the cells to 100 μM carbachol results in an increase in O_2 consumption. Carbachol is a drug that binds to the m1 muscarinic receptors expressed in the CHO M1 WT3 cells and elicits a response in them [19]. The carbachol action, however, is not directly linked to the aerobic energy metabolism, as opposed to the amobarbital action above. The carbachol-induced increase in aerobic turnover must therefore be a more general effect of cell stimulation on the aerobic metabolism. Exposure of the cells to carbachol in the presence of 10 μM atropine does not result in such an increase. Atropine prevents binding of carbachol to m1 receptors - therefore, this experiment confirms that the previously observed increase in O_2 consumption must be due to cell stimulation caused by carbachol binding to the m1 receptors.

6.4 Conclusions

The chapter described a method for detection of O_2 consumption by adherent cell cultures within a time frame of minutes. Its operation is based on the following advantages given by the bead injection-based reagent handling and optical O_2 sensing:

1) Bead injection allows packing a relatively large number of adherent cells (on the order of 10^4) in a small (ca. 3 μL) volume, in a closed environment. This is an absolute requirement for being able to detect O_2 consumption within the minute time scale. A graphical comparison of the open and closed setups is shown in Figure 6-3.
2) Bead injection also allows rapid renewal of inspected cells. Thus, each assay can be conducted on a fresh set of cells.
3) Optical O_2 sensing allows placement of the sensing element right next to the cells. Consequently, O_2 consumption can be measured on the spot rather than down-

stream, resulting in maximal sensitivity because the deoxygenated solution is not diluted.

4) In this case, optical and electrochemical detection share the disadvantage that detection itself consumes oxygen. However, the optical method still retains the advantage that it can be switched on without a charging current that initially obscures the signal.

The three minute period needed for reliable quantitation of O_2 consumption compares favorably to existing measurement techniques for suspended cell cultures [2,3]. It should be further pointed out that the cultured cells, both in this work and the above references, were obtained from immortal cell lines, which typically derive most of their energy through the anaerobic pathway. Application of any of these techniques to primary cell cultures, which are fully aerobic and thus consume far greater amounts of O_2, should necessitate even shorter measurement periods.

It was demonstrated that stimulation of the muscarinic m1 receptors on the CHO M1 WT3 cells increases their oxygen consumption. These results are especially interesting since the rate of the overall (i.e. aerobic + anaerobic) cellular energy metabolism has been shown to reflect a broad array of perturbations in a cell's environment caused by various biochemical effector agents [20]. Presently, the overall metabolic rate is quantitated by measuring the rate of CO_2 and lactic acid extrusion from the cells with the commercial Cytosensor Microphysiometer®. The results presented in this chapter indicate that O_2 measurements might be used as an alternative, or complementary, indicator of stimulation for aerobic cells.

Table 6-1 The most usual competing decay mechanisms for luminescent O_2 indicators. k_r, k_{nr} and k_q are the rate constants of the different decay processes. Other possible pathways, such as intersystem crossing and charge transfer, are left out for simplicity.

Type of decay	*Reaction scheme*	*Decay rate*
radiative decay	$X^* \rightarrow X + h\nu$	$k_r[X^*]$
non-radiative decay (internal conversion)	$X^* \rightarrow X$	$k_{nr}[X^*]$
O_2-mediated quenching	$X^* + {}^3O_2 \rightarrow X + {}^1O_2$	$k_q[X^*][O_2]$

Table 6-2 Bead injection protocol used in the oxygen consumption assays.

BI step	*Illumination*	*Recorded event*
1. Pack beads	OFF	
2. Wash beads	OFF	
3. Aspirate blank and deliver onto cells	OFF→ON	baseline
4. Stop flow for 180 s:		
a. 174 s	OFF	
b. 6 s	ON	O_2 consumption in absence of drug
5. Wash beads	ON→OFF	
6. Aspirate drug and deliver onto cells	OFF→ON	baseline
7. Stop flow for 180 s:		
a. 174 s	OFF	
b. 6 s	ON	O_2 consumption in presence of drug
8. Wash beads	ON→OFF	
9. Discard beads	OFF	

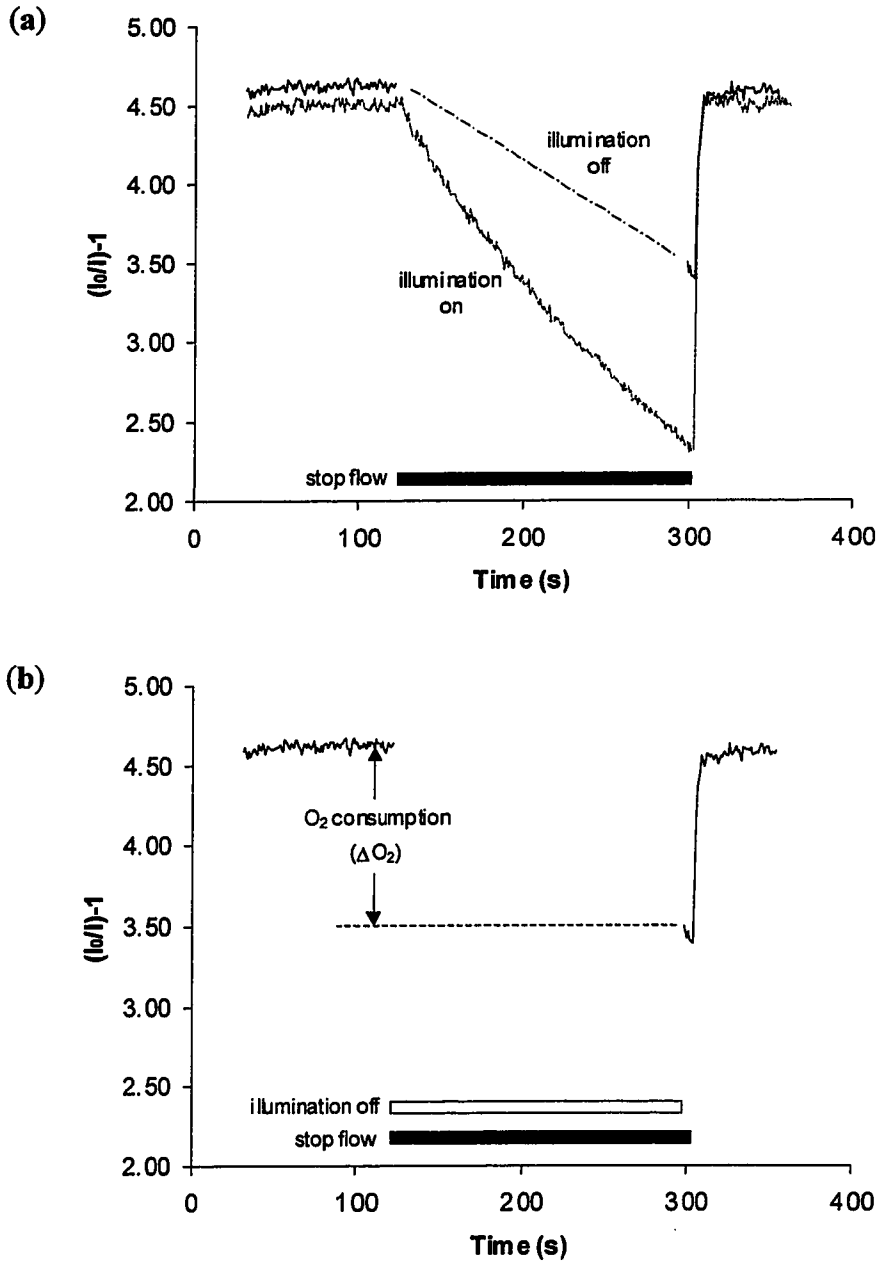

Figure 6-1 (a) Oxygen depletion during stopped flow period with illumination on (consumption due to cells and sensing, grey trace) and illumination off (consumption due to cells only, black trace). The dashed line represents the approximate oxygen consumption trend during the "illumination off" period. (b) Measurement of cellular oxygen consumption as the difference between the initial baseline (average of ten data points before switching off illumination) and the level at the end of the stopped flow period (average of the first two data points after switching on illumination). Cells were grown on Cytodex-3 microcarrier beads.

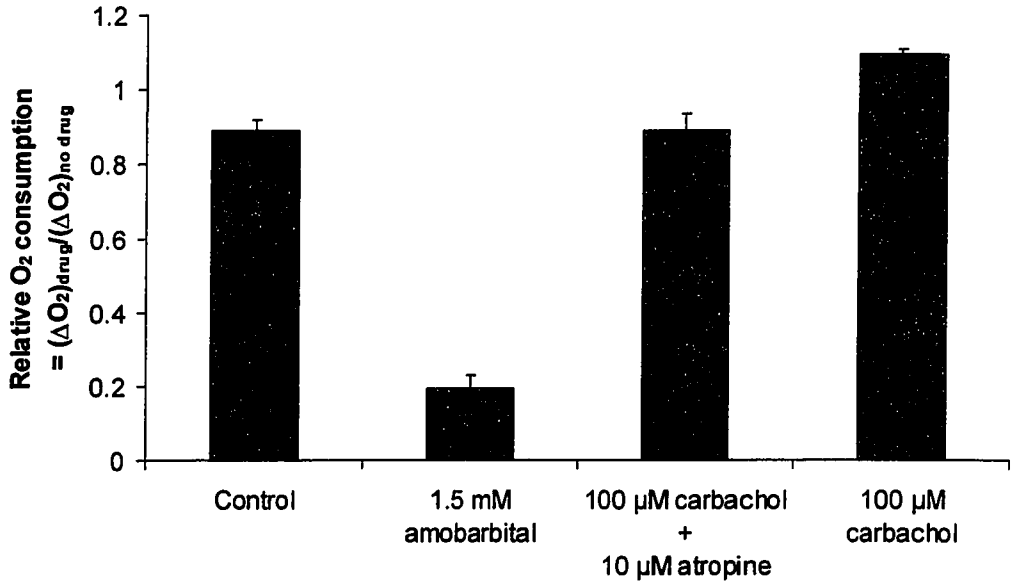

Figure 6-2 Oxygen consumption by the CHO M1 WT3 cells exposed to 1.5 mM amobarbital, 100 µM carbachol + 10 µM atropine and 100 µM carbachol. The control refers to basal oxygen consumption measured in plain phosphate buffer. The reported standard deviations are based on four experiments (n=4).

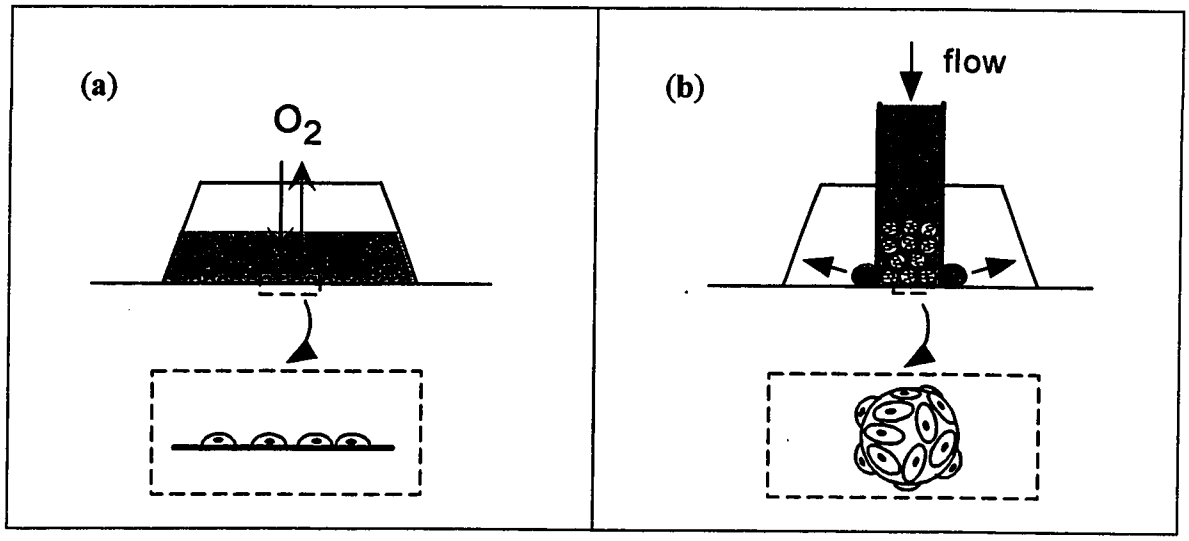

Figure 6-3 (a) Conventional setup for inspection of adherent cells by microscope, where cells are grown as a monolayer on the glass bottom of a microscope chamber. The open architecture causes consumed O_2 to be replenished from surrounding air. (b) Bead injection flow through chamber has microcarrier beads packed inside a steel tube pressed against the glass bottom of a microscope chamber. Pumped liquid can trickle through the junction between the steel and glass but exchange of O_2 between the bead layer and air is negligible.

Notes to Chapter 6

[1] Garrett R.H., Grisham C.M. *Biochemistry*, Saunders College Publishing: Orlando, 1995; Chapter 20.

[2] James P.E., Jackson S.K., Grinberg O.Y., Swartz H.M. *Free Radic. Biol. Med.* **1995**, *18*, 641-647.

[3] Motterlini R., Kerger H., Green C.J., Winslow R.M., Intaglietta M. *Am. J. Physiol.* **1998**, *275*, H776-H782.

[4] Gesinski R.M., Morrison J.H., Toepler J.R. *J. Appl. Physiol.* **1968**, *24*, 751-754.

[5] Shenoy M.A., Biaglow J.E., Varnes M.E., Hetzel F.N. *Adv. Exp. Med. Biol.* **1983**, *159*, 359-369.

[6] Rumsey W.L., Schlosser C., Nuutinen E.M., Robolio M., Wilson D.F. *J. Biol. Chem.* **1990**, *265*, 15392-15402.

[7] Rumsey W.L., Vanderkooi J.M., Wilson D.F. *Science* **1988**, *241*, 1649-1651.

[8] Saltiel J., Beauford W.A. in Volman D.H., Hammond G.S., Gollnick K. (eds.) *Advances in photochemistry*, vol. 14, Wiley, New York, 1988.

[9] Timpson C.J., Carter C.C., Olmsted J. *J. Phys. Chem.* **1989**, *93*, 4116-4120.

[10] Demas J.N., Harris E.W., McBride R.P. *J. Am. Chem. Soc.* **1977**, *99*, 3547-3551.

[11] Gouterman M. *J. Chem. Edu.* **1997**, *74*, 697-702.

[12] Stern O.. Volmer M. *Physik. Z.* **1919**, *20*, 183-188.

[13] Wolfbeis O.S. in Wolfbeis O.S. (ed.) *Fiber optic chemical sensors and biosensors, vol. II*, CRC Press, Boca Raton, 1991.

[14] Demas J.N., DeGraff B.A. *J. Chem. Educ.*, **1997**, *74*, 690-695.

[15] Vanderkooi J.M., Maniara G., Green T.J, Wilson D.F. *J. Biol. Chem.*, **1987**, *262*, 5476-5482.

[16] Kavandi J., Callis J., Gouterman M., Khalil G., Wright D., Green E., Burns D., McLachlan B. *Rev. Sci. Instrum.* **1990**, *61*, 3340-3347.

[17] Shankland E. *Ph.D. thesis*, University of Washington: Seattle, 1988; Chapter 2.

[18] Slater E.C. *Methods Enzymol.* **1967**, *10*, 48-57.

[19] Buck M.A., Fraser C.M. *Biochem. Biophys. Res. Commun.* **1990**, *173*, 666-672.

[20] McConnell H.M., Owicki J.C., Parce J.W., Miller D.L., Baxter G.T., Wada H.G., Pitchford S. *Science* **1992**, *257*, 1906-1912.

Chapter 7 Summary

The work in the thesis was aimed at designing tools for cell response studies, utilizing the fact that many responses have been noticed to alter the cellular energy metabolism. This goal was achieved by developing the following methods to measure the rate of energy metabolism:

1) detection of metabolic acid generation through acid release measurements
2) detection of metabolic acid generation through intracellular pH changes
3) detection of respiration rate through O_2 consumption measurements

The advantage in measuring metabolic parameters - as opposed to traditional, specific parameters such as [Ca^{2+}], [cAMP] or membrane potential – is that they provide a more universal way of probing the response. The downside of the approach is that the connection between the response and the measured parameter is more complex than it is in the case of the traditional parameters. Both are due to the fact that metabolic parameters are a consequence of the whole response cascade whereas the traditional ones are involved in a specific, integral step in the response.

Future directions of the work would include evaluating the generality of intracellular pH and O_2 consumption responses on different cell lines and drug-receptor systems. In particular, elucidating the utility of O_2 consumption measurements for primary cell lines would be of great interest. Future research in the area of metabolic response measurements could, perhaps, also be enhanced by the use of a fluorescent temperature probe developed by Engeser *et al.* [1]. As mentioned in a recent interview of one of the authors [2], the probe may make it possible to probe the metabolic activity in a cell through the heat released in energy generation.

Notes to Chapter 7

[1] Engeser M., Fabbrizzi L., Licchelli M., Sacchi D. *Chem. Commun.*, **1999**, 1191-1192.

[2] *Chemical and engineering news*, **1999**, *July 12*, 6.

BIBLIOGRAPHY

Alberts B., Bray D., Lewis J., Raff M., Roberts K., Watson J.D. *Molecular Biology of the Cell*, Garland Publishing, New York, 3rd ed., 1994.

Austin C., Dilly K., Eisner D., Wray S. *Biochem. Biophys. Res. Commun.* **1996**, *222*, 537-540

Azuma E.K., You A., Matsushima K., Kasahara T., Mizoguchi H., Saito M., Takaku F., Kitagawa S. *Exp. Hematol.*, **1996**, *24*, 169-175.

Baxter G.T., Young M.-L., Miller D., Owicki J.C. *Life Sciences*, **1994**, *55*, 573-583.

Bianchini L., Pouyssegur J. *J. Exp. Biol.*, **1994**, *196*, 337-344.

Bidet M., Tauc M., Gastineau M., Poujeol P. *Pflugers Arch.*, **1992**, *421*, 523-529.

Boron W.F. in Seldin D.W., Giebisch G. (eds) *The Regulation of Acid-Base Balance*, Raven Press, New York, 1989, Chapter 2.

Boyer M.J., Hedley D.W. *Meth. Cell. Biol.*, **1994**, *41*, 135-148.

Buck M.A., Fraser C.M. *Biochem. Biophys. Res. Commun.* **1990**, *173*, 666-672.

Busa W.B. *Ann. Rev. Physiol.*, **1986**, *48*, 389-402.

Chaillet J.R., Amsler K., Boron W.F. *Proc. Natl. Acad. Sci. USA*, **1986**, *83*, 522-526.

Chemical and engineering news, **1999**, *July 12*, 6.

Demas J.N., DeGraff B.A. *J. Chem. Educ.*, **1997**, *74*, 690-695

Demas J.N., Harris E.W., McBride R.P. *J. Am. Chem. Soc.* **1977**, *99*, 3547-3551.

Egorov O., Ruzicka J. *Analyst* **1995**, *120*, 1959-1962.

Ekokoski E., Törnquist K. *Biochim. Biophys. Acta*, **1994**, *1223*, 274-278.

Engeser M., Fabbrizzi L., Licchelli M., Sacchi D. *Chem. Commun.*, **1999**, 1191-1192.

Frelin C., Vigne P., Ladoux A., Lazdunski M. *Eur. J. Biochem.*, **1988**, *174*, 3-14.

Garrett R.H., Grisham C.M. *Biochemistry*, Saunders College Publishing, Orlando, 1995.

Gesinski R.M., Morrison J.H., Toepler J.R. *J. Appl. Physiol.* **1968**, *24*, 751-754.

Gouterman M. *J. Chem. Edu.* **1997**, *74*, 697-702.

Graber M.L., DiLillo D.C., Friedman B.L., Pastoriza-Munoz E. *Anal. Biochem.*, **1986**, *156*, 202-212.

Grinstein S., Cohen S., Rothstein A. *J. Gen. Physiol.*, **1984**, *83*, 341-369.

Grynkiewicz G., Poenie M., Tsien R.Y. *J. Biol. Chem.*, **1985**, *260*, 3440-3450.

Haugland R.P. *Handbook of Fluorescent Probes and Research Chemicals*, Molecular Probes, Eugene, OR, USA, 6th ed., 1996.

Herman, B. *Fluorescence microscopy*, Springer, New York, 1998.

Hodder P.S., Ruzicka J. *Anal. Chem.* **1999**, *71*, 1160-1166.

Holman D.A., Christian G.D., Ruzicka J. *Anal. Chem.* **1997**, *69*, 1763-1765.

Incerpi S., Rizvi S.I., DeVito P., Luly P. *J. Cell Physiol.*, **1997**, *171*, 235-242.

Inoué, S. *Video Microscopy*, Plenum Press, New York, 1986, Chapter 5.

James P.E., Jackson S.K., Grinberg O.Y., Swartz H.M. *Free Radic. Biol. Med.* **1995**, *18*, 641-647.

Katzung B.G. *Basic and clinical pharmacology*, 7th ed., Appleton & Lange, Stamford, CT, 1998, Chapter 1.

Kavandi J., Callis J., Gouterman M., Khalil G., Wright D., Green E., Burns D., McLachlan B. *Rev. Sci. Instrum.* **1990**, *61*, 3340-3347.

Kenakin, T. *Pharmacologic analysis of drug-receptor interaction*, Lippincott-Raven, Philadelphia, 1997, Chapters 1 and 5.

Lähdesmäki I., Beeson C., Ruzicka J. unpublished results

L'Allemain G., Paris S., Pouyssegur J. *J. Biol. Chem.*, **1985**, *260*, 4877-4883.

Martínez-Zaguilán R., Martínez G.M., Lattanzio F., Gillies R. *Am. J. Physiol.*, **1991**, *260*, C297-C307.

Martínez-Zaguilán R., Parnami G., Lynch R.M. *Cell Calcium*, **1996**, *19*, 337-349.

McConnell H.M., Owicki J.C., Parce J.W., Miller D.L., Baxter G.T., Wada H.G., Pitchford S. *Science,* **1992**, *257*, 1906-1912.

Motterlini R., Kerger H., Green C.J., Winslow R.M., Intaglietta M. *Am. J. Physiol.* **1998**, *275*, H776-H782.

Negulescu P.A., Machen T.A. Meth. Enzymol., **1990**, *192*, 38-81.

Ohara T., Takeda K., Asano Y. *Jpn. Circ. J.*, **1992**, *56*, 133-141.

Pitchford S., Hirst M. *J. NIH Res.*, **1994**, *6*, 84.

Poch E., Botey A., Gaya J., Cases A., Rivera F., Revert L. *Biochem. J.*, **1993**, *290*, 617-622.

Roos A., Boron W.F. *Physiol. Rev.*, **1981**, *61*, 296-434.

Rumsey W.L., Schlosser C., Nuutinen E.M., Robolio M., Wilson D.F. *J. Biol. Chem.* **1990**, *265*, 15392-15402.

Rumsey W.L., Vanderkooi J.M., Wilson D.F. *Science* **1988**, *241*, 1649-1651.

Ruzicka J. *Analyst* **1998**, *123*, 1617-1623.

Ruzicka J., Baxter P.J., Thastrup O., Scudder K. *Analyst*, **1996**, *121*, 945-950.

Ruzicka J., Gübeli T. *Anal. Chem.* **1991**, *63*, 1680-1685.

Ruzicka J., Hansen E.H. *Anal. Chim. Acta*, **1975**, *78*, 145-157.

Ruzicka J., Hansen E.H. *Flow injection analysis*, Wiley, New York, 1988.

Ruzicka J., Ivaska A. *Anal. Chem.* **1997**, *69*, 5024-5030.

Ruzicka J., Marshall G.D. *Anal. Chim. Acta* **1990**, *237*, 329-343.

Ruzicka J., personal communication.

Ruzicka J., Scampavia L.D. *Anal. Chem.*, **1999**, *71*, 257A-263A.

Saltiel J., Beauford W.A. in Volman D.H., Hammond G.S., Gollnick K. (eds.) *Advances in photochemistry*, vol. 14, Wiley, New York, 1988.

Shankland E. *Ph.D. thesis*, University of Washington: Seattle, 1988; Chapter 2.

Shenoy M.A., Biaglow J.E., Varnes M.E., Hetzel F.N. *Adv. Exp. Med. Biol.* **1983**, *159*, 359-369.

Slater E.C. *Methods Enzymol.* **1967**, *10*, 48-57.

Staub F., Winkler A., Peters J., Kempski O., Kachel V., Baethmann A. *J. Cereb. Blood Flow Metab.*, **1994**, *14*, 1030-1039.

Stern O.. Volmer M. *Physik. Z.* **1919**, *20*, 183-188.

Tallarida R.J., Jacob L.S. *The dose-response relation in pharmacology*, Springer Verlag, New York, 1979, Chapter 3.

Thomas R.C. *Nature*, **1989**, *337*, 601-601.

Timpson C.J., Carter C.C., Olmsted J. *J. Phys. Chem.* **1989**, *93*, 4116-4120.

Touyz R.M., Schiffrin E.L. *Hypertension*, **1997**, *30*, 1440-1447.

Tsien R.Y. *Meth. Cell Biol.*, **1989**, *30*, 127-156.

Vanderkooi J.M., Maniara G., Green T.J, Wilson D.F. *J. Biol. Chem.*, **1987**, *262*, 5476-5482.

Vicentini L.M., Villereal M.L. *Life Sciences*, **1986**, *38*, 2269-2276.

Wada H.G., Indelicato S.R., Meyer L., Kitamura T., Miyajima A., Kirk G., Muir V.C., Parce J.W. *J. Cell. Physiol.*, **1993**, *154*, 129-138.

Wiegmann T.B., Vamos S., Welling L.W., Beatty D.M., Morris S.J. *Int. Rev. Exp. Pathol.* **1996**, *36*, 175-196.

Wolfbeis O.S. in Wolfbeis O.S. (ed.) *Fiber optic chemical sensors and biosensors, vol. II*, CRC Press, Boca Raton, 1991.

Yoshizaki K., Ohtomo K., Fukuhara K., Kawaguchi T., Kawaguchi J. *Adv. Exp. Med. Biol.* **1996**, *410*, 221-226.

VITA

Ilkka Lähdesmäki received a Master of Science degree in chemical engineering from the Åbo Akademi University (Turku, Finland) in 1993. For the next two years, he was a graduate student at the Åbo Akademi University. In 1995 he transferred to the University of Washington and received the Ph.D. degree in 1999.